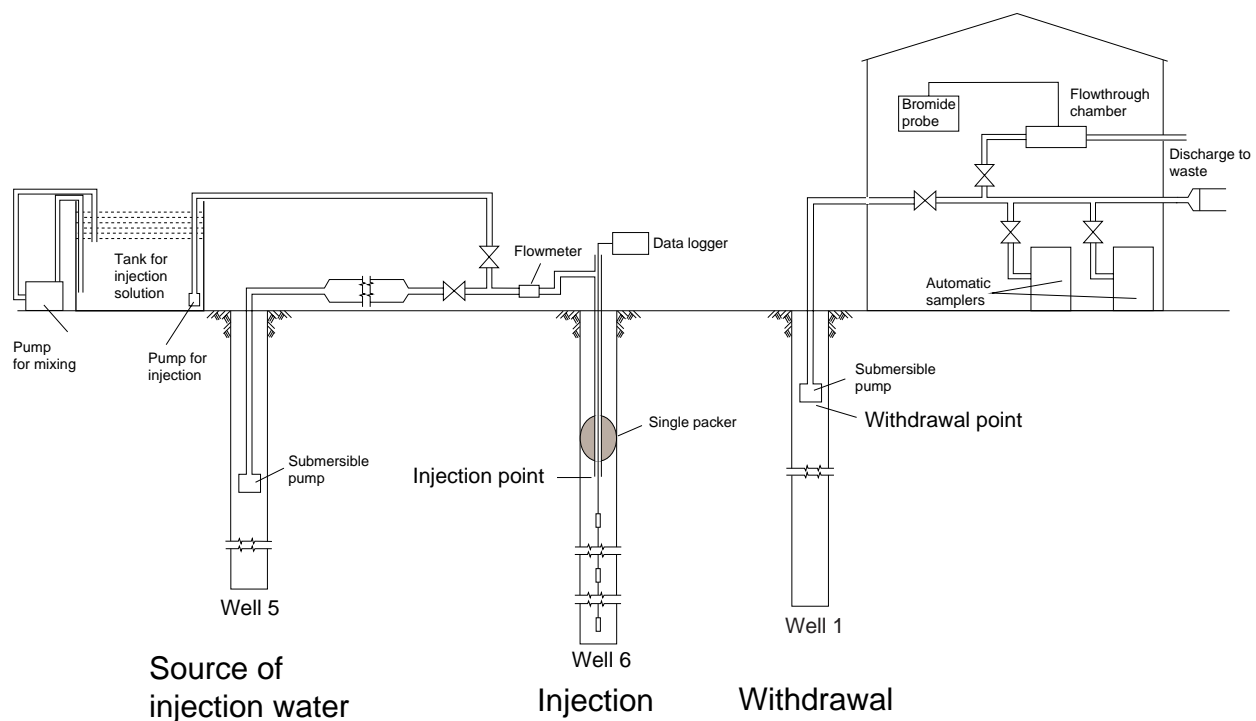# DESIGN AND ANALYSIS OF TRACER TESTS TO DETERMINE EFFECTIVE POROSITY AND DISPERSIVITY IN FRACTURED SEDIMENTARY ROCKS, NEWARK BASIN, NEW JERSEY

Water-Resources Investigations Report 98-4126A

Prepared in cooperation with the

NEW JERSEY DEPARTMENT OF ENVIRONMENTAL PROTECTION

USGS
science for a changing world

The cover sketch depicts the field installation of injection, withdrawal, and sampling equipment for a doublet tracer test.

DESIGN AND ANALYSIS OF TRACER TESTS TO DETERMINE EFFECTIVE POROSITY AND DISPERSIVITY IN FRACTURED SEDIMENTARY ROCKS, NEWARK BASIN, NEW JERSEY

By Glen B. Carleton[1], Claire Welty[2], and Herbert T. Buxton[1]

U.S. Geological Survey

Water-Resources Investigations Report 98-4126A

[1]U.S. Geological Survey, West Trenton, New Jersey

[2]Drexel University, School of Environmental Science, Engineering, and Policy, Philadelphia, Pennsylvania

West Trenton, New Jersey

1999

USGS

science for a changing world

U.S. DEPARTMENT OF THE INTERIOR

BRUCE BABBITT, *Secretary*

U.S. GEOLOGICAL SURVEY

Charles G. Groat, *Director*

CONTENTS

Page

ILLUSTRATIONS

ILLUSTRATIONS--Continued

TABLES

CONVERSION FACTORS, VERTICAL DATUM, AND ABBREVIATED WATER-QUALITY UNITS

Multiply	By	To obtain
	Length	
meter (m)	3.281	foot
kilometer (km)	0.6214	mile
	Area	
square meter (m^2)	10.76	square foot
hectare (ha)	2.471	acre
	Volume	
liter (L)	0.2642	gallon
	Flow	
liter per minute (L/min)	0.2642	gallon per minute
	Mass	
kilogram (kg)	2.205	pound, avoirdupois
	Hydraulic conductivity	
meter per day (m/d))	3.281	foot per day
	Transmissivity	
meter squared per day (m^2/d)[1]	10.76	foot squared per day

Sea level: In this report "sea level" refers to the National Geodetic Vertical Datum of 1929-- a geodetic datum derived from a general adjustment of the first-order level nets of the United States and Canada, formerly called Sea Level Datum of 1929.

Water-quality abbreviations:

mg/L- milligrams per liter

---

[1]This unit is used to express transmissivity, the capacity of an aquifer to transmit water. Conceptually, transmissivity is cubic meter (of water) per day per square meter (of aquifer area) times meter (of aquifer thickness), or $(m^3/d)/m^2$ x m. In this report, this expression is reduced to its simplest form, m^2/d.

DESIGN AND ANALYSIS OF TRACER TESTS TO DETERMINE EFFECTIVE POROSITY AND DISPERSIVITY IN FRACTURED SEDIMENTARY ROCKS, NEWARK BASIN, NEW JERSEY

By Glen B. Carleton, Claire Welty, and Herbert T. Buxton

ABSTRACT

Investigations of the transport and fate of contaminants in fractured-rock aquifers require knowledge of aquifer hydraulic and transport characteristics to improve prediction of the rate and direction of movement of contaminated ground water. This report describes an approach to estimating hydraulic and transport properties in fractured-rock aquifers; demonstrates the approach at a sedimentary fractured-rock site in the Newark Basin, N.J.; and provides values for hydraulic and transport properties at the site. The approach has three components: (1) characterization of the hydrogeologic framework of ground-water flow within the rock-fracture network, (2) estimation of the distribution of hydraulic properties (hydraulic conductivity and storage coefficient) within that framework, and (3) estimation of transport properties (effective porosity and dispersivity). The approach includes alternatives with increasingly complex data-collection and analysis techniques.

The local geologic structure of the site, located in Hopewell Township, Mercer County, is dominated by a gently northwest-plunging syncline. Bedding planes in the main part of the site strike approximately east-west and dip to the north. The two dominant fracture sets in the study area are bedding-plane partings and east-west-striking structural fractures that dip steeply to the south. Transmissive layers correspond to bedding-plane zones and contain bedding-plane separations and near-vertical structural fractures. The transmissive layers are separated by massive rock zones through which water flows vertically at very low rates, apparently through near-vertical fractures. Transmissive zones were identified using single-well hydraulic tests and water-level data collected under static and pumping conditions. Transmissive zones occur about every 9 meters, on average.

A 9-day, site-scale aquifer test was designed and conducted to test the basic concept of hydrogeologic framework and to estimate the distribution of hydraulic properties. Application of an analytical solution, in which an equivalent homogenous, anisotropic porous medium was assumed, provided estimates of principal values of hydraulic conductivity of 6.4, 0.30, and 0.0043 m/d (meters per day) and specific storage of 9.2×10^{-5} meters^{-1}; the maximum principal direction of hydraulic conductivity was nearly aligned with strike and nearly horizontal in space. A three-dimensional numerical ground-water-flow model with model layers aligned with the bedding planes provided best-fit, average values of hydraulic conductivity of about 7, 3, and 4×10^{-5} m/d for the strike, dip, and normal-to-bedding plane directions, respectively. The numerical model results indicate that heterogeneities and boundary conditions significantly affect estimates of the hydraulic properties.

Three non-recirculating doublet tracer tests were conducted at spacings of 30.5, 91.4, and 183 meters in approximately 40-meter-long open boreholes using a pulsed bromide injection. Longitudinal dispersivity was found to increase with the scale of the experiment, indicating that a minimum scale (spacing) tracer test is required to provide values of transport properties representative of processes on the order of tens to hundreds of meters, the scale of many contaminant plumes. For the

tracer test conducted at the 183-meter spacing, effective porosities of 3.7×10^{-4} to 7.6×10^{-4} and a longitudinal dispersivity of 12.8 meters were obtained using an analytical technique. An effective porosity of 1.2×10^{-3} and a longitudinal dispersivity of 12.8 meters were obtained using a two-dimensional numerical solute-transport model. An effective porosity of 1.4×10^{-3} was estimated from tracer-test data using particle-tracking methods and the three-dimensional numerical flow model used to interpret the site-scale aquifer test.

The hydraulic and tracer tests were successfully evaluated using the approach presented, including mathematical models developed for porous-media applications. This success indicates that flow and transport through fractured sedimentary rocks such as those in the Newark Basin can be simulated as flow and transport through an equivalent porous medium at the scales considered in this study.

INTRODUCTION

Investigations of transport and fate of contaminants in fractured-rock aquifers are often hampered by lack of knowledge of the hydraulic and transport properties typical of these aquifers. At present, significant uncertainty exists in estimates of ground-water flow rates and directions and in prediction of the movement of contaminated ground water in fractured-rock aquifers. Hydraulic and tracer tests based on an interpretation of the hydraulics associated with fracture geometries can be used to calculate values of hydraulic conductivity, specific storage, effective porosity, and dispersivity. Of particular interest are the applicability of porous-media approaches to estimating these properties in fractured rock, the transport properties of fractured media, and the influence of test scale on calculated dispersivity.

A field site underlain by fractured sedimentary rocks typical of the Newark Basin in northern New Jersey was selected to develop an approach for characterizing the hydraulic and transport properties in this terrane and to determine these properties at a representative site. The scale of the investigation was intended to be representative of plume-scale processes at contaminated sites. The U.S. Geological Survey (USGS) conducted the investigation in cooperation with the New Jersey Department of Environmental Protection (NJDEP), through the Division of Science and Research (DSR) and New Jersey Geological Survey (NJGS). The NJGS identified as a priority the estimation of values for hydraulic and transport properties of common fractured-rock aquifers in New Jersey and the demonstration of methods to estimate those properties at the plume scale as critical information needs for contamination characterization and remediation in New Jersey (Robert Canace, New Jersey Geological Survey, oral commun., 1997). The NJDEP DSR implemented that priority as part of its 1993–94 research agenda and provided matching funds for the investigation under a grant from the 1981 hazardous waste bond issue.

Although considerable research has been done on contaminant transport in porous media (similar to the Coastal Plain aquifers of New Jersey), fewer studies have described transport in complex and variable fractured-rock terranes such as those of northern New Jersey. For this reason, studies such as the one described herein have the potential to significantly contribute to the data base of information available on hydraulic and transport properties of these aquifers. About 90 Mgal/d of ground water is withdrawn from Newark Basin aquifers to supply some of the approximately 5 million people living in the basin, yet more than 300 hazardous waste sites have been identified in

the basin. Careful testing and analysis at these sites can aid in better prediction of the extent of contamination, leading to improved management of human-health and environmental risk, as well as considerable time and cost savings during site remediation. Information on how to design, implement, and interpret field studies to determine hydraulic and transport properties is needed by practitioners and regulators alike.

Purpose and Scope

This report (1) presents an approach to characterize the hydrogeologic, hydraulic, and transport properties at a representative fractured-sedimentary-rock site in the Newark Basin, N.J., and (2) reports values for hydraulic and transport properties of the site. The report is divided into three sections. The first section describes development of a conceptual model of the hydrogeologic framework of the site, based on the assumptions of ground-water flow in an equivalent porous medium. The second section describes the design and analysis of a site-scale aquifer test to determine the hydraulic conductivity and specific storage of the aquifer and to verify the conceptual model of the hydrogeologic framework. The third section describes the design and analysis of tracer tests and includes discussions of the importance of scale and heterogeneity, different hydraulic flow regimes for tracer tests, considerations for determining the type and amount of tracer to inject, field plumbing, and analysis of tracer-test data to determine longitudinal dispersivity and effective porosity.

Approach

The approach for the design and interpretation of field experiments to characterize the hydraulic and transport properties of the fractured sedimentary-rock aquifer has three components: (1) characterization of the hydrogeologic framework of ground-water flow within the network of rock fractures, (2) estimation of the distribution of hydraulic properties (hydraulic conductivity and storage coefficient) within that framework, and (3) estimation of transport properties (effective porosity and dispersivity). For this study, increasingly complex data-collection and analysis techniques were used until satisfactory results were obtained. Those methods of lower complexity and difficulty may be sufficient for applications where risks are low and (or) resources are limited.

The hydrogeologic framework was defined on the basis of existing information, field geologic mapping, borehole geophysics, and single- and double-well hydraulic tests. Layered sedimentary rocks in the Newark Basin commonly contain water-bearing partings along bedding planes in fissile layers separated by massive layers with virtually no such partings. Joint sets perpendicular to bedding planes can transmit water across the massive layers separating fissile zones. A concept of the hydraulics of the system was based on an equivalent porous media approach; that is, an initial concept of the flow through the fracture network was based on assumption of an equivalent set of unconsolidated aquifers and confining units, in which fissile bedding-plane zones and massive layers are treated as aquifers and confining units, respectively (fig. 1). Although this description dramatically simplifies the complexities of the fractured sedimentary-rock aquifer, it illustrates the concept of an equivalent porous medium representation, which, if properly applied, facilitates use of a wide range of interpretive methods developed for analysis of porous media.

A. Fractured rock media

Joint set

Massive rock
(confining unit)

Rock with abundant
bedding-plane partings
(aquifer)

B. Unconsolidated media

Clay and silt
(confining unit)

Sand and gravel
(aquifer)
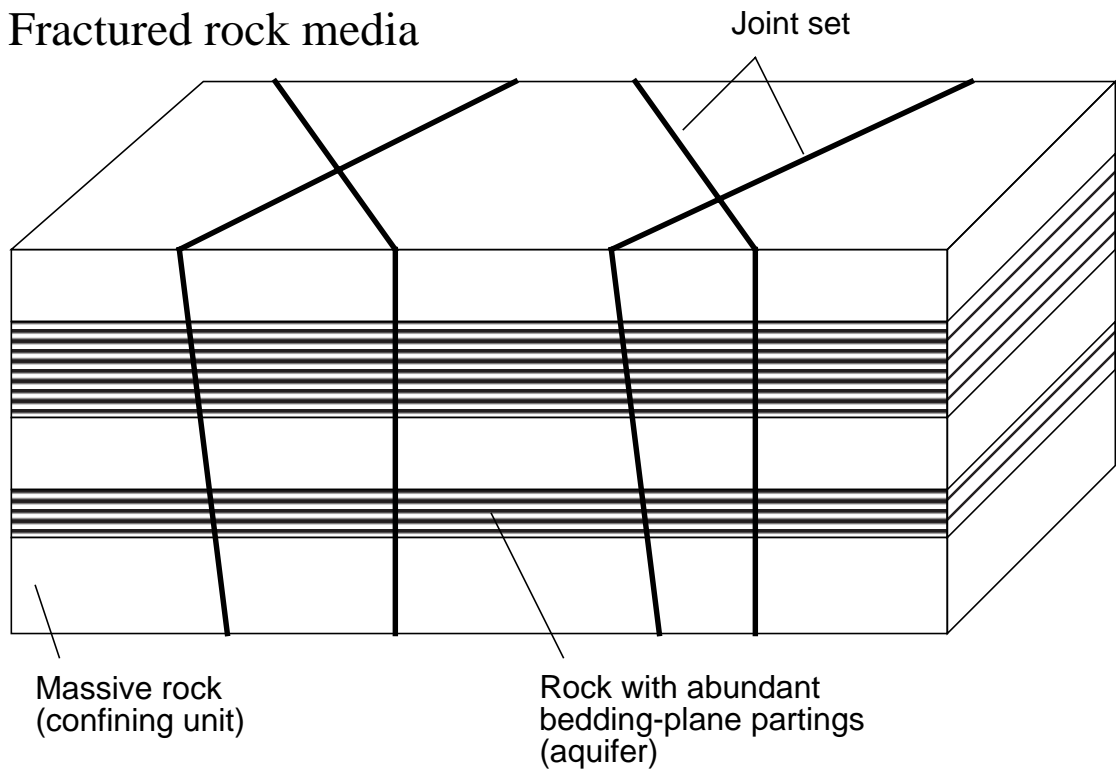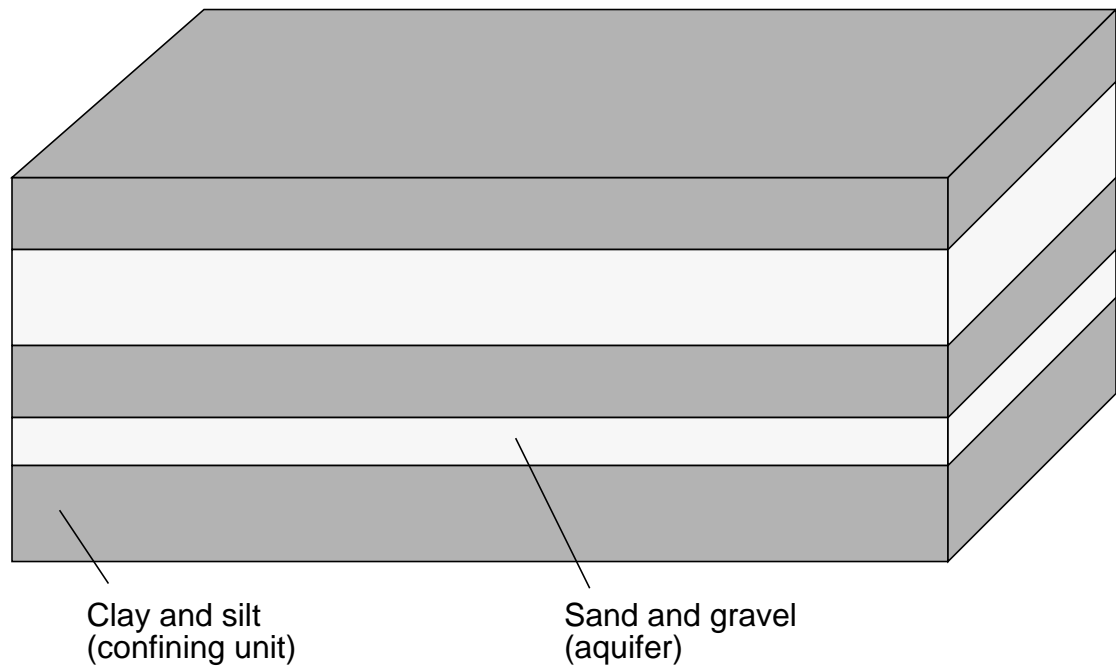
Figure 1. Diagrammatic comparison of (A) sedimentary rock aquifer system and
(B) equivalent unconsolidated aquifer system.

The initial concept of the hydrogeologic framework of the study site was tested and refined through design and interpretation of an aquifer test, in which aquifer (water-level) response to pumping at a sitewide scale was interpreted. The distribution of hydraulic properties within the hydrogeologic framework was estimated. The aquifer test was analyzed by means of analytical and numerical techniques. Analytical techniques typically are relatively quick to carry out, but they include simplifying assumptions that may not be acceptable for some applications. In contrast, numerical models can require considerable time to construct, but they can be modified to represent boundary conditions and complex aquifer-confining unit relations exhibited by layered sedimentary-rock aquifers.

Aquifer transport properties were estimated by conducting and analyzing tracer tests in which a harmless solute was introduced to the aquifer and its dispersal within a prescribed flow field was interpreted. The analysis yielded estimates of effective porosity and dispersivity, both of which significantly affect the rate of solute movement and the mixing caused by random heterogeneity within the aquifer. The conceptual model of the hydrogeologic framework was used as the basis to design the tracer test and, consequently, confidence in that concept was increased through successful interpretation of the tracer tests. As with hydraulic tests, tracer-test results can be analyzed by means of analytical or numerical techniques, with similar benefits and restrictions.

A continuum approach to modeling the fractured-rock aquifer was used in this study. Alternative approaches for modeling flow and transport in fractured-rock environments include discrete-fracture models or models that are hybrids between the continuum approach and discrete-fracture models. A recent report by the National Research Council (1996) discusses strengths and weaknesses of the various alternatives.

Site Description

The study site is located in Hopewell Township, Mercer County, N.J., on a 250-ha nature reserve owned by the Stony Brook-Millstone Watershed Association (fig. 2). It is in the Newark Basin, part of the Piedmont Physiographic Province. Thirteen observation wells were drilled by the air rotary method at the site in 1966 for a study of anisotropic flow in fractured rock (Vecchioli and others, 1969). The observation-well network consists of eight wells located at a radius of about 90 m from a central well (well 1), three wells located at greater distances approximately along strike (183, 195, and 280 m for wells 10, 7, and 12, respectively), and one additional well (well 6) located 30.5 m downdip. (Two privately owned wells, 14 and 15, are shown in figure 1 and are discussed later in the report.) The observation wells are all constructed with about 6 m of steel surface casing, have a nominal diameter of about 15 cm, and are about 46 m deep, except for well 6, which was drilled to 61 m in order to penetrate the same bedding planes intersected by well 1. The wells yielded as much as 400 L/m at the time of drilling (Vecchioli and others, 1969). The small stream (Honey Branch) running through the site was dammed shortly after the wells were drilled, creating a small pond that is as much as 2 m deep.
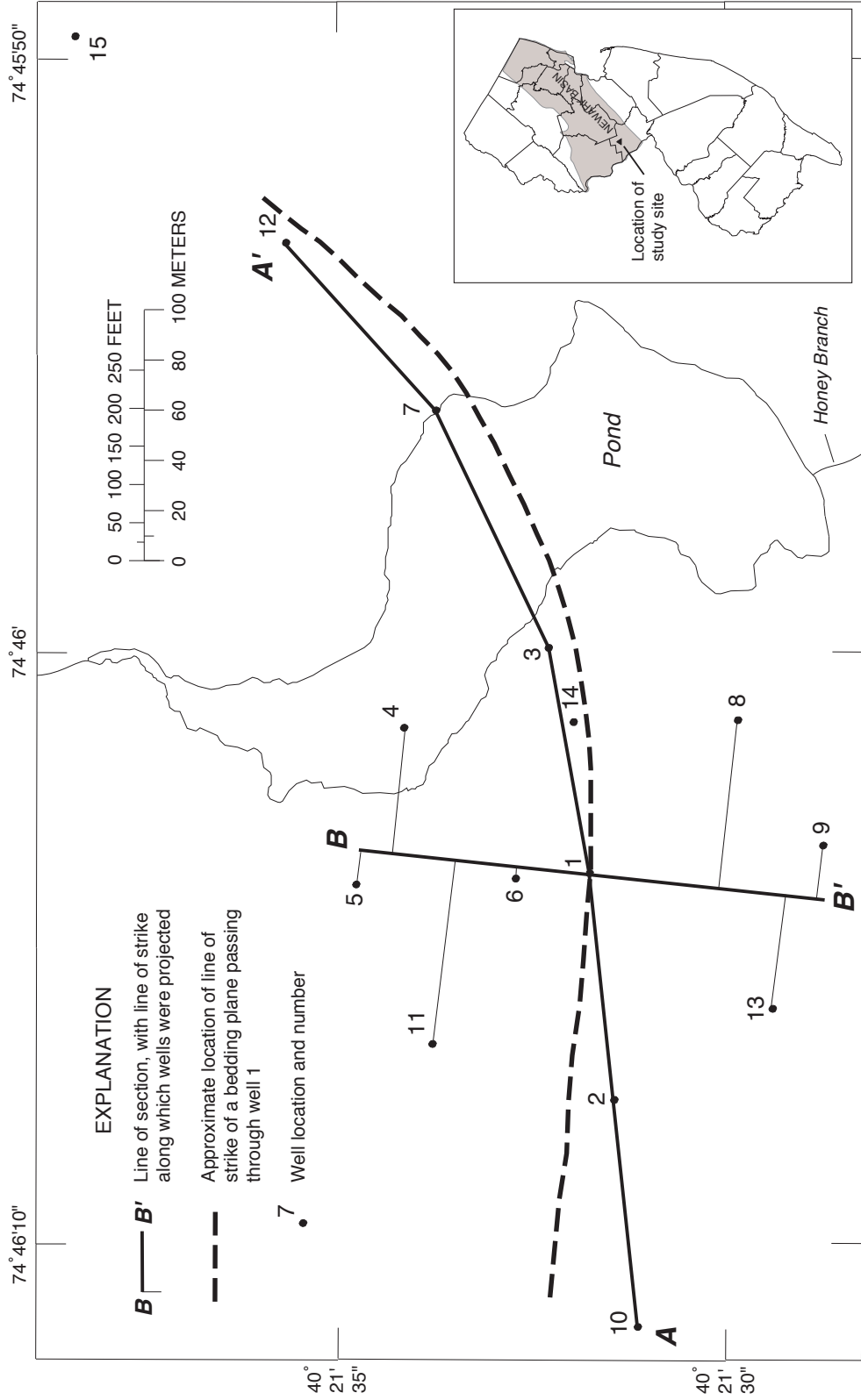
Figure 2. Location of wells and significant features in study area, Hopewell Township, N.J.

6

Acknowledgments

HYDROGEOLOGIC FRAMEWORK

A conceptual model of the hydrogeologic framework of the site was developed on the basis of observational geology and borehole geophysical information, which describe the hydrogeologic structure of the rock-fracture network; and single- and dual-well (small zone of influence) hydraulic tests, which indicate the comparative productivity of fracture zones within individual wells and correlate those zones between wells. No new boreholes were drilled for this study; therefore, no cores or drill-cutting data were available. Collection of surface geophysical data was considered unnecessary because of the abundant data available from the existing wells.

Geologic and Geophysical Interpretations

The Newark Basin is an elongate (210 by 55 km), northeast-southwest-trending fault trough filled with late Triassic and early Jurassic fluvial and lacustrine sediments and igneous intrusions (Olsen, 1980; Parker and others, 1988; Houghton, 1990). The sedimentary rocks of the Newark Basin are similar to deposits in about 30 inland rift basins along the East Coast from South Carolina to Nova Scotia. The site is underlain by the Late Triassic Passaic Formation (an important aquifer in New Jersey and Pennsylvania), consisting of red arkosic mudstones, siltstones, and fine-grained sandstones. The Hopewell Fault is a major regional structure that lies about 2 km northwest of the site and trends northeast-southwest. Other regional structures include broad, low-amplitude folds (Lyttle and Epstein, 1987) that are secondary features related to the Hopewell Fault (Gregory Herman, New Jersey Geological Survey, written commun., 1995).

The local structure of the site is dominated by a gently northwest-plunging syncline, the axis of which runs about through the center or slightly northeast of the pond on the east side of the site (Vecchioli and others, 1969; Gregory Herman, written commun., 1995). On the western limb of the broad syncline, the bedding planes strike approximately east-west and dip moderately to the north. The two dominant fracture sets in the study area are bedding-plane partings and east-west-striking structural fractures that dip steeply to the south.

Standard laboratory testing of three cores of massive rock matrix, stratigraphically similar to Passaic Formation rock found at the site, including one core collected about 16 km west of the site, yielded total porosities of 3 to 5 percent and hydraulic conductivities ranging from undetectable to 7.8 x 10^{-4} m/d (Core Laboratories, written commun., 1991). The very low permeability of the rock matrix indicates that virtually all of the flow occurs in fractures, but the significant porosity of the matrix can be a source or sink for dissolved contaminants or chemical tracers.

A full suite of borehole geophysical logs—including gamma, electric, electromagnetic conductance (EM), caliper, fluid temperature and resistivity, and video—was collected at and interpreted for all of the wells. In addition, all of the wells except for wells 7 and 12 (inaccessible) and well 5 (collapsed at 21 m shortly after construction) were logged with the acoustic borehole televiewer (BHTV) and heat-pulse flowmeter (HPFM). Detailed information regarding geophysical tools and their principles of operation in ground-water investigations can be found in Keys (1990). Results of the geophysical logging are summarized below; more detailed discussion of the results can be found in Morin and others (1997).

The geophysical logs were used to determine location and orientation of fractures and to construct lithologic sections that correlated producing zones on the basis of geologic characteristics. EM logs were used to construct lithologic sections (figs. 3 and 4) on which EM anomalies can be correlated across the site, including across the axis of the syncline. The BHTV data show the bimodal distribution of fractures (fig. 5); about 80 percent of the 280 identified fractures are either bedding-plane partings dipping gently northward or structural fractures dipping steeply southward (Morin and others, 1997). The average strike and dip of the bedding-plane partings measured on the BHTV logs (on the western limb of the synform only) are N. 276° E., 19° N., although the average dip estimated from the lithologic sections is slightly greater, about 27° N. The average strike and dip of the major set of structural fractures is approximately N 79° E., 71° S. A minor set of structural fractures imaged by the BHTV strikes about N. 170° E. and dips 82° W., on average.

The probability of intersecting a near-horizontal fracture with a vertical borehole is very high, whereas the probability of intersecting a near-vertical fracture is very low; therefore, the ratio of horizontal to vertical fractures detected is likely to be higher than the actual ratio. A statistical correction of fracture frequency based on the dip angle of the fractures may be applied to predict the frequency of fractures of a particular orientation that would be intersected by a well drilled normal to the fracture plane (Terzaghi, 1965; Barton and Zoback, 1992). This statistical correction was applied to the cumulative fracture population from the 10 wells logged with the BHTV (Morin and others, 1997). About 50 percent of the identified fractures dip less than 35°, and about 33 percent dip more than 65°. When the statistical correction is applied, the bimodal distribution is still apparent, but about 25 percent of the predicted fractures dip less than 35°, and about 60 percent dip more than 65°. Although the results of applying the statistical correction imply that more than twice as many steeply dipping fractures as bedding-plane partings exist, these data alone do not indicate in which fractures ground-water flow occurs.
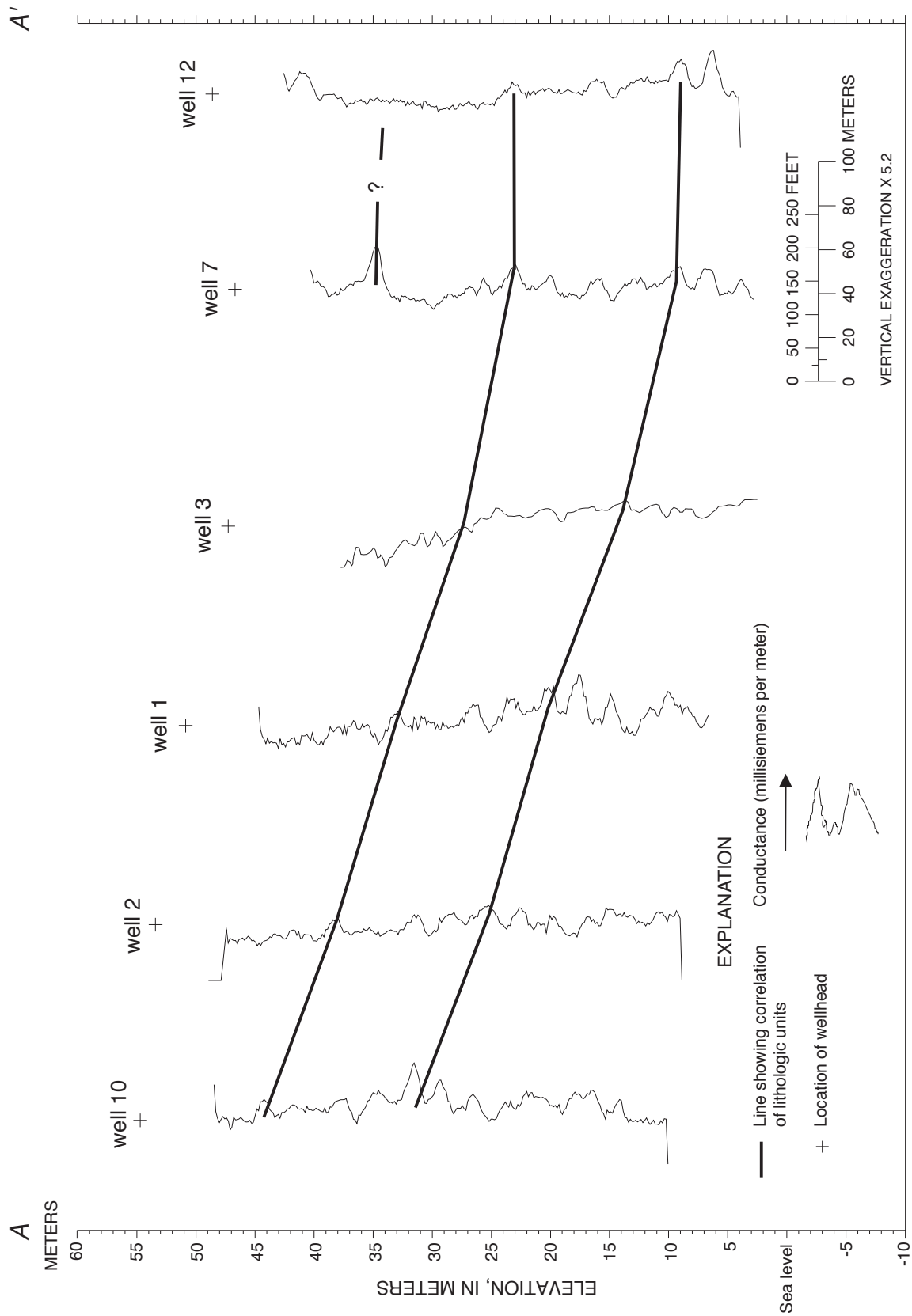
Figure 3. Section *A-A'* showing lithologic correlations determined from electromagnetic conductance geophysical logs, Hopewell Township, N.J. (Trace of section shown in fig. 2.)

9
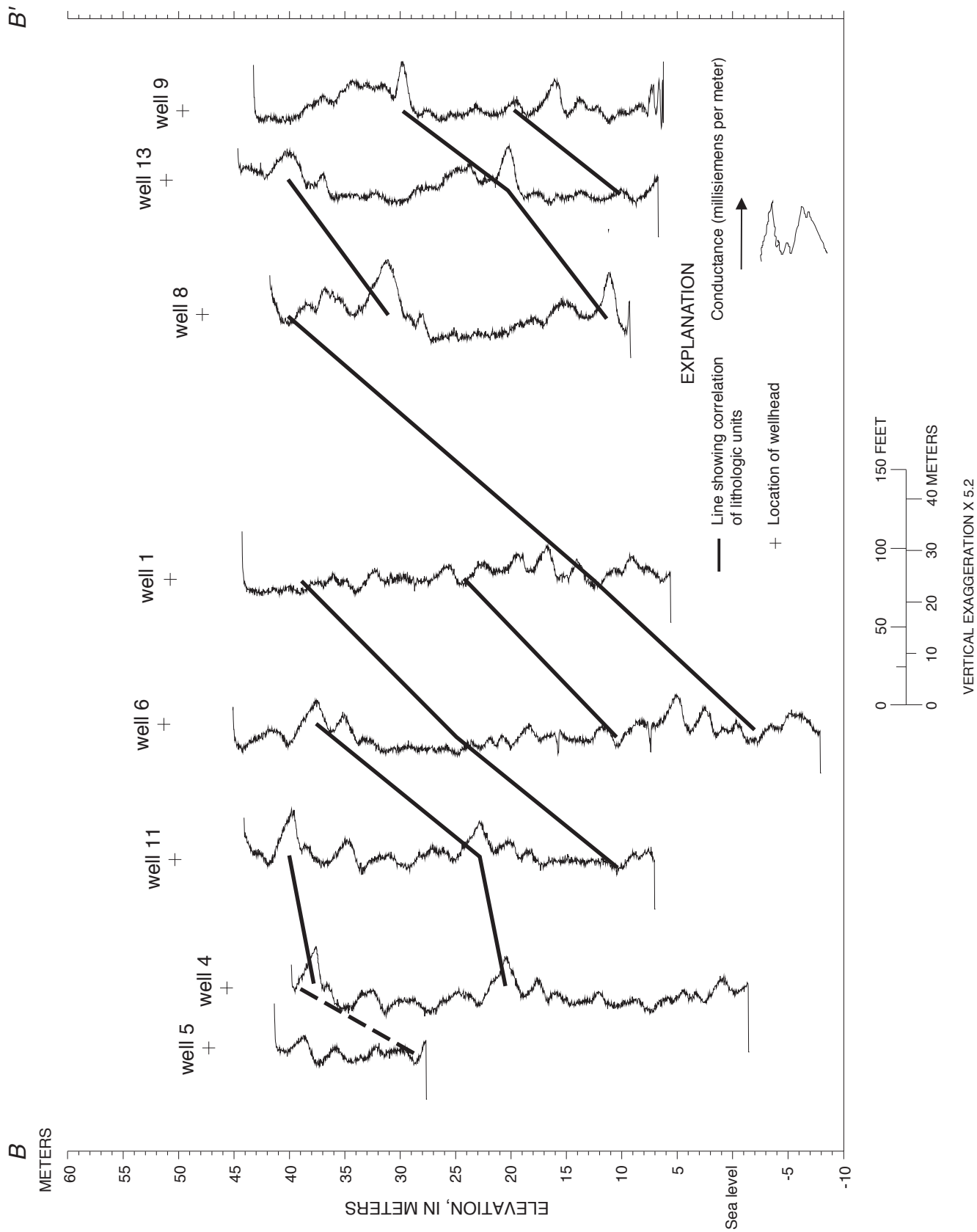
Figure 4. Section *B-B'* showing lithologic correlations determined from electromagnetic conductance geophysical logs, Hopewell Township, N.J. (Trace of section shown in fig. 2.)

Equal Area

N = 280   Circle = 15 percent

N = 280   Contour interval = 4.2 sigma
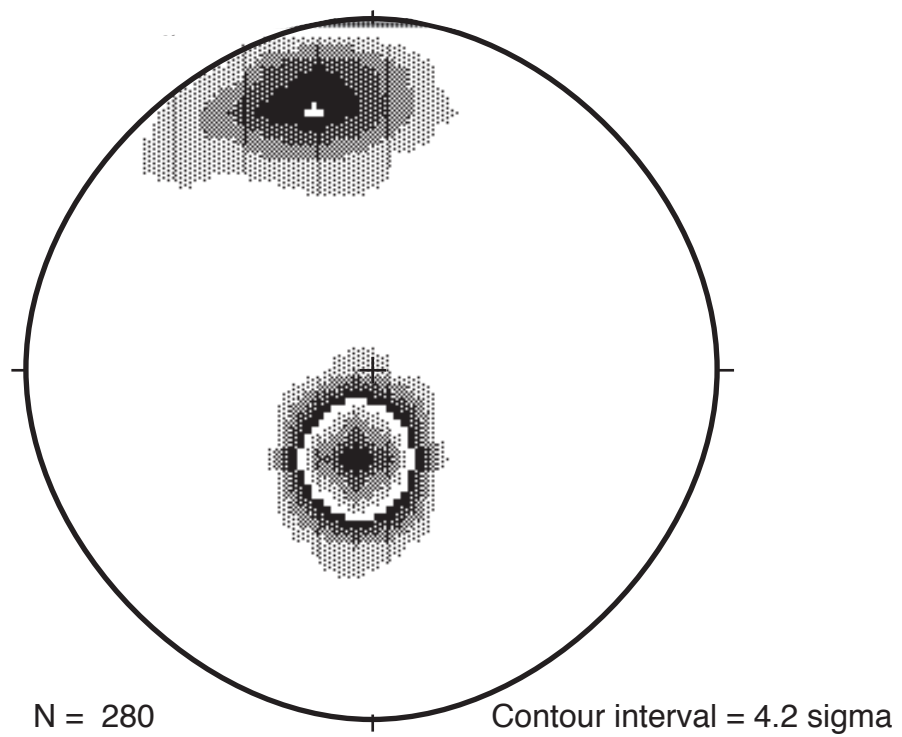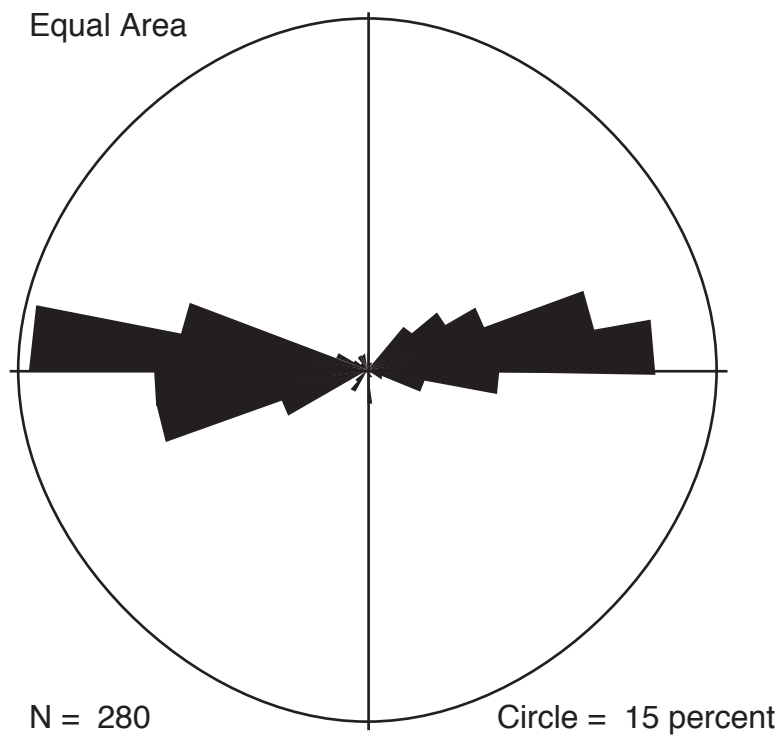
Figure 5. Rosette and stereographic diagrams of fracture orientations at 10 wells (N = 280 fractures) Hopewell Township N.J. (From Morin and others, 1997).

Productive-Zone Hydraulic Testing

The HPFM measures vertical fluid movement in a well under ambient and pumping conditions (Hess and Paillet, 1990). Measurements are typically made at discrete intervals, and changes in velocity indicate that water is entering or leaving the borehole. Data from other geophysical logs, such as fluid temperature and resistivity, caliper, and BHTV, can help identify specific producing fractures. In some cases, the borehole is too damaged to identify a specific producing fracture, or multiple producing fractures are present; therefore, only a producing zone is identified. If drawdown data are collected and fluid velocity data are converted to discharges, then analytical solutions may be used to estimate the transmissivity of producing fractures or zones (Morin and others, 1988; Molz and others, 1989).

Fluid temperature and resistivity and HPFM logs from the study site indicate little or no vertical flow in any of the wells under ambient conditions, although low-velocity uphole flow was observed with the borehole video in well 8. The lack of significant vertical flow in the boreholes indicates that different producing zones intersected by the wells are not productive enough and (or) at sufficiently different heads to cause water to flow vertically at a rate above the detection limit of the HPFM (about 1 cm/min (Hess, 1982), which translates to about 2 L/min in a 15-cm-diameter well).

HPFM logs also were collected in each of 10 wells while water was being withdrawn at a median rate of 47 L/min. From 2 to 6 producing zones were identified in each well, and in most cases flow could be attributed to a specific fracture or two intersecting fractures. The many fractures visible in outcrop indicate that individual fractures are not extensive; rather, they join other fractures in an interconnected network. Nonetheless, to gain a better understanding of the system, the orientation of specific producing fractures was determined where possible. Among the 10 wells, 51 producing fractures were identified, representing about 18 percent of the total fracture population (Morin and others, 1997). In eight cases, fluid exchange could not be attributed to a unique fracture because of a highly damaged borehole and a lack of corroborating responses from the fluid-property logs. The orientation of 43 of the producing fractures was determined from BHTV data. Of these 43 fractures, the hydraulics of 4 could not be determined because of equipment problems, and 8 pairs of bedding-plane partings and steeply dipping structural fractures were characterized as forming 8 fracture intersections. Thus, the orientation and hydraulic properties of 31 of the 51 producing fractures were characterized.

The transmissivity of these zones was calculated using the flow-meter-pumping technique of Morin and others (1988) and Molz and others (1989). Transmissivities of the 31 fractures range from about 0.1 to 20 m^2/d. Transmissivities associated with each fracture type are presented as a function of depth in figure 6, and average transmissivities are listed in table 1. Bedding-plane partings exhibit a wide range of transmissivity (two orders of magnitude) and diminish in magnitude and frequency with depth. The most transmissive fractures identified at the site are the bedding-plane partings near the surface, but no permeable partings were found below about 35 m (fig. 6). The high-angle fractures have a slightly narrower range of transmissivity, and there is no apparent correlation between depth and transmissivity. The intersections of bedding-plane partings and high-angle fractures also have a narrower range of transmissivity (less than one order of magnitude), and transmissivities also vary independently of depth.

Table 1. Average transmissivities of three categories of fractures observed in a fractured sedimentary rock, Newark Basin, Hopewell Township, New Jersey [From Morin and others, 1997]

[T_{avg}, average transmissivity; m^2/d, square meters per day]

Fracture type	Number of fractures	T_{avg} (m^2/d)
Bedding-plane partings	11	5.0
High-angle structural fractures	12	2.6
Bedding-plane parting/structural fracture intersections	8	4.2

Although the results of the borehole logging indicate that high-angle structural fractures are significantly transmissive within narrow water-producing zones, data collected over a larger zone of influence indicate they do not interconnect these water-producing zones. Houghton (1990) and Michalski (1990) report that near-vertical fractures at outcrops commonly terminate at lithologic contacts. Thus, although some high-angle fractures provide significant pathways for fluid transport, they are not necessarily extensive in the vertical direction and may be transmissive only in specific rock layers, primarily along strike, separated by low-permeability layers.

To verify the confining properties of these low-permeability layers, a packer was placed in a nonproducing zone in well 6 at a depth of 16.3 to 17.5 m below land surface, thereby isolating the strata common to wells 6 and 1 from those stratigraphically higher than well 1 (fig. 4). Water was withdrawn from well 1 at a rate of 108 L/min and drawdown above and below the packer in well 6 was measured. A hydraulic response was detected below the packer in well 6 (in the strata that occur in well 1) less than 10 seconds after the onset of pumping, and drawdown reached 3.62 m after 9 hours. Conversely, drawdown was not detected above the packer until more than 1 hour after pumping began, and reached only 0.19 m after 9 hours.

These results indicate that certain intervals have very low permeabilities (both horizontal and vertical) and serve as efficient confining units. Sections showing the locations of producing zones (figs. 7, 8) reveal that about 30 percent of the producing zones in one well correspond to producing zones at the same stratigraphic level in a neighboring well at the site. Other strata show no evidence of fluid exchange, and they apparently impede vertical flow. Thus, although high-angle fractures are important to flow within a fractured, water-producing bedding-plane zone, they apparently do not typically conduct flow between these bedding-plane zones, indicating that bedding-plane zones act as aquifers and confining units at a site scale. Jean Lewis-Brown (U.S. Geological Survey, written commun., 1997) and Michalski and Britton (1997) reached similar conclusions at other sites in the Newark Basin in New Jersey.
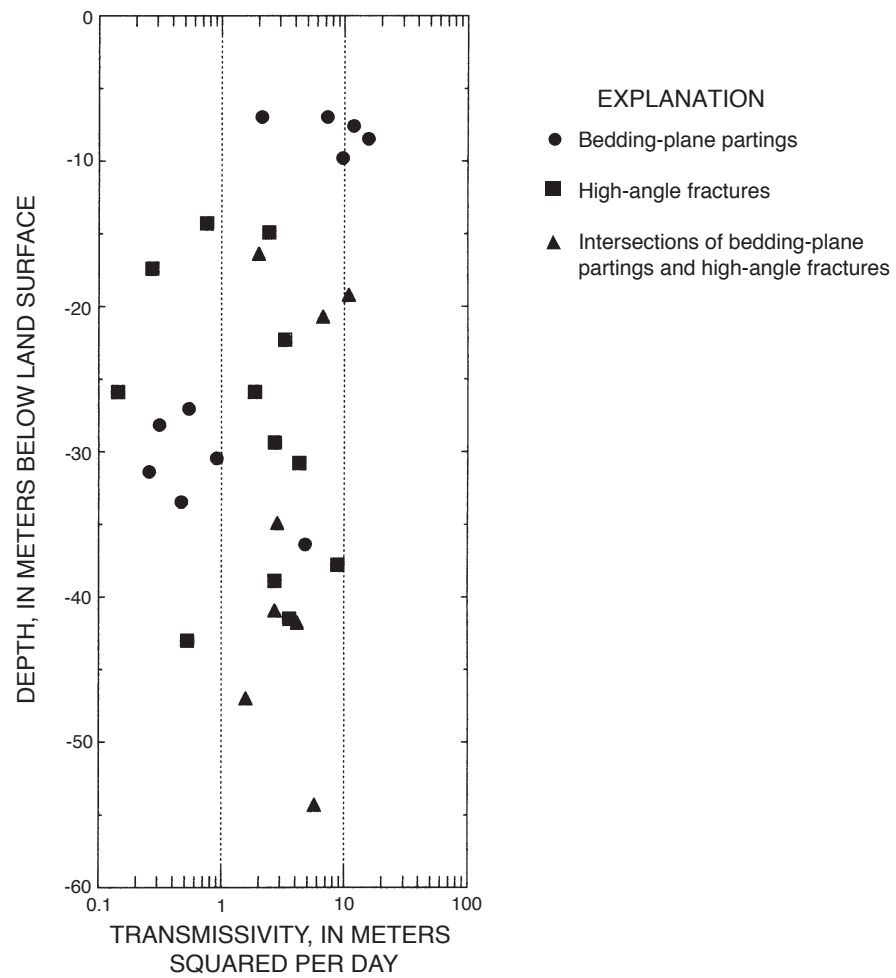
Figure 6. Transmissivities of different fracture types and associated depths below land surface, Hopewell Township, N.J.
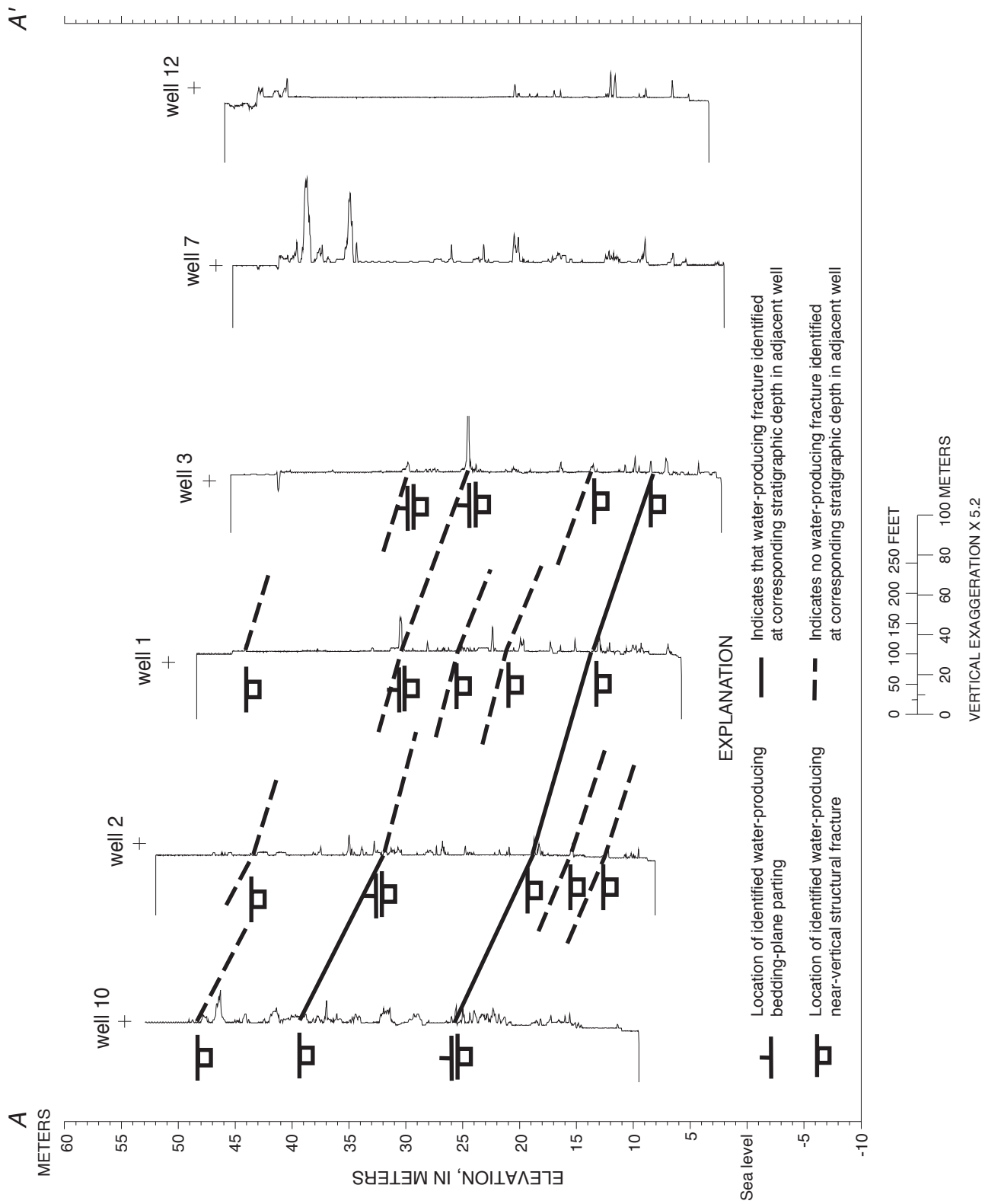
Figure 7. Section *A-A'* showing caliper logs and location of producing zones, Hopewell Township, N.J. (Trace of section shown in fig. 2.)

15
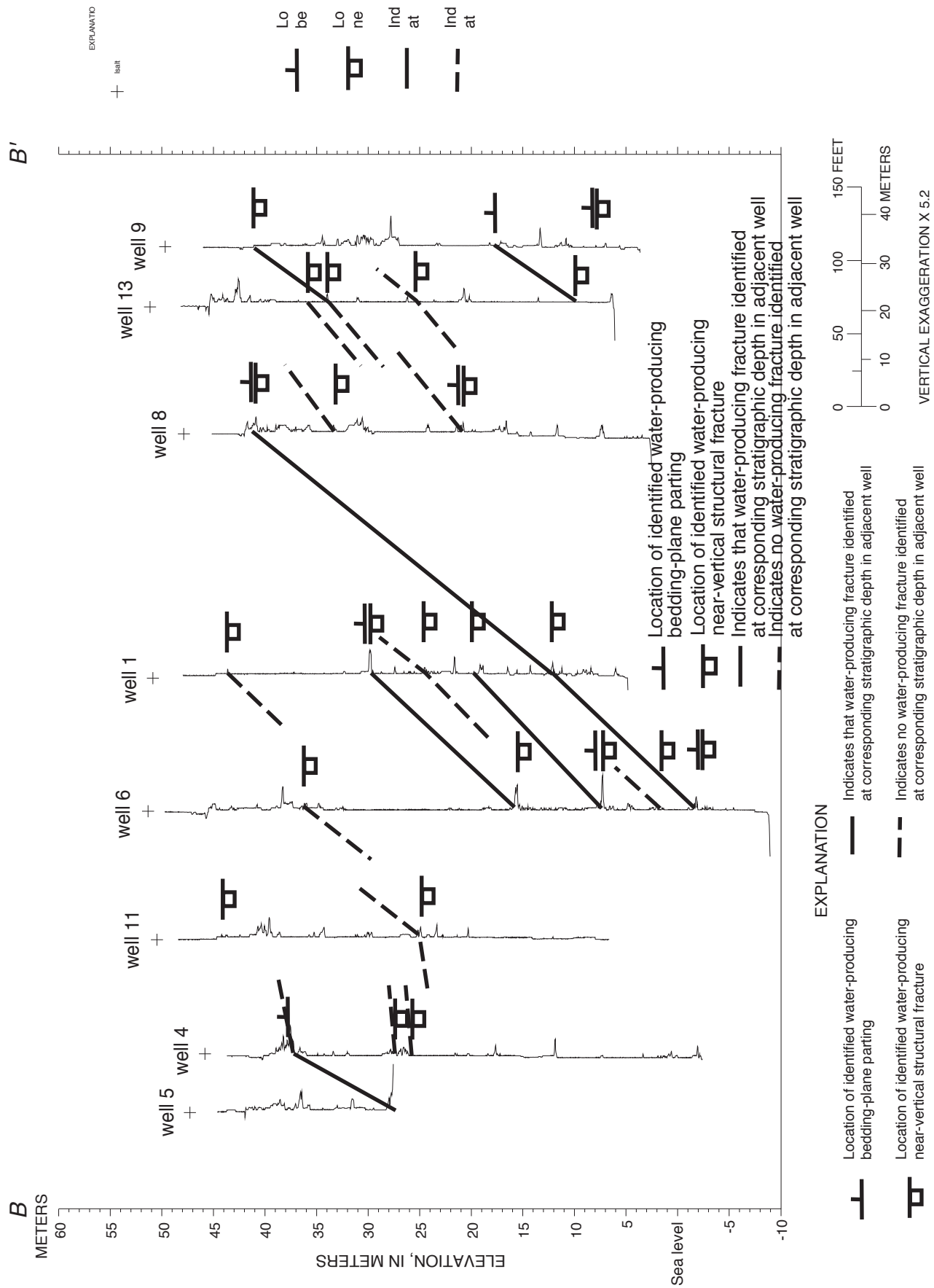
Figure 8. Section *B-B'* showing caliper logs and location of producing zones, Hopewell Township, N.J. (Trace of section shown in fig. 2.)

16

Static water levels also indicate that hydraulic conductivity is greater within bedding-plane zones than perpendicular to the planes. Water-level altitudes measured in all 13 observation wells on April 1, 1994 (fig. 9), indicate that gradients are as much as two orders of magnitude lower within bedding planes than between bedding planes (1 x 10^{-4} m/m and 2 x 10^{-2} m/m, respectively). The results of these water-level measurements show that the wells can be divided into four groups: "strike" wells (wells 10, 2, 1, 6, 3), wells "across the pond" (wells 7, 12), "north" wells (wells 4, 5, 11), and "south" wells (wells 8, 9, 13). Water levels in the strike group are within 0.04 m of each other, an indication of good hydraulic connection and a high hydraulic conductivity. The water levels in wells 9 and 13, south of the strike wells and open to stratigraphically lower beds, are as much as 1.69 m higher than in the strike group, an indication of significant hydraulic separation. The water level in well 8 is similar to other strike-group water levels because the top of well 8 intersects strata that occur in the bottom of well 1 and other strike wells, a fact that also explains the upward flow observed with the borehole video at the bottom of well 8. The effects of short circuits in open bore-holes, such as occurs in well 8, require that water-level data from wells with long open intervals be used cautiously. The head in wells open to multiple producing zones is weighted towards the zone with the highest transmissivity and may obscure substantially different heads in zones with lower transmissivities.

SITE-SCALE HYDRAULIC CHARACTERIZATION

The conceptual model of the hydrogeologic framework was tested by conducting and analyzing an aquifer test, which provides estimates of hydraulic conductivity and specific storage on a site scale. Borehole hydraulic tests, discussed in the previous section, provide transmissivities on the scale of about 1 meter; the range of values at this scale reflects the heterogeneity of the system. The site-scale aquifer test characterized average flow-system hydraulics at the scale of tens to hundreds of meters.

Vecchioli and others (1969) previously conducted an aquifer test at the site to study the anisotropy of flow in the Passaic Formation. In this test, the central well (well 1) was pumped at 60 L/min for 8 hours, and drawdown at wells 1 through 13 were reported at the end of the pumping period. The investigators concluded that the aquifer was anisotropic mainly from the difference between water-level responses in the strike and dip directions. Interpretive tools available at that time were insufficient to estimate hydraulic conductivity and specific storage. The availability of this well network provided an opportunity to conduct additional aquifer tests and to interpret them using current methods. A description of the test design and execution, a discussion of the methods used to analyze the data, and the resulting estimates of the aquifer properties are presented.

Aquifer-Test Design and Execution

The aquifer-test design was based on the assumption that the site contains a series of north-ward-dipping, transmissive units that correspond to layers with abundant fractures along bedding planes and less-transmissive, massive units that transmit water between transmissive zones. The existing well network provided the opportunity to withdraw water from the central well (well 1) and monitor the propagation of drawdown along strike and across massive layers to observation wells to the north (downdip and stratigraphically higher) and to the south (updip and stratigraphically lower). This arrangement of wells enabled estimation of hydraulic properties along bedding planes, and
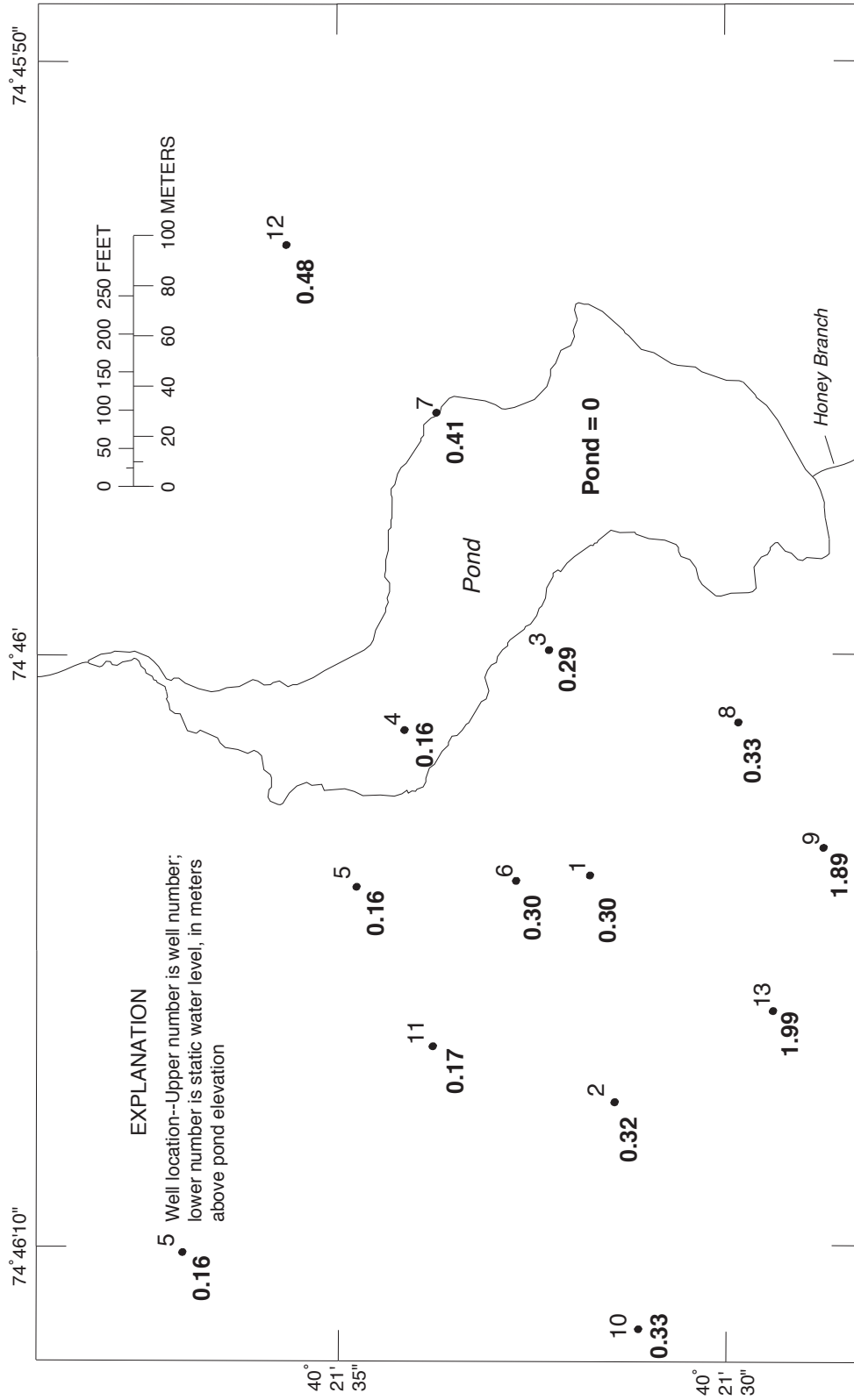
Figure 9. Static water levels, April 1994, Hopewell Township, N.J.

through massive layers, corresponding to the transmissivity of an aquifer layer and a confining unit, respectively, in the corresponding porous media equivalent. Use of packers to eliminate hydraulic short circuits between layers would have been desirable but was not possible in the investigation.

After preliminary withdrawal tests to determine a suitable pumping rate, a 9-day aquifer test was conducted in October 1994. Well 1 was pumped at a rate of 108 L/min, plus or minus 2 percent. No significant precipitation fell during the 5 days before the test or during the test; therefore, no recharge affected the water levels. The withdrawn water was discharged to the nearby pond to avoid recharging the aquifer.

Drawdowns were recorded in 15 wells, each instrumented with an electronic data logger recording data from either a shaft-encoder and float or a pressure transducer. In addition to the 13 observation wells described previously, water levels were measured in an irrigation well (well 14) and a nearby domestic well (well 15). The irrigation well, installed for a nearby farm in 1983, is cased to 18 m and is 38 m deep. The domestic well is cased to about 18 m and is about 37 m deep (Mr. Taylor, well owner, oral commun., 1994). Maximum drawdown at each well is shown in figure 10, and drawdown as a function of time for all of the wells is shown in figure 11.

Water levels in the strike wells (2, 3, 14, and 10) responded to pumping in less than 6 seconds; maximum drawdowns were between 6.6 and 6.9 m (fig. 10). Water levels in wells 7, 12, and 15, on the eastern limb of the synform, responded in 6 to 15 minutes and maximum drawdowns were between 1.9 and 3.9 m. Drawdown in well 12 was greater than in well 7 despite well 12's location farther from the pumping well, an indication that well 12 is more directly connected to well 1. Water levels in the northern wells (4, 5, and 11) responded in 5 to 9 minutes, and drawdown stabilized at about 0.6 m between 1,500 and 3,000 minutes after pumping began. Water levels in the southern wells (9 and 13, located updip but downsection) responded more slowly than those in the northern wells (at approximately 23 and 200 minutes, respectively), but the drawdowns at the end of the test were approximately three times those in the northern wells. The response in well 8 was more similar to the responses in wells 7 and 12 than to the responses in wells 9 and 13.

Well 6 is immediately downdip from well 1, yet it penetrates the same strata as well 1; therefore, the response in well 6 can be compared to the responses in wells 2 and 3 to determine the significance of northerly dipping bedding-plane partings as opposed to southerly dipping structural fractures. The similarity of the time-drawdown curves in wells 2, 3, and 6 supports the conclusion that flow occurs predominantly in bedding-plane zones and that near-vertical fractures are not vertically extensive. The importance of bedding-plane zones also partly explains drawdown responses in the northern (downdip) and southern (updip) wells. The drawdown response in well 8 is similar to the responses in wells 7 and 12, apparently because the top of well 8 is open to a producing zone that some of the strike wells are open to. Similarly, the early response in wells 4, 5, and 11 to the north is partially explained by a hydraulic connection (short circuit) to well 1 through the open borehole in well 6.

The effect of the hydraulic connection in well 6 on drawdown response in well 11 was tested by pumping well 1 when a packer was inflated in well 6. The packer isolated the zones tapped by the northern wells from the zones tapped by well 1. Drawdown in well 11 during this test occurred later and was less than when the zones were not isolated, but the drawdown curves are similar in shape.
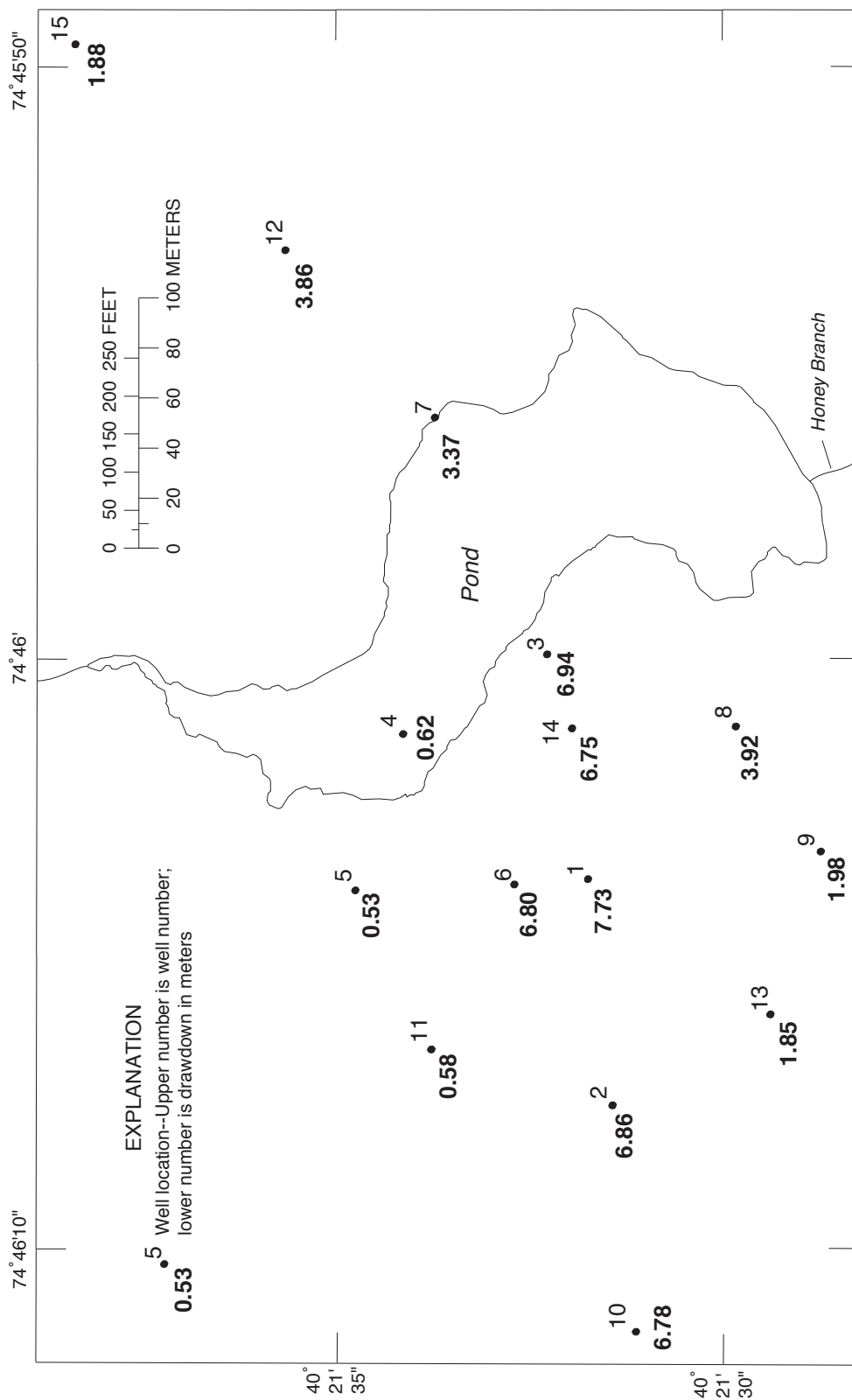
Figure 10. Measured drawdown at the end of a 9-day aquifer test, Hopewell Township, N.J.
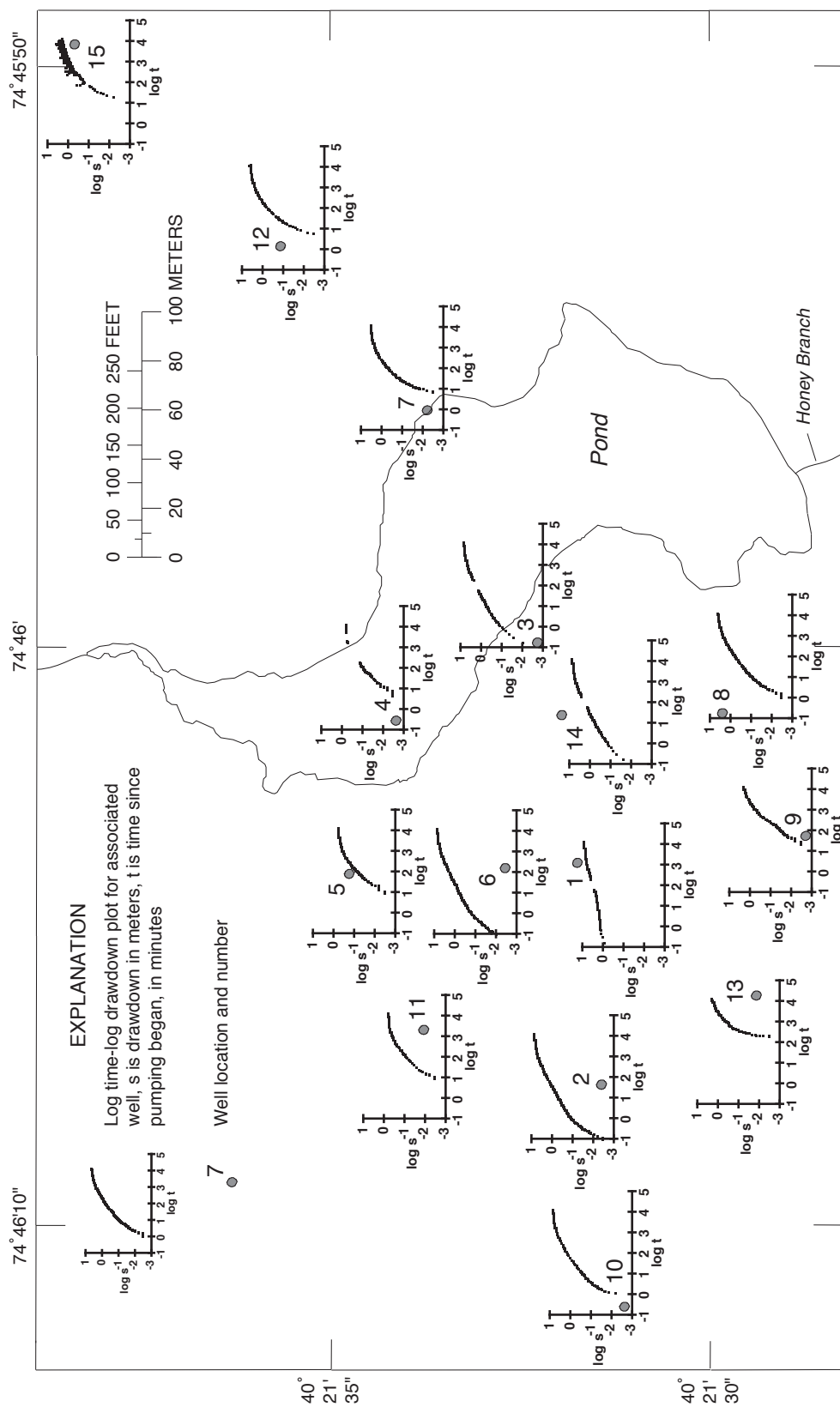
Figure 11. Measured log-drawdown as a function of log-time associated with each well location during a 9-day aquifer test, October 1994, Hopewell Township, N.J.

21

For example, drawdown in well 11 during the first and second tests was detected 9 minutes and about 30 minutes after pumping began, respectively; after 60 minutes of pumping, drawdown in the first and second tests was 0.046 m and 0.024 m, respectively. These results indicate that hydraulic connections through the open boreholes affect the aquifer response but that aquifer characteristics can still be interpreted from the results.

Aquifer-Test Analysis

The aquifer-test data were evaluated using analytical and numerical methods. The analytical method was used to obtain an initial estimate of the aquifer properties, with the assumption that the heterogeneous site could be modeled as an equivalent homogeneous and anisotropic system. The subsequent numerical evaluation enabled the authors to improve the representation of the hydrogeologic framework, incorporate boundary effects specific to the site, and represent spatially variable hydraulic conductivity.

The geologic structure of an aquifer, including sedimentary layering or the presence of uniformly oriented fractures, can give rise to anisotropic hydraulic conductivity—that is, calculated hydraulic conductivity that is direction-dependent. In the most general case, hydraulic conductivity is defined by a nine-component tensor containing six independent quantities that can be used to determine the three principal directions and three principal components of hydraulic conductivity. In the case of the Hopewell site, it was of interest to test the hypothesis that the site could be modeled as an equivalent homogeneous anisotropic system; therefore, an appropriate analytical technique was needed to calculate the desired parameters from the field data available.

Analytical Method

The analytical method of Hsieh and Neuman (1985) was used because it allows determination of unknown principal directions and principal values of hydraulic conductivity for a homogeneous and anisotropic medium. Hsieh and Neuman (1985) present analytical solutions for drawdown as a function of time, space, specific storage, pumping rate, and the nine-component hydraulic conductivity tensor. From their solutions, dimensionless time-drawdown type curves can be constructed, and type-curve matching can be performed. From the match-point information, directional hydraulic diffusivities (directional hydraulic conductivity divided by specific storage $[K_d/S_s]$) can be calculated along the lines connecting the centers of each withdrawal and observation interval, and the values of hydraulic conductivity and specific storage also can be computed.

The analysis using the method of Hsieh and Neuman (1985) yielded a specific storage value of $S_s = 9.2 \times 10^{-5}$ m^{-1} (2.8×10^{-5} ft^{-1}) and principal values of hydraulic conductivity of 6.4, 0.30, and 0.0043 m/d in the x, y, and z directions, respectively. Additional discussion of the analysis is in appendix A. Principal directions of hydraulic conductivity are listed in table A-2. The resulting anisotropy ratios are 1,500:70:1. The greatest hydraulic conductivity value is in the general direction of the strike. The hydraulic conductivity ellipsoid estimated in this analysis dips slightly away from the horizontal plane to the north and plunges longitudinally slightly south of east (table A-2). One interpretation of these results is that the dip angle of the vertical joints (to the south) and that of the bedding planes (to the north) influence the principal directions in addition to the general strike direc-

tion. The largest principal value of hydraulic conductivity is in the general direction of the strike, a result that was expected given the shape of the hydraulic response data. The flat, linear trend of the drawdown data (1/2 slope on log-log paper) exhibited by wells 2, 3, and 14 is likely caused by the preferential flow of water in the strike direction. The fact that the dip of the ellipsoid is not greater and more comparable to that of the bedding planes may be due to the lack of adequate well spacing in the vertical.

The high value of anisotropy indicated by this analysis indicates that hydraulic conductivity within bedding planes is significantly greater than across bedding planes. However, the lack of data in the vertical may also contribute to this effect. A major consideration for using the method of Hsieh and Neuman (1985) to interpret the subject aquifer test is whether sufficient vertical variability in the location of the center points of wells is available. As indicated in table A-1, the vertical distance between the centers of boreholes of observation wells ranges from 0.2 to 7.2 m from the pumped well. An additional step that could be employed to yield further information on the nature of the vertical hydraulic conductivity would be to conduct a second aquifer test, withdrawing water from a well having the highest or lowest borehole center elevation (such as well 6). The additional data set would provide an additional set of directional diffusivities and add robustness to the results from this method.

Additional difficulties arising from application of this analytical method to open boreholes at this site include the potential for erroneous results due to possible hydraulic connections (short-circuiting) among wells, as well as the possible contribution of the wells to unnaturally high permeability in the vicinity of the open boreholes. However, the ultimate benefit of the type of calculation described in this section can be to provide approximate values of the specific storage and orientation and magnitude of the principal components of hydraulic conductivity.

Numerical Method

The numerical analysis of the aquifer test was done with the ground-water flow model MODFLOW (McDonald and Harbaugh, 1988). The analysis started with the conceptual model of the hydrogeologic framework developed from the hydrogeologic and simple hydraulic analyses. The concept was tested and revised during a trial-and-error calibration analysis until the simulated drawdown curves matched the measured data reasonably well. The conceptual model of the system includes producing zones along bedding planes that act as thin, areally extensive aquifers. The aquifers are separated by nonproducing, massive zones. Although high-angle structural fractures are locally transmissive, they do not conduct water across the massive zones in significant quantities. Therefore, the vertical hydraulic conductivities of massive zones are assumed to be orders of magnitude lower than those of the aquifer layers and to function as confining units. The aquifers extend thousands of meters in the strike direction but only a few hundred meters in the dip direction, from their outcrop down to an extinction depth of about 150 m. The transmissivity of the aquifers is considered to be insignificant below the extinction depth. Diabase dikes and faults can be lateral boundaries, and streams and ponds are upper boundaries.

The model rows and columns are aligned with the strike and dip of the bedding planes (N. 96° 80 E., 27° N.); the model has nine layers that are estimated to slope at the dip angle. Each layer includes one or more producing zones but also includes nonproducing zones. The confining

properties of the nonproducing zones are represented by the vertical conductivity between model layers. Layers 1 and 9 are above and below, respectively, the zones intersected by the observation wells (fig. 12); they serve to extend the model boundaries beyond the area in which drawdown occurred during the aquifer test. Layers 2 and 3 include bedding planes intersected by the northern (downdip) wells; layers 3, 4, and 5 include bedding planes intersected by the strike wells (including the three wells on the east side of the pond); and layers 7 and 8 include bedding planes intersected by the southern (updip) wells.

The model grid is variably spaced, centered on the pumped well (fig. 13). The grid spacing is 0.30 m at the pumped well and expands out by a multiplication factor of about 1.3 to the most distant observation wells (wells 10 and 15, to the west and east, respectively), past which the multiplication factor is 1.5. The multiplication factor was adjusted in the region containing observation wells so that each well was at the center of a cell.

Two characteristics of the system were simplified considerably in the model. First, the synform was represented by, in effect, "straightening" the synform such that the pond and wells 3, 7, 12, and 15 were located in the model relative to their position from the line of strike passing through well 1 (fig. 13). This adjustment is not believed to introduce error in the immediate area of the pumped well (well 1), but it does affect model results near distant wells (12 and 15). Second, because the aquifer layers dip at an angle of $27°$, the model was constructed so as to align with these layers; therefore, the actual distance between cells in the dip direction was 1.12 times the distance in map view. Using the multiplier of 1.12 in this way correctly located wells (which are all vertical and therefore not perpendicular to the bedding planes) that intersect more than one model layer.

The southern boundary of each layer is a no-flow boundary representing the outcrop of the dipping layer. The northern boundary is also a no-flow boundary, representing the extinction depth of significant, interconnected water-bearing fractures. The extinction depth is assumed to be 150 m because extending well depths beyond 150 m usually does not increase well productivity (Greenman, 1955, p. 25; Lewis-Brown and Jacobsen, 1995, p. 13). The horizontal width of each layer from outcrop to extinction is between 300 and 350 m, depending on its thickness. The eastern boundary is a no-flow boundary representing a diabase intrusion located about 1,800 m from the pumped well. The western boundary is a constant-head boundary located 18,550 m from the pumped well. This boundary does not represent an actual hydrologic feature; rather, it is designed to be far enough from the pumped well that the boundary can represent the aquifer beyond this distance within the resolution needed. The pond is simulated as a head-dependent boundary that intersects the outcrop areas of layers 1 through 7. Stony Brook, flowing from north to south and located 1,400 m west of the pumped well, is simulated as a river (head-dependent boundary) sequentially intersecting the outcrops of each model layer.

The aquifers are assumed to be confined—transmissivities are constant, regardless of drawdown—but a higher storage value is assigned to the outcrop area of each layer to represent specific yield. In addition, well-bore storage in 15 wells in a relatively small area can potentially add to the storage capacity of the formation; therefore, well-bore storage was accounted for by increasing the storage of model cells containing a well by the ratio of the area of the well divided by the area of the cell. The simulated aquifer properties are nearly uniform in all layers. The vertical conductance between layers is related to the vertical hydraulic conductivity and the distance between the midpoint
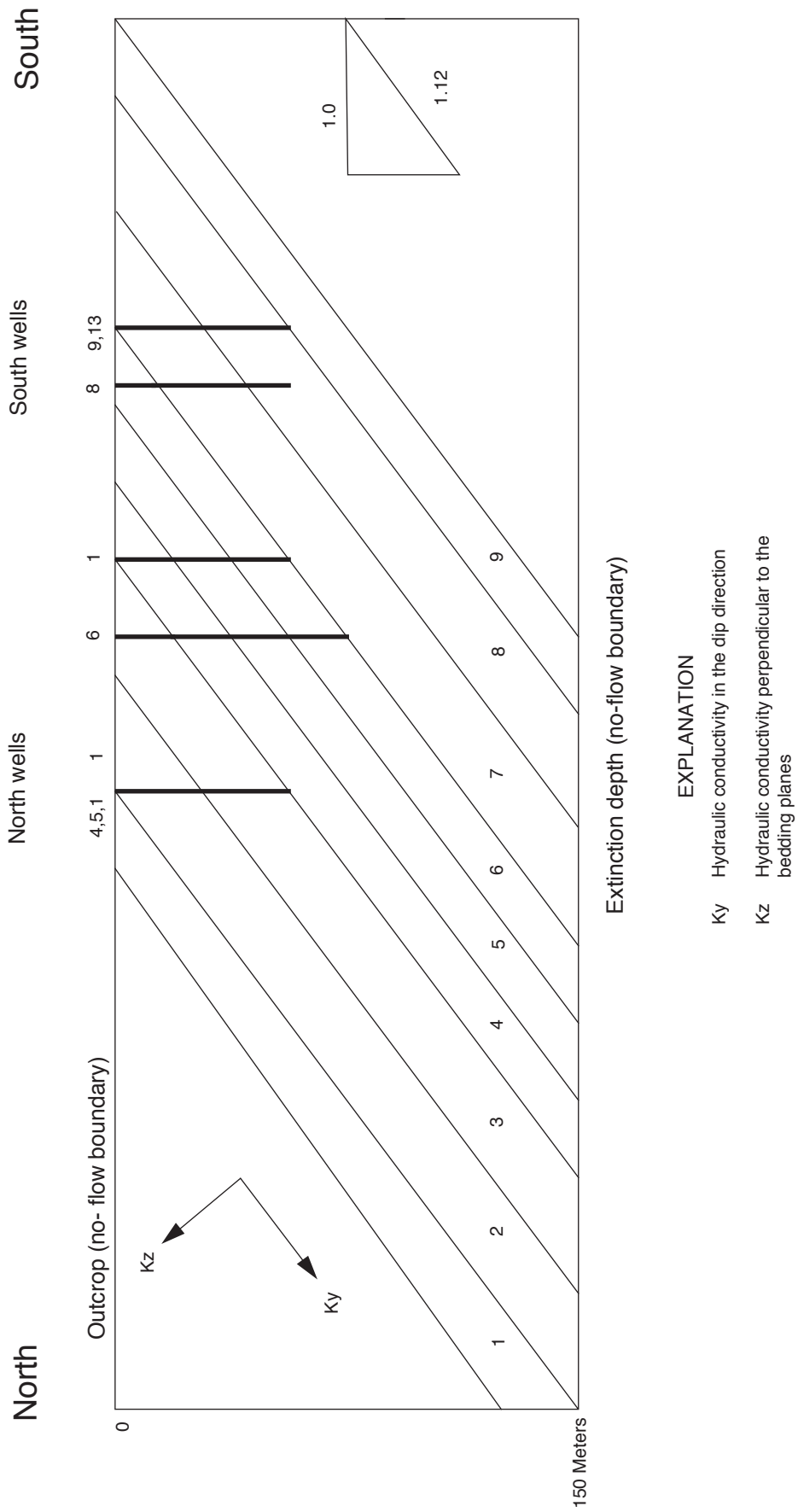
Figure 12. Schematic section of the three-dimensional finite-difference (MODFLOW) model of the study area, Hopewell Township, N.J.
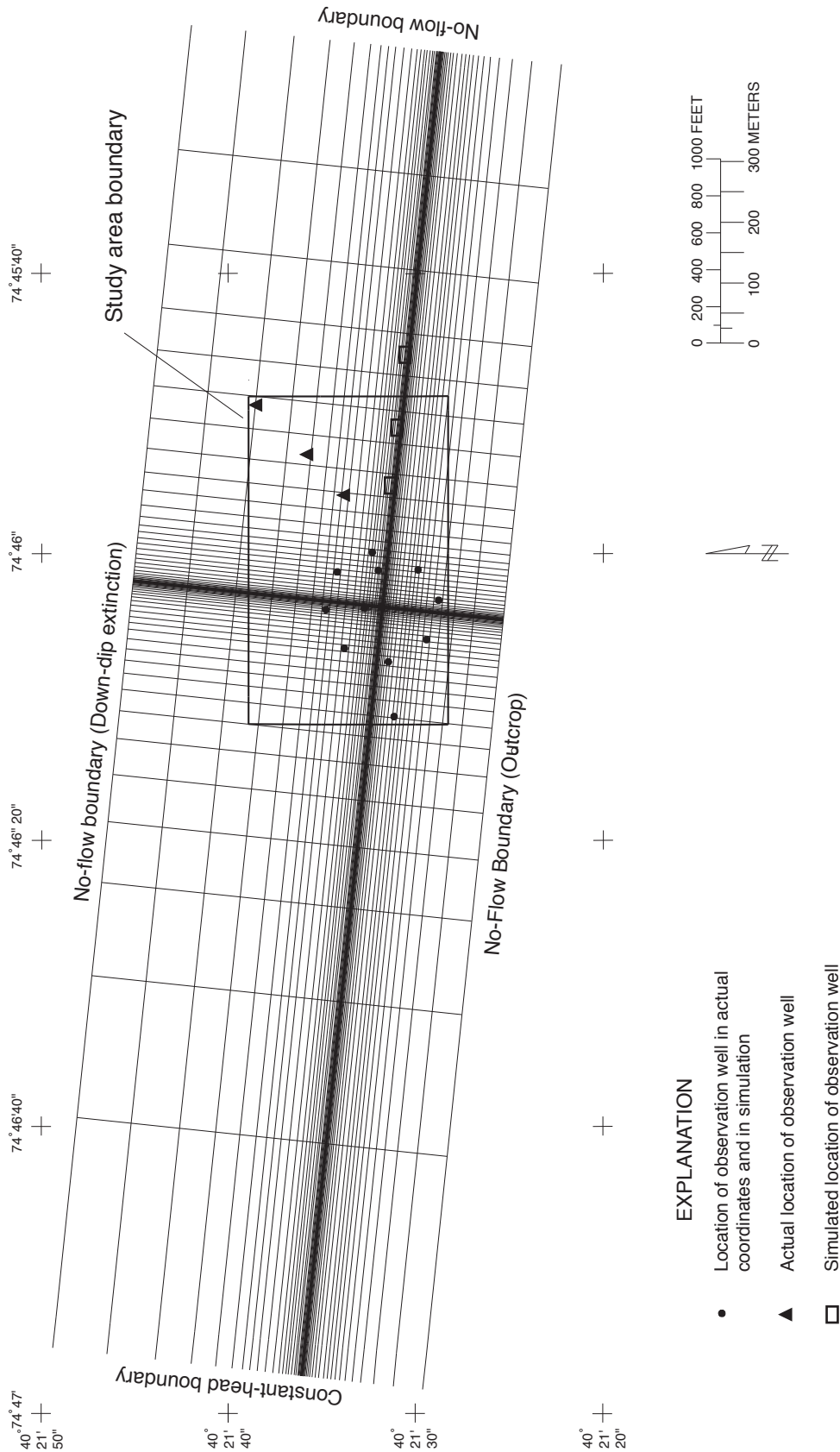
Figure 13. Finite-difference grid and horizontal boundaries of the three-dimensional finite-difference (MODFLOW) model of the study area, Hopewell Township, N.J. (Simulated head values at the easternmost three wells were taken from the model cells in which the wells would be located if the strata were not folded.)

of each layer. The same vertical hydraulic conductivity is used for all of the layers. Transmissivities are the product of horizontal hydraulic conductivity and the thickness of the layer. The same horizontal hydraulic conductivity is used for each layer, except layers 4 and 5.

Heat-pulse flowmeter logging in well 1 (the pumped well) indicates the transmissivities of producing zones simulated in layers 4 and 5 are 1.7 and 1.5 times those of layer 6, respectively; thus the transmissivities of these two layers are increased in the model. These local heterogeneities are included because they were identified in the pumped well; variations in transmissivity identified in other wells are not included. Results of the HPFM logging also indicate that the transmissivity of producing zones is greater in the top one-third (13 m) of the well. It is further assumed that transmissivity is not significant below 150 m; therefore, it is logical to conclude that transmissivity decreases with depth by a smooth function. Therefore, horizontal hydraulic conductivity is decreased with depth by an exponential factor: $K_{(d)} = K_{(0)} e^{(-a\,d)}$, where $K_{(0)}$ is the maximum hydraulic conductivity in the strike direction, $e = 2.718$, a is a small positive number estimated during calibration, and d is the depth below the water table. The same set of assumptions was applied to all layers, except for a few minor heterogeneities described in the results section farther on.

Objective matching of simulated and measured time-drawdown data included consideration of the time of first arrival of drawdown, the curve shapes, and the maximum drawdown. Time-drawdown curves for all 15 wells were matched concurrently. Although ideally all 15 curves would be matched with similar accuracy, in the final analysis, a match in one well could be improved only at the expense of the match for another well. Therefore, the criteria that were used were (in decreasing order of importance) curve shape, final drawdown, and initial drawdown detection for the strike wells, southern wells, northern wells, and wells east of the pond. Parameters that were adjusted in calibration include (in approximately decreasing order of effect on model results) horizontal hydraulic conductivity, specific yield of shallow cells, specific storage of confined cells, bed-sediment conductivity of the pond, vertical conductance between layers, decreasing horizontal conductivity with depth, horizontal anisotropy, hydraulic conductivity of borehole connections between layers, and bed-sediment conductivity of Stony Brook.

The best-fit parameters for the model, determined from a trial-and-error calibration, are the following. The maximum hydraulic conductivity in the strike direction (K_x) is 10 m/d. The hydraulic conductivity in the dip direction (K_y) is 5 m/d. Average hydraulic conductivities are about 7 and 3 m/d in the strike and dip directions, respectively. Hydraulic conductivity decreases with depth by the function $K_{(d)} = K_{(0)} e^{(-a\,d)}$, where $a = 0.02$ and d is depth. Hydraulic conductivity perpendicular to bedding planes (K_z) is 4×10^{-5} m/d. Specific yield is 1×10^{-4}, and specific storage is 1×10^{-7} m^{-1}. Finally, the hydraulic conductivity of pond bed sediment (and Stony Brook bed sediment) is 2.0×10^{-3} m/d.

Simulated and measured time-drawdown plots from the best-fit simulation of the aquifer test are shown in figure 14. The simulated curves for the pumped well and strike wells 2, 6, and 10 are shown in figure 14; data curves for strike wells 3 and 14 have similar shapes but are not shown. Early-time discrepancies for this group of wells are considered to be small, given that the first arrival of drawdown is on the order of seconds; late-time matches are close. The late-time matches are also close for the southern (updip) wells (wells 8 and 9 shown in fig. 14; well 13 not shown), and the entire match for well 9 is very close. The early- to mid-time matches for wells 8 and 13 are not as close.
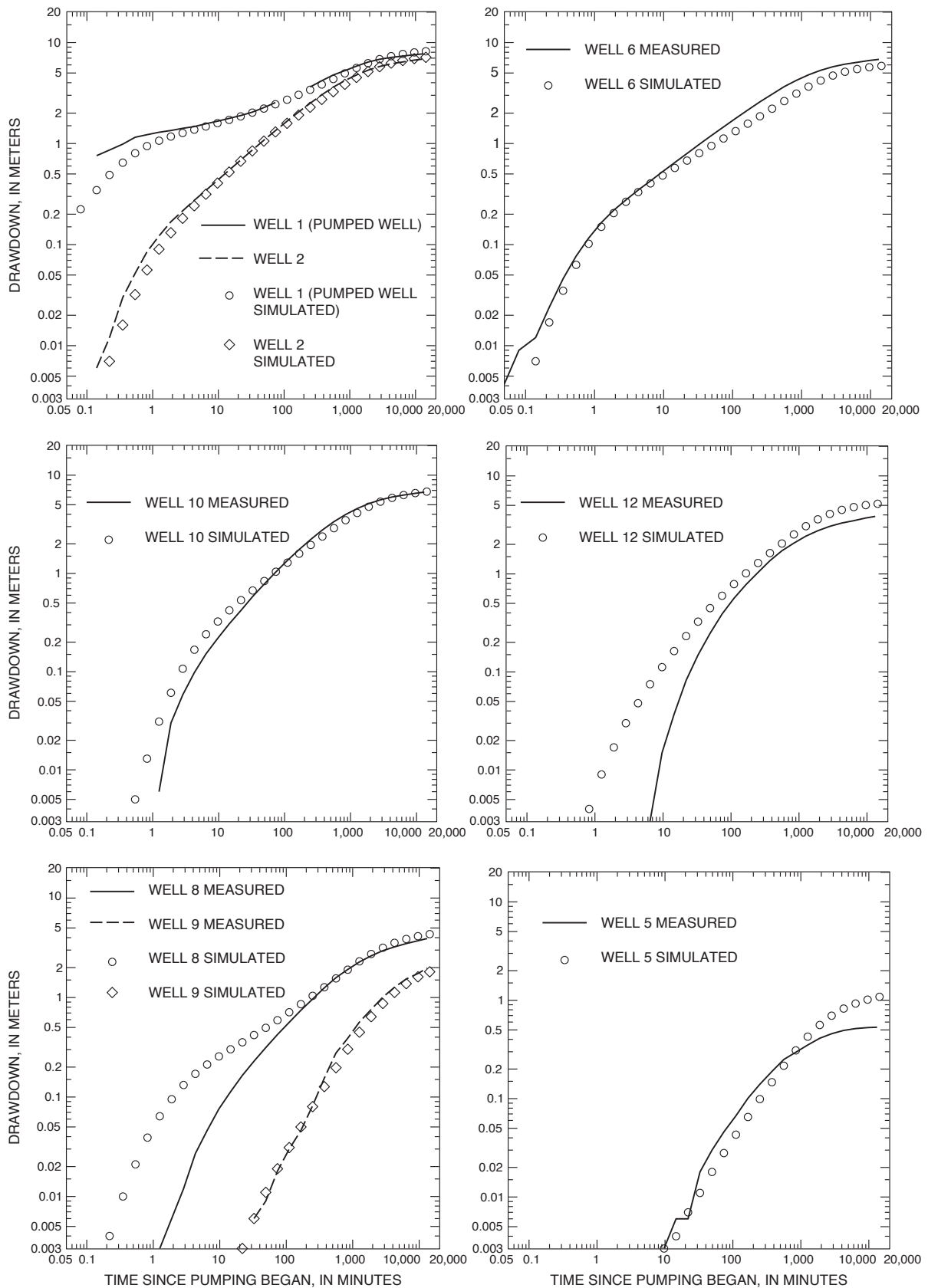
Figure 14. Measured and simulated drawdowns in wells 1, 2, 5, 6, 8, 9, 10, and 12 during a 9-day aquifer test, October 1994, Hopewell Township, N.J.

Well 8 is hydraulically well connected to the pumped well because the top of the well is stratigraphically higher than that of wells 9 and 13; therefore, the initial drawdown onset is earlier and the magnitude is greater than at wells 9 and 13. Although simulation of the hydraulic connection between layers in well 8 yields close matches in later time, the model predicts a much earlier initial drawdown, indicating that the heterogeneity is not accurately simulated. Similarly, well 13 is a low-yielding well that is poorly connected to the producing zones that well 9 is connected to. Therefore, although the modeled initial drawdown at well 13 occurs too early, this mismatch is considered acceptable because the late-time matches are close.

The matches between simulated and measured data for the northern (downdip) wells (well 5 shown in fig. 14; wells 4 and 11 not shown) are acceptable but are not as close as those for the southern wells. Drawdown was first detected in these wells considerably earlier than in wells 9 and 13 (occurring at about 10 minutes compared to at about 25 and 150 minutes, respectively), yet the drawdown virtually stabilizes about 1,000 to 3,000 minutes into the test. The presence of the short circuit between layers in the open borehole of well 6 and the hydraulic connection to the pond were explicitly simulated and contributed to earlier drawdown onset and less total drawdown in the northern wells, respectively, but the match was never as close as for the southern wells or the strike wells. The matches for wells on the eastern side of the pond (well 12 shown in fig. 14; wells 7 and 15 not shown) are also considered acceptable but are not as close as those for wells near the pumped well; the simulated drawdown is too large in all three cases, and the initial drawdown occurs too early. Mid- and late-time matches, however, are fairly close.

Steady-state hydraulic conditions developed during a tracer test between well 10 and well 1 (described later in this report) also were simulated. The simulation included withdrawal of 118 L/min from well 1 and reinjection into well 10; the water was originally withdrawn from well 5 (hydraulically distant from wells 1 and 10). For this simulation, the model grid was refined around the pumped well and the injection well. The simulated drawdowns (fig. 15) are within 0.3 m of measured drawdowns for most of the observation wells and within 30 percent for the pumped well. Drawdown was not well matched in well 8, presumably because of effects of the short circuit between layers in the well. Drawdowns also were not well matched in wells 7 and 12, a result that is attributed to an incomplete understanding of the connection of these wells to the different layers because of their location on the fringe of the study area.

The simulated head buildup and drawdown in wells 10 and 1 were 30 and 15 percent too low, respectively; the simulated drawdown in well 5 was within 1 percent of measured drawdown. The simulation of head buildup in well 10 (from injection into that well) was improved when low-conductivity zones immediately surrounding wells 10 and 2 were included in the model. The hydraulic conductivities around wells 10 and 2 are one-fifth and two-thirds, respectively, of the hydraulic conductivity elsewhere. The zone around well 10 is about 160 m in the strike direction and 80 m in the dip direction. The zone around well 2 is about 100 m in the strike direction and 80 m in the dip direction. These heterogeneities, based on HPFM results, would not be necessary if the models did not include multiple injection and withdrawals wells that highlighted the natural heterogeneities of the system. Their presence did not significantly affect the aquifer-test model. The successful simulation of the different hydraulic conditions of the aquifer test and tracer test increases the confidence in the numerical model results.
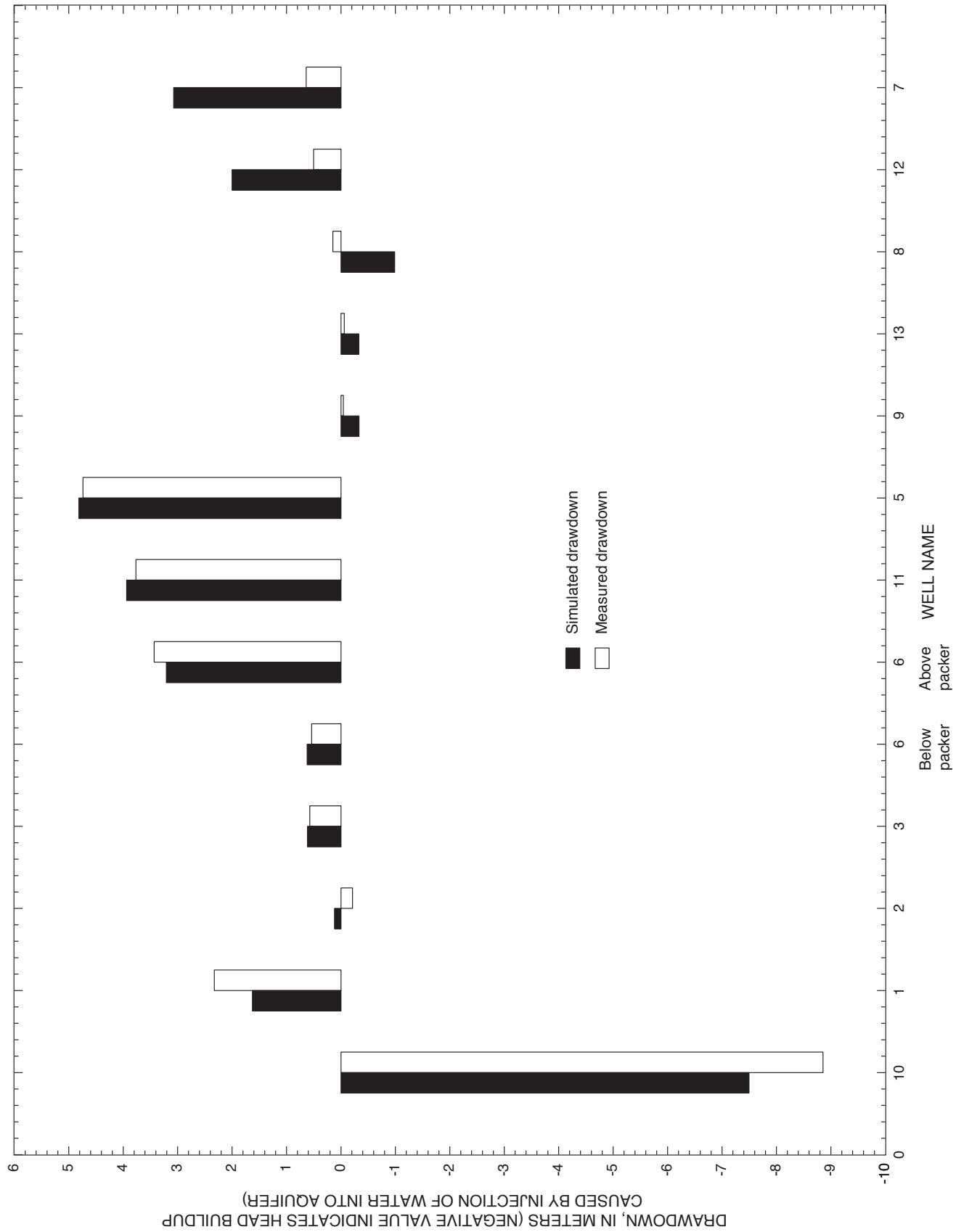
Figure 15. Simulated and measured head drawdowns or build-ups in wells 1-3 and 5-13 during a doublet tracer test, with withdrawal from well 1, April 1995, Hopewell Township, N.J.

30

The results obtained using the numerical models indicate that the fractured sedimentary rocks of the Newark Basin can be modeled as an equivalent porous medium at a scale of several hundred meters if the model is sufficiently detailed. Furthermore, consistency between the analytical and numerical analyses indicates that the conceptual model of the site is accurate as applied.

The results of the analytical and numerical analyses have some similarities, although a direct comparison must allow for the different assumptions inherent in the two analyses (table 2). Specific storage (S_s) from the analytical model is 9.2×10^{-5} m^{-1}, higher than the numerical model result of $S_s = 1.0 \times 10^{-7}$ m^{-1} but close considering that the numerical model includes specific yield of $S_y = 1.0 \times 10^{-4}$ in shallow cells. Values of K_x are similar for the two analyses, but the horizontal anisotropy is higher in the analytical model than in the numerical model. Conversely, the vertical anisotropy is higher in the numerical model.

Table 2. Hydraulic conductivity and storage values from analytical and numerical analyses of a 9-day aquifer test and borehole flowmeter logging, Hopewell Township, New Jersey

[K_x, hydraulic conductivity in the strike direction; K_y, hydraulic conductivity in the dip direction; K_z, hydraulic conductivity in the direction perpendicular to the bedding planes; m/d, meters per day; --, not applicable]

Type of analysis	K_x (m/d)	K_y (m/d)	K_z (m/d)	K_{avg} (m/d)	Specific storage
Borehole flow meter	--	--	--	0.36	--
Analytical (Hsieh and Neuman, 1985)	6.4	0.30	0.0043	--	9×10^{-5} m^{-1}
Numerical (MODFLOW)	7 (avg.) 10(max.)	3 (avg.) 5 (max.)	4×10^{-5}	--	1×10^{-5} m^{-1} (shallow) 1×10^{-7} m^{-1} (deep)

The borehole geophysical data yield hydraulic-conductivity estimates that are about one order of magnitude lower than the average of the numerical model estimates, most likely because of the smaller scale at which the values were obtained. The borehole data are useful for identifying producing and nonproducing zones and establishing comparative values for hydraulic conductivity. The cumulative total of flow below the detection limit of the instrument and the simplifying assumptions necessary to solve for hydraulic conductivity using the borehole flowmeter technique, however, reduce the accuracy of the results compared to a larger scale, multiwell aquifer test.

The ability to test heterogeneities and aspects of the system such as the pond, borehole connections, well-bore storage, and variations in hydraulic conductivity make the numerical model the more flexible tool. The analytical method was useful to test selected hydrologic concepts and to obtain preliminary estimates of parameter values.

TRACER-TEST DESIGN AND ANALYSIS

Tracer tests are conducted to determine the transport properties—effective porosity and dispersivity—of an aquifer. Ground-water velocity is inversely proportional to effective porosity. For fractured-rock aquifers, where porosities can vary greatly and be very small (10^{-3}, compared to 10^{-1} for unconsolidated deposits), dissolved contaminants can move significantly more quickly than in unconsolidated deposits with a similar hydraulic conductivity. Determination of effective porosity is therefore essential in characterizations of fractured-rock aquifers. Whereas the effective porosity directly influences the mean displacement of a solute body, the spreading of a solute ahead of and behind the mean displacement is affected by the dispersivity. Dispersivity is a length scale related to the degree of heterogeneity of an aquifer that characterizes the potential for aquifer materials to cause mixing of a contaminant mass within the native ground water. In highly heterogeneous aquifer materials such as fractured rock, the dispersivity can be on the order of meters to tens of meters (Webster and others, 1970; Gelhar and others, 1992), which can cause the first arrival of a contaminant to be significantly in advance of the mean displacement. For this reason, determination of dispersivity is also of principal importance in predicting solute transport.

A tracer test consists of introducing a tracer into ground water and monitoring the tracer's movement and spreading. Natural-gradient tracer tests involve monitoring a tracer as it moves through the aquifer with ambient ground-water flow (for example, LeBlanc and others, 1991). Induced-gradient tests, such as those conducted for this study, typically involve creating a flow field with injection and (or) withdrawal, injecting a slug (pulse) of tracer in one well, and monitoring the arrival of the tracer at a second well. Dispersivity and effective porosity are determined from the shape and position of the time-concentration (breakthrough) curve.

Three-dimensional transport of a nonreactive solute in saturated porous media can be described by the following differential equation (Bear, 1972):

$$\frac{\partial c}{\partial t} + v_i \frac{\partial c}{\partial x_i} = \frac{\partial}{\partial x_i}\left(D_{ij} \frac{\partial c}{\partial x_j} \right) \ , \tag{1}$$

where c is solute concentration [mass/mass],
     v_i is mean pore (solute) velocity in the x_i direction (i = 1, 2, 3) and equals q_i/n [L/t],
     q_i is Darcy velocity in the x_i direction [L/t],
     n is effective porosity, and
   D_{ij} is tensor of hydrodynamic dispersion, (i, j = 1,2,3) [L^2/t].

For isotropic aquifers, the elements of the tensor of hydrodynamic dispersion can be defined as follows (Konikow and others, 1996):

$$D_{11} = \alpha_L \frac{v_1^2}{|v|} + \alpha_{T_H} \frac{v_2^2}{|v|} + \alpha_{T_v} \frac{v_3^2}{|v|} + D_m,$$

$$D_{22} = \alpha_L \frac{v_2^2}{|v|} + \alpha_{T_H} \frac{v_1^2}{|v|} + \alpha_{T_v} \frac{v_3^2}{|v|} + D_m,$$

$$D_{33} = \alpha_L \frac{v_3^2}{|v|} + \alpha_{T_H} \frac{v_2^2}{|v|} + \alpha_{T_v} \frac{v_1^2}{|v|} + D_m,$$

$$D_{12} = D_{21} = (\alpha_L - \alpha_{T_H}) \frac{v_1 v_2}{|v|} + D_m,$$

$$D_{13} = D_{31} = (\alpha_L - \alpha_{T_v}) \frac{v_1 v_3}{|v|} + D_m, \text{ and}$$

$$D_{23} = D_{32} = (\alpha_L - \alpha_{T_v}) \frac{v_2 v_3}{|v|} + D_m,$$

where $|v| = \sqrt{v_1^2 + v_2^2 + v_3^2}$ $[L/t]$,

α_L is longitudinal dispersivity $[L]$,

α_{T_H} is transverse horizontal dispersivity $[L]$,

α_{T_v} is transverse vertical dispersivity $[L]$, and

D_m is coefficient of molecular diffusion in a porous medium $[L^2/t]$.

A prediction of contaminant movement depends on estimates of effective porosity and dispersivity, in addition to characterization of the flow field as defined by the boundary conditions and the distribution of hydraulic conductivity.

In isotropic media, the principal directions of the dispersion tensor are aligned with direction of flow, whereas such an alignment is not necessarily the case for anisotropic media (Gelhar and Axness, 1983; Voss, 1984). Analytical models available for modeling solute transport do not incorporate effects of anisotropy on the directional dependence of dispersivity. The solute transport code SUTRA (Voss, 1984) employs an ad hoc model of anisotropic dispersivity by assuming that principal directions of the dispersivity tensor are aligned with the principal directions of the hydraulic conductivity tensor, although the two tensors may not necessarily be aligned (Gelhar and Axness, 1983).

The tracer tests described herein were designed to estimate dispersivity within representative transmissive bedding-plane layers of the fractured-rock medium. Although water flows at higher rates and in the general strike direction within these bedding-plane transmissive layers, solute transport within the medium occurs through bedding-plane layers and the massive intervening layers. Therefore, the results provide parameter-value estimates for solutes transported within transmissive, bedding-plane layers, but these estimates are not representative of flow through both transmissive and massive layers. Tests to estimate solute transport properties of the massive layers were beyond the scope of this study but could include conducting a tracer test across a massive layer between transmissive bedding-plane layers or conducting a tracer test perpendicular to strike and across both transmissive and massive layers.

Design

Many important issues must be considered in designing a tracer test, including representative volume of the aquifer to be tested, aquifer orientation, test scale (length of flow field), flow-field geometry, mechanics of tracer injection, tracer-test duration, and selection of a suitable tracer. In the following sections, these issues are discussed for the tracer tests conducted during this study.

Hydraulic Flow Regime

Conducting a tracer test under ambient flow (natural gradient) conditions enables an investigator to obtain the most information about the dispersive properties of an aquifer, because the three principal values of dispersivity can be calculated if appropriate data are collected. This procedure is not practical as a routine tool for determining dispersivity of an aquifer, however, because it requires a large monitoring network and substantial time to allow ambient ground-water flow to disperse the plume sufficiently so that an appropriate test scale is achieved. As a practical alternative, induced-gradient flow regimes can be used in which the duration of the test is reduced by orders of magnitude—that is, from years to days—and, in most cases, the tests can be done with two wells. The drawbacks are that (1) only the longitudinal dispersivity can be determined with the techniques currently available, (2) longitudinal dispersivity is calculated in the direction of the forced flow, which may underestimate or overestimate the principal longitudinal dispersivity in the natural flow system in anisotropic porous media, and (3) tests conducted over days or weeks may not demonstrate other physical processes that affect chemical migration over years or tens of years, such as diffusion into the rock matrix (matrix diffusion). Because few tracer tests have been conducted in fractured sedimentary rock, it is not currently (1998) known how results from natural-gradient tests would compare to those from forced-gradient tests. Testing under ambient conditions could help determine the difference, and is strongly recommended by the National Research Council (1996), but was beyond the scope of this project.

The options for creating a hydraulic flow regime include convergent radial flow, divergent radial flow, and doublet (a test using injection and withdrawal wells). The setups, advantages, and disadvantages of each of these types of tests are discussed in Welty and Gelhar (1989, 1994). Doublet tests (also called dipole or dual-well tests) with a pulse input of tracer and without recirculation of withdrawn water were chosen for this study because of (1) the superior control of the flow field and initial conditions of tracer input, (2) the sensitivity of the test to longitudinal dispersivity, and (3) the

reduced time required to run the test at a given distance compared to the other two options. The principal drawbacks to utilizing this flow regime are (1) the intricate design of field plumbing that is required, (2) the need for a source of injection water when recirculation is not employed, and (3) the need for a place to dispose of the wastewater from the test. Despite these practical drawbacks, the principal advantages of the doublet test make it more strongly recommended than the radial flow tests. Examples in the literature in which doublet tests have been successfully applied include cases described in Webster and others (1970) and Leonhart and others (1985).

In a doublet tracer test, a steady flow field is first established by injecting water into one well and pumping water from another well until the flow circulation pattern between the wells stabilizes. Equal flow rates at the injection and pumped wells are not necessary, but this choice simplifies the calculations. After a steady flow field is established, a pulse of tracer is inserted into the injection line and samples from the effluent line are analyzed for the tracer.

If the aquifer behaves as an equivalent isotropic confined system, the data can be evaluated by application of available analytical techniques. An approximate solution for a pulse input in a doublet tracer test is presented by Gelhar (1982) and Welty and Gelhar (1994). Figure 16 is a simple set of
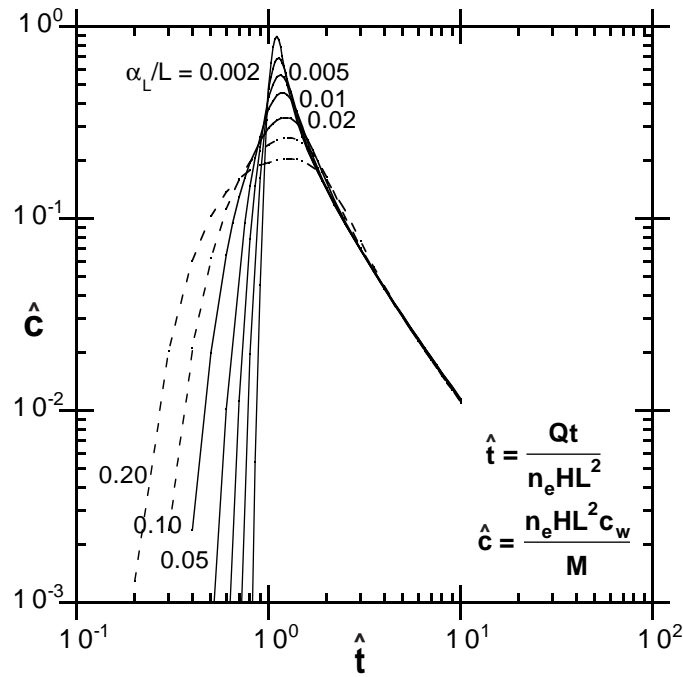

Figure 16. Type curves for a doublet tracer test with a pulse input and equal flow at the pumped and injection wells. (Modified from Gelhar, 1982; $\hat{t}$ is dimensionless time and $\hat{c}$ is dimensionless concentration)

35

type curves depicting the analytical solution (equation 45 in Welty and Gelhar, 1994) under assumptions of isotropy, confined aquifer flow, and fully screened pumped and injection wells. The method of analysis involves plotting the field data (solute concentration as a function of time) obtained at the pumped well and matching the field data with the type curves to obtain dispersivity and effective porosity values.

Heterogeneity and Scale Effects

Until recently, users of equation 1 often assumed that dispersivity was constant over the scale of a given problem, so that dispersivity was treated as little more than a fitting parameter, such that the equation adequately matched any field data on solute distribution. Evidence in recent years indicates that this empirical approach is an oversimplification of what is observed and that the values of the dispersivity tensor depend on, among other things, the scale of displacement of the solute body.

Field data and theoretical considerations have both shown that the longitudinal dispersivity of an aquifer increases as a function of distance or scale. Figure 17a (from Gelhar and others, 1992) consists of data taken from 59 sites around the world where values of dispersivity have been calculated, for both fractured-rock and porous-media environments. This figure shows a general trend of increasing longitudinal dispersivity with distance. What is not clear is whether the dispersivity increases linearly with scale indefinitely or levels off to an asymptotic value for a given aquifer. When Gelhar and others (1992) critically evaluated the reliability of the data of figure 17a, the result as depicted in figure 17b was that the values judged to be of high reliability were few, as indicated by the large circles. The high-reliability data of figure 17b show that longitudinal dispersivities no greater than 11 m have been reported for solute displacement distances up to about 250 m. Figure 17b also shows that an accurate description of the behavior of dispersivity as a function of distance data does not exist for distances greater than 250 m.

In the field, longitudinal dispersivity has been observed to be on the order of meters and about an order of magnitude larger than transverse horizontal dispersivity, and two orders of magnitude larger than transverse vertical dispersivity (for example, LeBlanc and others, 1991). This observation has two important implications: (1) solute plumes are three-dimensional and are longer than they are wide or thick, (2) the longitudinal dispersivity value is the most important in determining the dispersive properties of contamination because its value plays the largest role in spreading a solute mass about its mean advective position in the aquifer. For porous media, field data (for example, LeBlanc and others, 1991) and theoretical results (for example, Gelhar and Axness, 1983) have shown that longitudinal dispersivity is proportional to the heterogeneity of an aquifer. This relation implies that, at a given scale, a more heterogeneous aquifer will be characterized by a larger dispersivity value, and it could partly account for the range of dispersivity values at a given scale evident in figures 17a and 17b. Theoretical results also predict that longitudinal dispersivity increases as a function of scale (mean displacement distance of the solute body) and levels off to a constant asymptotic value at a distance of about 10 times the value of the asymptotic dispersivity for aquifers that can be described by one scale of heterogeneity (Gelhar, 1993). For aquifers that can be described as exhibiting a wide range of scales of heterogeneity, recent research results indicate that the values of the dispersivity components are also dependent on the size of the solute body injected (Rajaram and Gelhar, 1995). Because this latter result is too recent to have yet been evaluated for a variety of aquifer settings, the effect of the plume scale in aquifers with a wide range of scales of heterogeneity will not be considered in this report.
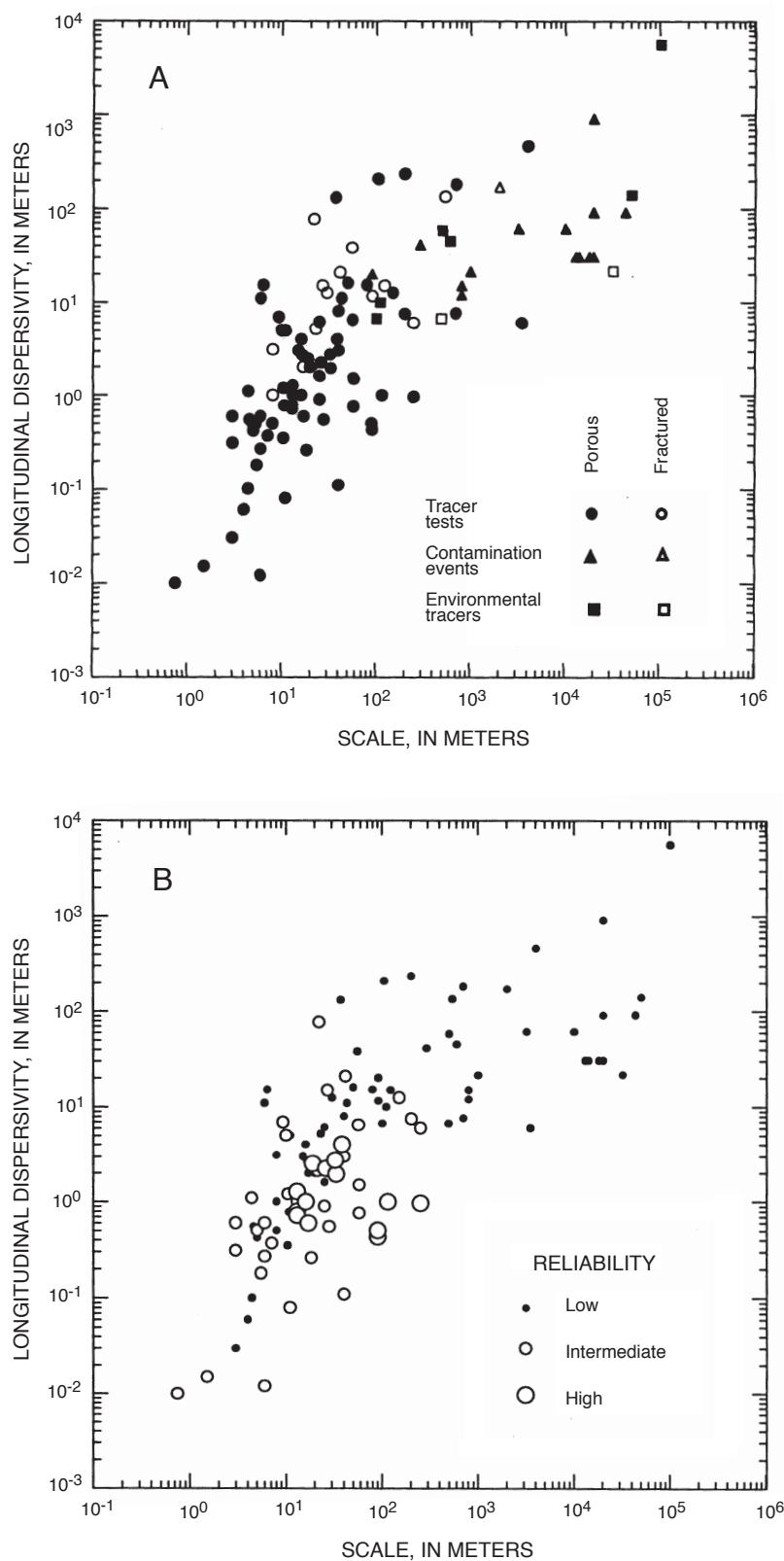
Figure 17. (A) Longitudinal dispersivity as a function of scale of observation identified by type of observation and aquifer (Data from 59 field sites characterized by widely differing geologic materials), and (B) longitudinal dispersivity as a function of scale with data classified by reliability. (Both graphs modified from Gelhar and others, 1992.)

37

Field evidence has borne out some of the above theoretical findings for some porous media (for example LeBlanc and others, 1991; Boggs and others, 1992), but quantitative evidence of similar behavior in sedimentary rock is not currently (1998) available. It would be expected that the degree of heterogeneity is greater in fractured rock aquifers than in many porous media settings and, therefore, that the longitudinal dispersivity may be larger for fractured rock at a given scale. Evidence for this expected behavior can be seen in figure 17a, where most of the symbols for dispersivity in fractured rock are in the upper part of the chart. Although the dispersive behavior of fractured sedimentary rocks has not been well investigated, the tests conducted for this project are a first step in trying to understand whether this type of aquifer behaves similarly to observed porous media settings as just described.

The effects of heterogeneity and scale must be considered in the design of a tracer test. First, a tracer test needs to be conducted at a scale that is estimated to be large enough so that the dispersivity has reached a representative (for example, asymptotic) value for the prediction scale of interest. This is a difficult criterion to implement when a representative dispersivity value for a given scale is not known beforehand. The probability of error in determining the asymptotic value of dispersivity is much greater if a tracer test is conducted at a scale much smaller than the overall scale of interest (an approach that is tempting, owing to the shorter time required to collect data). An investigator restricted to drilling only two wells for tracer injection and observation for an investigation on the order of 100 m will have a higher likelihood of completing a successful tracer test with wells on the order of 100 m apart than with wells on the order of 10 m apart. Although tracer breakthrough would occur more quickly at the smaller well spacing, the data could be useless if the distance between wells is not sufficient to allow the dispersivity to reach a representative value.

The second consideration in designing a tracer test, on the basis of previous findings, is that the more heterogeneous the aquifer appears to be, the greater the large-scale values of dispersivity that can be expected, and therefore, the greater the distance that will be required to reach the asymptotic dispersivity value. In the case of the Hopewell Township site used for this study, the geophysical logs and the hydraulic tests indicated the sedimentary fractured-rock formation is highly heterogeneous, an indication that dispersivity at a given scale would be at the higher end of the range given in figure 17b.

At the study site, the choice of distance between injection and observation wells was limited because the wells were already in place. The authors explicitly wished to demonstrate the scale effect and, therefore, chose to run tracer tests at three scales: 30.5 m (well 6 to well 1), 91.4 m (well 2 to well 1), and 183 m (well 10 to well 1). If only one tracer test had been possible, the largest of these distances would have been chosen.

Choice of Tracer

The tracer injected into the aquifer must be nontoxic, conservative (will not biodegrade, sorb to aquifer material, or undergo radioactive decay), absent in the native ground water, easy to detect and inexpensive to analyze with current chemical techniques. Tritiated water is the ideal tracer, in the sense that water molecules that contain tritium are the same size as those of nontritiated ground water and are easy to detect. This tracer is widely used in Europe but cannot be legally injected into an aquifer used for drinking water in the United States because of its radioactive properties. The

halogen ions—chloride, bromide, and iodide—are currently the most widely used alternatives in the United States. There has been some concern that these ions do not always move precisely with the natural ground-water flow because of anion exclusion behavior in negatively charged aquifer materials, where the anion is pushed ahead of the natural flow velocity as a result of repulsive charges between the ion and negatively charged particle surfaces. There is also evidence that these ions in some cases may sorb onto aquifer materials (Koran, 1993). It is not feasible to use chloride at some sites because chloride is present in the native ground water and would interfere with the detection of the tracer. Samples collected prior to the design of the tracer tests from two wells at the Hopewell Township site had chloride concentrations of 4.7 and 6.6 mg/L, indicating that ambient concentrations and variability were too high to allow a low concentration of injected chloride to be reliably detected. Bromide and iodide were both considered to be suitable tracers for this study, and bromide was chosen because of its low toxicity and lower cost compared to iodide. Bromide was detected at concentrations of 0.03 and 0.04 mg/L in the two ambient water-quality samples collected, well below concentrations anticipated during the tests.

Determination of Injection Mass, Concentration, and Duration

Two opposing considerations must be balanced when determining the amount of tracer to inject. On the one hand, a high enough concentration must be injected so that the concentration at the observation well can be easily detected. On the other hand, in order to avoid density effects, the concentration of tracer injected should be kept as low as possible. Even at concentrations as low as 800 mg/L, some quantified sinking of an injected bromide solute body has been observed under ambient flow conditions (Garabedian and others, 1991). The forced flow field of a doublet test helps minimize this effect by forcing the injection solution quickly into the formation, where mixing reduces the concentration.

In order to determine the mass injection conditions, some initial estimate of the dispersivity must be made for a given scale, because dispersivity will affect the peak concentration at the observation well. In addition, an initial estimate of the effective porosity must be made to determine the approximate time at which the peak concentration will occur.

The analytic solution of Welty and Gelhar (1994) for the doublet test in isotropic homogeneous porous media was used to estimate the mass of tracer necessary for injection. Although the hydraulic test results indicate that the site is heterogeneous and anisotropic, the tracer tests isolated a specific interval of bedding-plane transmissive layers. Three effects that could contribute to solute breakthrough behavior that depart from the cited analytical solution, however, include (1) vertical leakage (flow across massive layers to adjacent transmissive layers), (2) matrix diffusion (Tsang, 1995), and (3) non-Fickian transport effects (Raven and others, 1988). These effects all tend to elongate the tails of the breakthrough curves, thereby spreading out the injected mass to a greater degree over time than predicted from the analytical solution of Welty and Gelhar (1994). The slope of the rising limb of the curve is dictated by the dispersivity value and is negligibly affected by matrix diffusion (Moench, 1995), however, so the dispersivity estimate would be unaffected by the late-time solute behavior. The late-time tailing will affect the estimate of the peak concentration in the arrival curve and, therefore, the estimate of the solute injection mass required. Also, the analytical solution is approximate in part because in the derivation it is assumed that $\alpha_L/L \ll 1$. Gelhar and Collins (1971) indicate that the method on which the solution is based should be accurate for values of $\alpha_L/L < 0.1$.

Therefore, some error is inherent in the determination of the desired parameters in application of this solution to cases where α_L/L is greater than 0.1. Where α_L/L is greater than 0.1, non-Fickian effects and scale-dependent dispersivity probably also affect transport processes; therefore, application of a Fickian transport equation under such conditions is not strictly valid (Gelhar and others, 1979).

The three tracer tests were designed sequentially beginning with the shortest scale test (well 6 to well 1) so that information gleaned from each test could be used in design of subsequent tests. The steps used to design all three tests were the same; details of the 6 to 1 test are provided here to illustrate sample calculations. The steady-state pumping and injection rates for the 6 to 1 test were 120 L/min. The well diameters for all tests were 0.15 m. A conservatively low initial estimate of effective porosity of 0.001 was chosen. Figure 17b was consulted to bracket the possible range of dispersivity values at the scale chosen (table 3).

Table 3. Input parameters used to design a doublet tracer test between wells 6 and 1, Hopewell Township, New Jersey

[m, meters]

Test name	Well spacing	Expected dispersivity range	Expected α_L/L range
Well 6 to well 1	30.5 m	0.45 - 4.5 m	0.015 - 0.15

Using the larger value of dispersivity in the design process provides a conservative estimate of the amount of mass to inject. In this case, the conservative value is $\alpha_L/L = 0.15$. A type curve was then generated using equation 45 of Welty and Gelhar (1994) with the value $\alpha_L/L = 0.15$ for the value of the parameter group. A plot of dimensionless concentration ($\hat{c}$) versus dimensionless time ($\hat{t}$) is generated, with the following:

$$\hat{c} = \frac{nHL^2 c_w}{M} \tag{2}$$

and

$$\hat{t} = \frac{Qt}{nHL^2}, \tag{3}$$

where t is time,

M is mass of solute injected [M],

H is aquifer thickness [L],

c_w is concentration observed at pumped well (mass fraction),

L is distance between wells [L],

Q is equal pumping and injection rates [L^3t^{-1}], and

n is effective porosity.

The peak dimensionless concentration for the generated breakthrough curve was $\hat{c}^* = 0.229$ at a peak value of dimensionless time $\hat{t}^* = 1.28$. The actual peak concentration c_w^* desired is at least 2 mg/L such that the lower concentration values will be above detection limits. Solving equation 2 for mass in terms of the peak scaled and desired concentrations,

$$M = \frac{c_w^* n H L^2}{\hat{c}^*} .$$

(4)

The value found was $M = 380$ g of bromide.

Solving equation 3 for t,

$$t = \frac{\hat{t}^* n H L^2}{Q} .$$

(5)

Substituting, the value of time at which the peak was predicted to occur was 0.36 d, or about 8.7 hours. The design parameters were, therefore, an injection mass of a minimum of 0.38 kg of bromide, with a peak expected to occur between 8 and 9 hours.

In order to provide as sharp a peak as possible, the mass should be injected as quickly as possible, while minimizing density effects. The desired injection time is calculated by dividing the design injection mass by the product of the desired injection concentration and the injection volumetric flow rate. To allow for possible spreading due to effects not accounted for in the analytical solution, the amount of bromide injected was increased. The final injection conditions for the well 6 to well 1 test were a total of 1.87 kg of bromide injected over a 20-minute period, at the steady-state flow rate of 120 L/min. The injection concentration was controlled by the injection time and was calculated at 760 mg/L. Injection was carried out by bleeding a concentration of bromide greater than 760 mg/L into the inlet line while maintaining a constant total flow rate.

Field Setup and Data Collection

Well 1 was used as the withdrawal well for each of the three doublet tests. Well 5 was pumped to provide a source of water to the injection well (wells 6, 2, and 10, respectively) for each of the three doublet tests. Well 5 (only 21 m deep) was considered to be sufficiently isolated from the strike wells that continuous pumping would not significantly affect the other wells. The drawdown in well 5 stabilized between 4.6 and 4.9 m for all three tests, compared to well 1, in which drawdown continued past 7.7 m during the 9-day aquifer test. Apparently the proximity of the pond to well 5, and the presence of a significant producing zone possibly cropping out in the pond, provided a source of recharge that stabilized drawdown in well 5 quickly. A packer was installed in well 6 between 16.6 and 17.8 m below land surface to eliminate a hydraulic connection (short circuit) with other wells.

The effectiveness of the packer is illustrated by the head difference in the borehole above and below the packer—about 8.6 m during the well 6 to well 1 doublet test (6 to 1 test) and about 3.2 m during both the well 2 to well 1 and well 10 to well 1 doublet tests (2 to 1 and 10 to 1 tests). In all three tests, the water and tracer injection setups were approximately the same (fig. 18).

Water was withdrawn from well 5 with a submersible pump and directed to the injection well through a flexible, 10.2-cm-diameter hose. About 3 m from the injection well, the 10.2-cm hose was reduced to 2.54-cm (nominal inside diameter) pipe, followed by a gate valve to control the flow from well 5. Following the gate valve was a pipe T, with a ball valve on the branching side, through which the tracer was injected; otherwise the ball valve was closed. Close to the injection well, a 2.54-cm impeller-type flowmeter measured instantaneous flow rate and total flow. The flow rate was monitored and kept constant by adjusting the gate valve as necessary.

The sodium bromide tracer was purchased in granular form, heated to drive off moisture, weighed, then dissolved in a tank just before injection. In order to inject about 5 kg of NaBr at a concentration of 1,000 mg/L, a 5,000-L tank would be necessary. It was deemed easier to dissolve the tracer in about 700 L of water, then inject the concentrated solution into the tracer-free stream coming from well 5. For the 6 to 1 test the 2,576 g of NaBr was mixed in approximately 720 L of water (concentration approximately 2,700 mg/L NaBr), and then pumped into the injection line at approximately 30 L/min, during which time the flow from well 5 was reduced by an equivalent amount so as to keep the injection flow rate constant. The mixture of the concentrated solution and tracer-free water from well 5 yielded the desired injection concentration of about 1,000 mg/L NaBr. The concentrated NaBr solution was mixed in a 1,100-L stock tank with a centrifugal pump, pumped into a standpipe, then injected into the main injection line with a pump having a 15 to 35 L/min capacity, depending on the back pressure.

For each test, the maximum capacity of the pump injecting the concentrated solution into the main line was determined, and the appropriate amount of water was put in the stock tank such that the full mass was injected into the formation as quickly as possible at the design concentration of about 1,000 mg/L. The mass of tracer, length of injection period, injection/withdrawal rate, injection concentration, and other parameters are listed in table 4.

In the 6 to 1 test, the tracer was injected through the center of the packer string, entering the borehole at a depth of about 18.3 m. In the 2 to 1 and 10 to 1 tests, the tracer was injected at a depth of about 5 m, inside the surface casing. For each test, the progress of the tracer in the injection borehole was monitored with submersible specific conductance (SC) probes connected to automatic data loggers. The SC probes were used primarily to confirm the arrival of the solute front in the borehole, the steady-state concentrations during tracer injection, and the arrival of the clean-water front after tracer injection. Secondly, using probes set at different depths (or a single probe lowered to multiple depths during injection), the velocity of the solute front was determined. Because an increasing percentage of the flow had left the borehole at increasing depth, the velocity of the flow decreased. Thus, a qualitative estimate of the percentage of flow entering each zone was made as a check of the HPFM (heat-pulse flowmeter) results. Finally, the SC probes were used to confirm that no tracer remained in the borehole after injection. Because of density effects, a small volume of solute sank to the bottom of the borehole in all three tests, but this volume was less than 45 L at a concentration of about 500 mg/L NaBr, and it diminished to near background concentrations over a period of days.
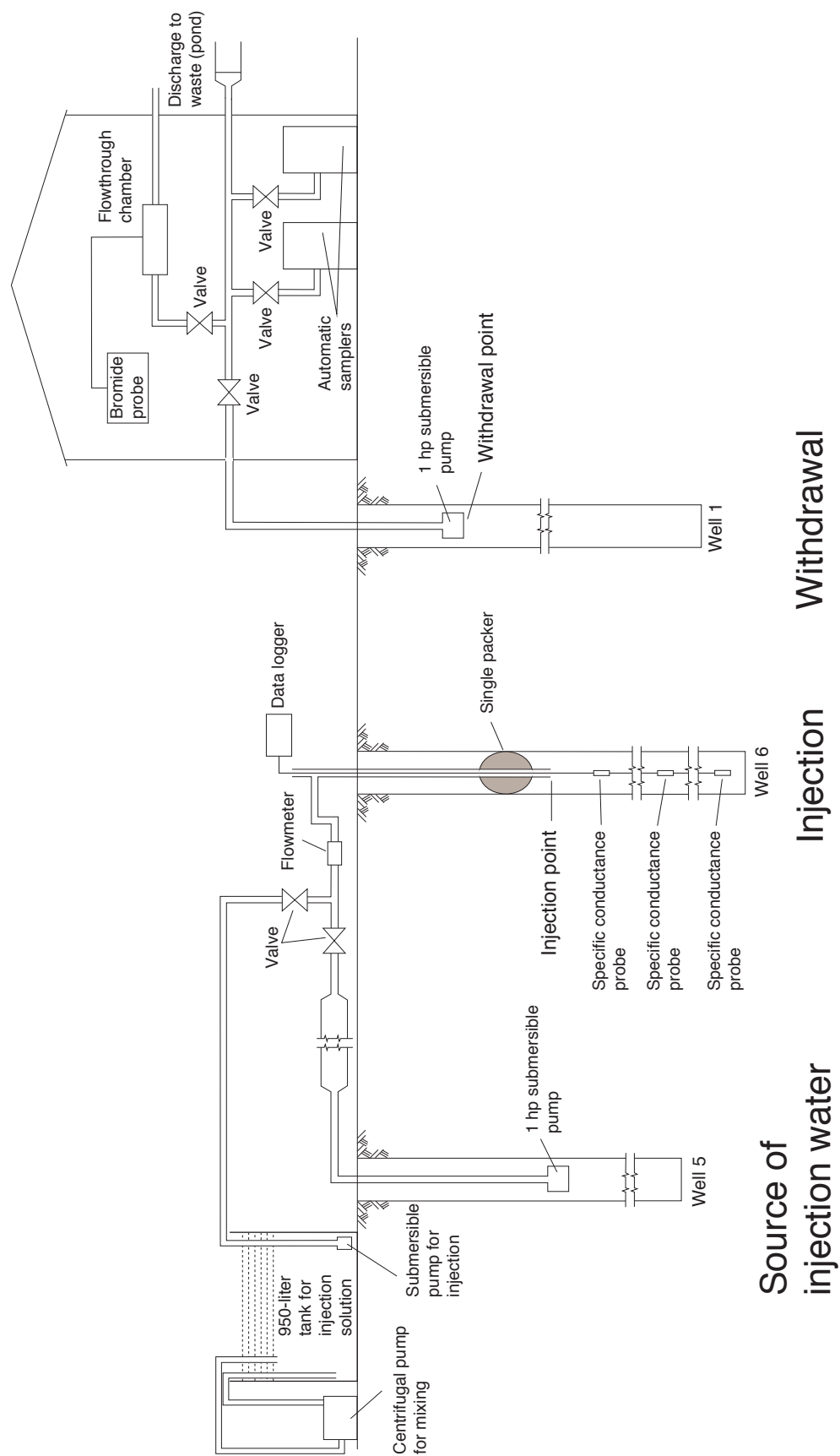
Figure 18. Schematic diagram for injection, withdrawal, and sampling equipment for a doublet tracer test.

43

Table 4. Injection data for the doublet tracer tests in wells 6 to 1, 2 to 1, and 10 to 1, March and April 1995, Hopewell Township, New Jersey

[L/min, liters per minute; mg/L, milligrams per liter; g, grams; min, minutes]

Tracer test name	Injection/ withdrawal rates (L/min)	Mass of sodium bromide injected (g)	Mass of bromide injected (g)	Duration of injection period (min)	Dimension-less injection time	Actual concentration of injection solution (mg/L)		Ambient Br$^-$ concen-tration at test begin-ning (mg/L)	First arrival time (min)	Peak arrival time (min)	Mass of Br$^-$ recovered (percent)
						NaBr	Br$^-$				
6 to 1	119/121	2,391	1,870	20.0	0.18	973	760	0.00	80	600	56
2 to 1	123/122	4,831	3,751	38.2	.04	1,031	800	.14	255	1,200	52
10 to 1	117/118	4,962	3,877	40.8	.01	1,038	810	.39	1,570	5,100	34

The water was withdrawn from well 1 with a submersible pump set at 11 m. The discharge-pipe diameter was reduced to 2.54 cm at the wellhead. This pipe was followed inline by a 2.54-cm impeller-type flowmeter, a gate valve, three pipe T's, and a 10.2-cm flexible discharge line. The discharge from well 1 was routed to the pond to avoid recharging the aquifer. The 2.54-cm section of pipe was routed through a 1.5-m x 2.0-m heated, insulated shelter, inside of which were a flowthrough chamber and two automatic samplers connected to the pipe T's. The automatic samplers contained 24 1-L bottles and could be set to collect samples at regular intervals spaced from 1 minute to several hours apart. Samples were collected as quickly as every 2 minutes at the beginning of the 6 to 1 test, then less frequently as time went on, but always sufficiently frequently to provide adequate definition of the time-concentration curve. Samples were collected alternately by the two samplers to ensure that samples were still collected at regular intervals in the unlikely event that one sampler malfunctioned. The samples were transferred from the automatic samplers to labeled 1-L bottles for subsequent analysis.

Approximately 400 to 500 samples were collected during each test to ensure that sufficient definition of the time-concentration curves was possible. Once the time of arrival and time of peak concentration were known, subsets of samples were used to generate the final data. The flowthrough chamber was used for continuous monitoring of the bromide concentration in the discharge, by means of an ion-selective electrode (ISE). Although the drift of the instrument did not allow accurate measurements to be made in real time, the ISE provided continuous, qualitative data helpful for making decisions on sampling intervals. In addition to the continuous monitoring, selected samples were tested in the field with a calibrated ISE every several hours until the peak concentration was determined to have passed. The field data were not adequate for rigorous analysis owing to significant fluctuation in the data caused by fluctuations in temperature of the samples of less than 1°C. Using the field data as a guide, 150 to 200 samples were, therefore, subsequently reanalyzed with the ISE under controlled laboratory conditions. The bromide ISE is accurate to within about 0.1 mg/L Br$^-$, with a detection limit of about 0.2 mg/L. The ISE readings (in millivolts) for standards were used to calibrate the meter. The samples were measured in the lab in terms of millivolts and subsequently converted to bromide concentrations. To confirm the ISE results, 40 samples were analyzed by standard colorimetric techniques at the USGS National Water Quality Laboratory (NWQL). The results obtained by using the colorimetric techniques and the ISE were in close agreement.

Time-concentration plots (breakthrough curves) of the results of the three tests are shown in figure 19, and results are summarized in table 4. During the 6 to 1 test, breakthrough occurred at 80 minutes, and the peak concentration was 3.0 mg/L Br$^-$ at about 600 minutes. During the 2 to 1 test, breakthrough occurred at 255 minutes, and the peak concentration was 4.0 mg/L Br$^-$ at about 1,200 minutes. During the 10 to 1 test, breakthrough occurred at 1,570 minutes, and the peak concentration was 1.6 mg/L Br$^-$ at about 5,100 minutes. The ambient bromide concentration in water discharged from well 1 was below the detection limit prior to the beginning of the 6 to 1 test. Because of time constraints, the 2 to 1 and 10 to 1 tests were both started before the bromide concentration in water from well 1 returned to below the detection limit. For the 2 to 1 test, the bromide concentration in water from well 1 was 0.14 mg/L immediately prior to start of the test. For the 10 to 1 test, the bromide concentration was 0.39 mg/L at the beginning of the test and decreased to about 0.37 mg/L
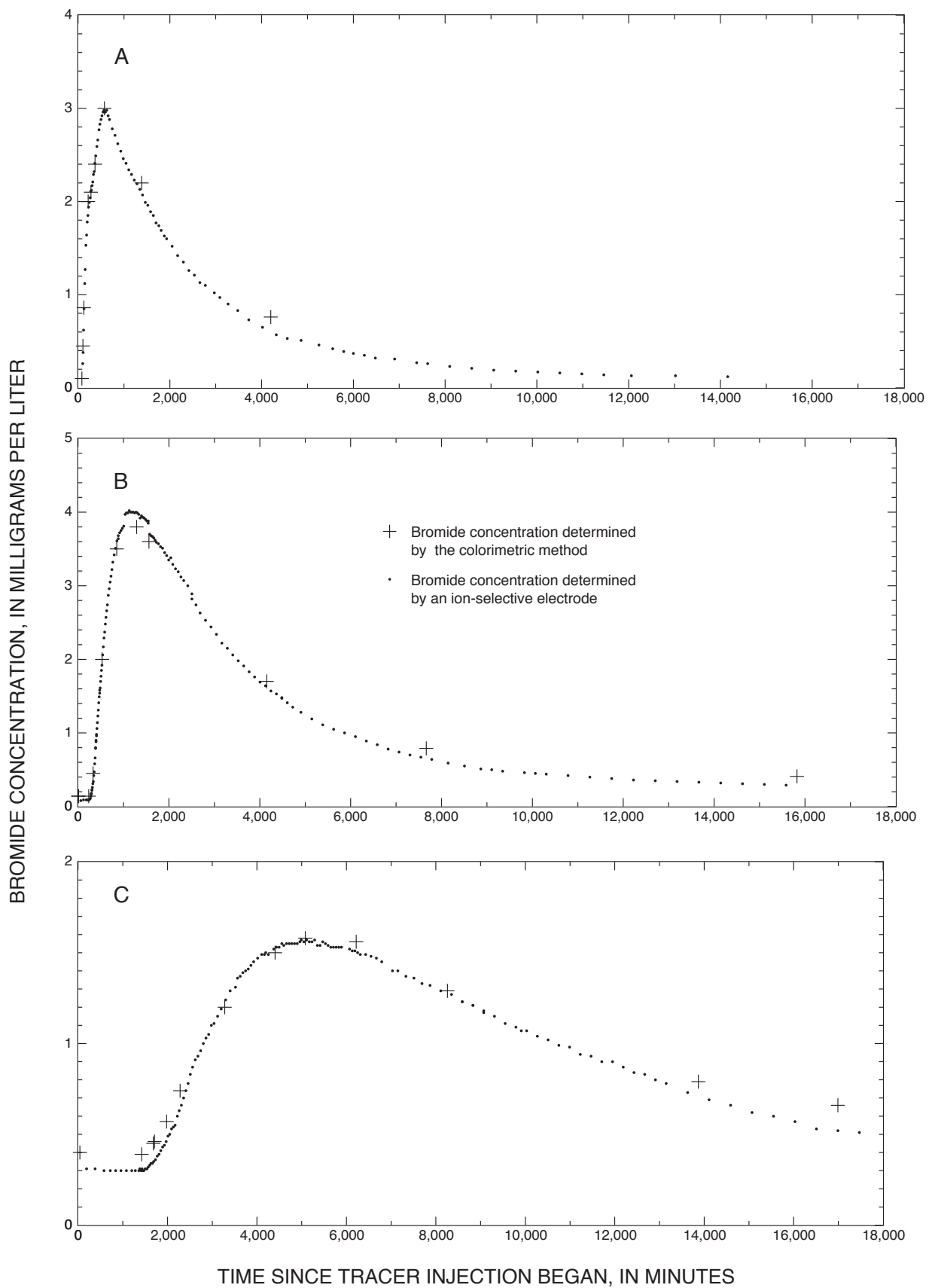
Figure 19. Bromide concentration as a function of time for three doublet tracer tests at well 1 during the (A) well 6 to well 1 test, (B) well 2 to well 1 test, and (C) well 10 to well 1 test, Hopewell Township, N.J.

before breakthrough occurred. For both tests, the decrease in background concentration during the test was small compared to the subsequent increase as a result of injection and is not believed to have significantly altered the shape and magnitude of the time-concentration curve.

The dimensionless injection times listed in table 4 are calculated as the ratio of the injection duration to the peak arrival time. If the dimensionless injection time exceeds about 10 percent, the breakthrough may be expected to depart from the breakthrough from a theoretical instantaneous (Dirac) input (Moench, 1995). According to this criterion, from table 4 it would be expected that the breakthrough curve from the 6 to 1 test would depart from that of a Dirac input—that is, exhibit a broad peak. Inspection of figure 20b, however, reveals that the breakthrough curve does not have a broad peak.

Analysis

The time-concentration data were analyzed to estimate effective porosity and dispersivity by two methods—through use of the analytical model used in the tracer design, and through development and calibration of a two-dimensional, numerical solute-transport model. In addition, effective porosity was estimated by using a particle-tracking technique with the flow model constructed for the aquifer-test analysis.

Analytical Methods

A preliminary interpretation of the first tracer test, at a 30.5-m scale, was made before the second tracer test to assist in designing the second test. A peak breakthrough concentration of 3.0 mg/L occurred at 8.4 hours. The resulting data were satisfactory in that the peak concentration was above the desired 2 mg/L and the test peak was near the predicted peak time of 8.7 hours. The data were evaluated by matching the rising limb of the data to the set of type curves in figure 16, because dispersivity is the predominant process that affects the shape of the rising limb (Moench, 1995). Using this approach to evaluate the field data is only an approximation because of the assumptions involved in deriving the type-curve analytical solutions—namely, Fickian transport, constant dispersivity, absence of boundary effects, and absence of diffusive processes. Nonetheless, this approach provides an estimate of the field parameters of interest, and any departures of the data from these type curves is an indication that physical effects that are not reflected by the assumptions associated with this analytical method are coming into play.

The ill-defined peak in the time-concentration curve plotted on log-log axes (fig. 20a) made interpretation difficult. What appears as a bimodal time-concentration distribution in figure 20a is exaggerated by the magnified ordinates at small time. This effect is seen to be small in the arithmetic plot of the data (fig. 20b). The long tails at this short distance may possibly be the result of non-Fickian dispersion (Raven and others, 1988; Gelhar and others, 1979). Separation of non-Fickian dispersion from other processes, such as matrix diffusion (Tsang, 1995; Gelhar, 1987) and vertical flow through adjacent layers, would be difficult without evaluating data from breakthrough curves at greater scales where the non-Fickian dispersion would be expected to disappear. For very short travel times, molecular diffusion into the rock matrix is not expected to be important (for example, Kuntsmann and others, 1997); however, other diffusion processes may be operating, such as the transport into immobile water trapped in low-permeability fracture zones. Other phenomena that may cause
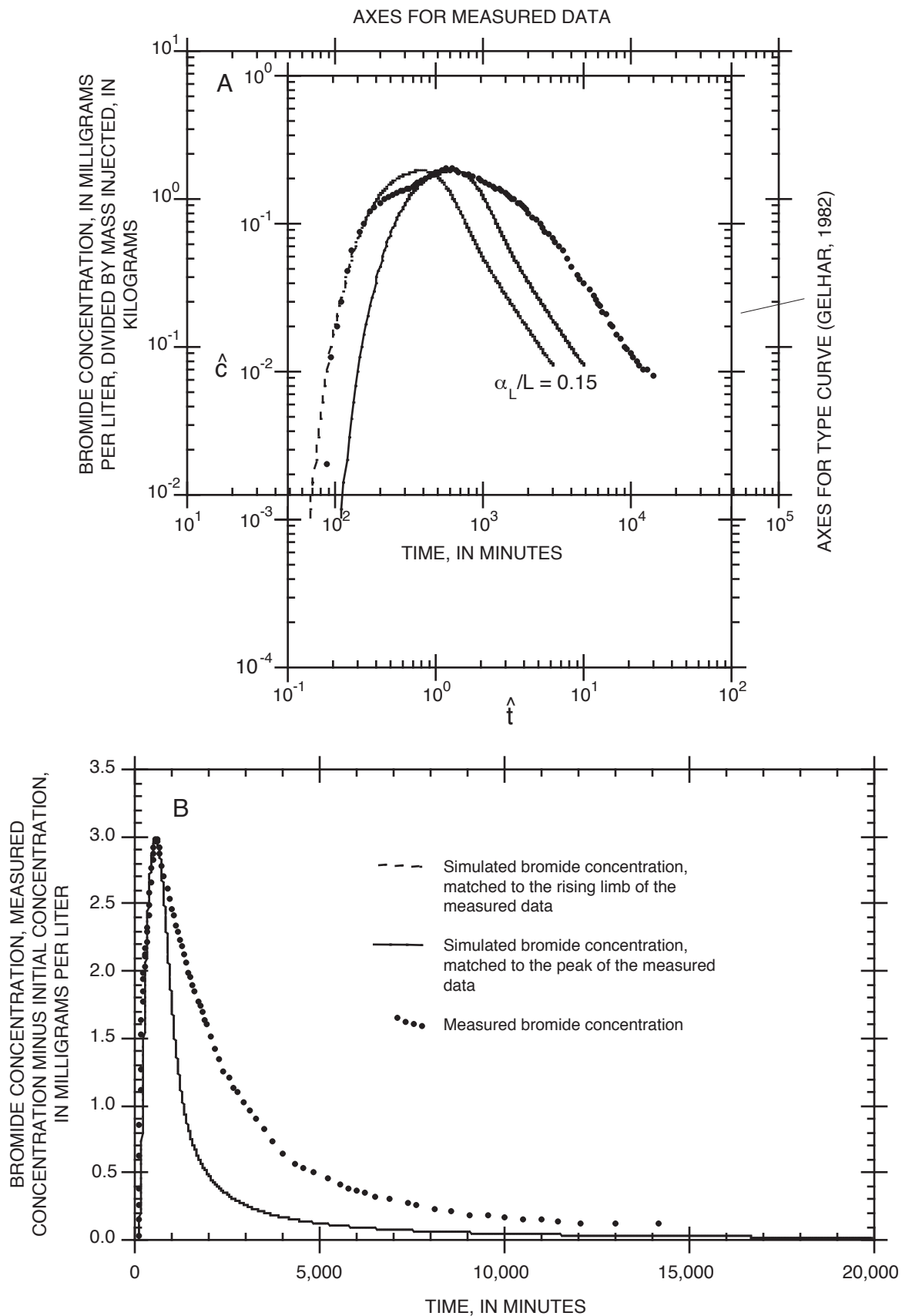
47

Figure 20. Best fit of the bromide breakthrough data from the well 6 to well 1 doublet tracer test, Hopewell Township, N.J., to the type curves shown in figure 16: (A) plotted on logarithmic (base 10) axes, ($\hat{t}$ dimensionless time and $\hat{c}$ dimensionless concentration) and (B) plotted on linear axes.

48

departures of breakthrough-concentration data in the tailing region from those of the ideal case presented in figure 16 include (1) large values of transverse dispersivity (on the order of half the longitudinal value) (Kuntsmann and others, 1997) and (2) inaccuracies in the analytical solution used to construct figure 16 at small distances from the injection well ($\alpha_L/L > 0.1$), especially in the neglect of transverse dispersivity, although some numerical testing has shown the error to be small (Goblet, 1984).

The type-curve match of the 6 to 1 test is shown in figure 20a. The best-fit value of dispersivity was chosen by matching the rising limb of the data to the type curve. The value of $\alpha_L/L = 0.15$ (the chosen design value) coincidentally appears to be the best-fit value of the parameter group. In addition to the best-fit value of α_L/L, a match point must be chosen from the curve matching to find effective porosity. To estimate the effective porosity for the 6 to 1 test, the best-fit type curve ($\alpha_L/L = 0.15$) was moved to the right to match the data peak, owing to the irregular curve in the early time data that is magnified on the log-log plot. The value of $\alpha_L/L = 0.15$ yields a dispersivity of 4.6 m (for this 30.5-m test). If the equation for dimensionless time (eq. 3) is solved for effective porosity, this yields a value of 0.0016 when the time match point is substituted into the equation. As a check on the value of effective porosity, the dimensionless concentration equation (eq. 2) can also be solved for effective porosity, but the results are subject to increased error. Carrying out this calculation indicates an effective porosity of 0.0030, the same order of magnitude as the first result but about double the value. This larger value from the second calculation could result from (1) error in estimation of the mass input and (2) poor match of the physical processes described by the analytical solution to the physical processes of the real system.

A twofold discrepancy in the estimate of effective porosity implies a twofold discrepancy in the estimate of mean pore velocity, which has significant implications for transport prediction. Improved confidence in the estimate of effective porosity could most likely be obtained by improved modeling of the breakthrough curve to better account for all mass in the system. The percentage of mass recovered in application of the analytical solution is 26 percent, compared to a 56-percent recovery of mass from the test at the same point in time. Finally, the scale of the first test is 30.5 m, less than 10 times the resulting dispersivity value (10 x 4.6 m = 46 m), indicating that the dispersivity may not have reached its asymptotic value and that non-Fickian effects could be influencing the solute distribution (Raven and others, 1988; Gelhar and others, 1979).

For the 2 to 1 test, the value of dispersivity of 4.6 m was chosen for design. Using similar calculations as for the first test, a minimum mass of 2.75 kg of bromide was predicted to reach a peak breakthrough of 2 mg/L at 3.2 days. The actual injection conditions were 3.75 kg of bromide, producing a peak concentration of 4.0 mg/L at 0.9 day. The best-fit type curve to the rising limb of the data is shown in figure 21a. The best-fit value of $\alpha_L/L = 0.11$ yields a value of longitudinal dispersivity of 10.1 m. From the curve match, a value of effective porosity is calculated as 3.7×10^{-4} from the time match point and 8.2×10^{-4} from the concentration match point, which is a similar twofold discrepancy compared with the 6 to 1 test. The percentage of mass recovery using the analytical solution is 29 percent compared to 53 percent from the data analysis.

From the results of the first two tracer tests, dispersivity appears to be scale-dependent. Because the dispersivity value of 10.1 m exceeds one-tenth of the 2 to 1 test scale of 91.4 m, it could be expected that the dispersivity may, in fact, not be constant and be increasing with scale (Gelhar, 1993) and also that other non-Fickian effects may be influencing transport.
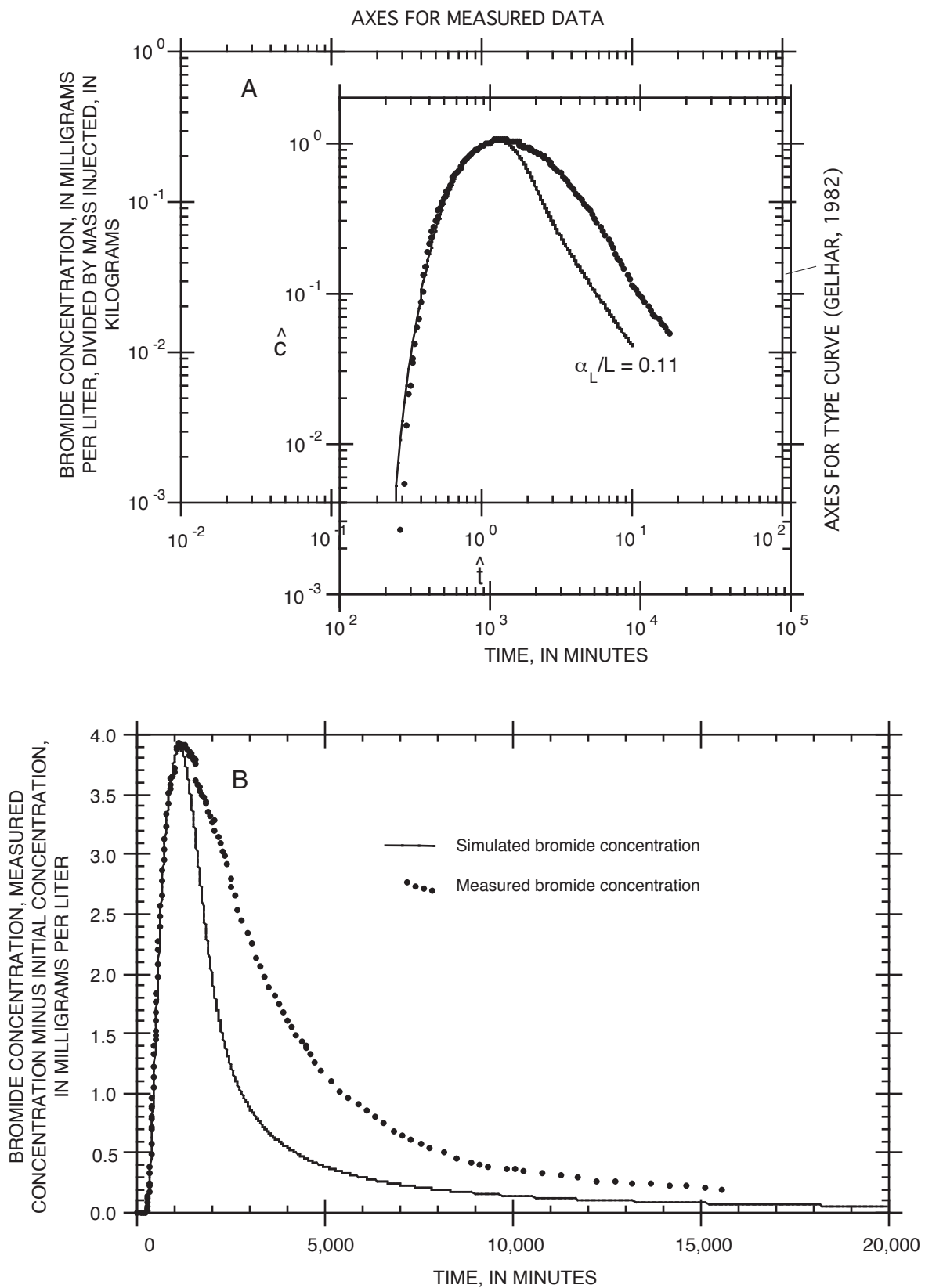
Figure 21. Best fit of the bromide breakthrough data from the well 2 to well 1 doublet tracer test, Hopewell Township, N.J., to the type curves shown in figure 16: (A) plotted on logarithmic (base 10) axes, ($\hat{t}$ dimensionless time and $\hat{c}$ dimensionless concentration) and (B) plotted on linear axes.

In examining the arithmetic plot of the data as shown in figure 21b, it is apparent that the shape of the breakthrough is similar to that of the 6 to 1 test. If non-Fickian processes were affecting the distribution of the solute tails, the effect would be expected to diminish with scale (Raven and others, 1988). Therefore, it may be the case that non-Fickian effects do not account for the tailing exhibited by the first two tracer tests and that this postulated effect could be ruled out.

The design of the third tracer test (well 10 to well 1) was based on the dispersivity of 10.1 m from the 2 to 1 test with a well spacing of 183 m. An estimate of 2.84 kg of bromide to be injected that would peak at 2 mg/L at 3.1 days was used as the design criteria. A total mass of 3.9 kg of bromide was injected over a period of 40.8 minutes, producing a peak at 1.57 mg/L at 3.46 days. The best-fit type curve to the rising limb of the data is shown in figure 22. A best-fit value of $\alpha_L/L = 0.07$ produces a value of longitudinal dispersivity of 12.8 m, and an effective porosity value of 3.7×10^{-4} is calculated from matching the time peaks of the type curve and data set. (A value of effective porosity of 7.6×10^{-4} is calculated from the concentration match point.) The percentage of mass recovered is 26 percent compared to the 34 percent recovered in the data analysis. Here, the scale of the test (183 m) exceeds 10 times the calculated dispersivity value, indicating that asymptotic conditions may have been attained. This assertion could be tested by conducting a tracer test at yet a larger scale. Tailing is evident in the data from the third tracer test, and there does not seem to be any significant change in the discrepancy between the analytical solution and the observed data, compared to the first two tracer tests. The similarities among the results of the three tests indicate that the cause of tailing behavior is not a scale- (time or space) dependent process. Further testing would be needed to determine the precise cause of the tailing.

Use of an analytic solution developed on an assumption of constant dispersivity to infer a scale-dependent dispersivity obviously is not precisely correct. If the dispersivity value were constant for the entire problem, however, then the dispersivity would not be found to increase with scale. Therefore, the type-curve matching procedure described above can be used as a diagnostic tool to determine whether the scale effect should be considered for a given site.

The parameters calculated from the tracer-test analysis using the analytical models are summarized in table 5. The values of dispersivity found from the analyses of the tracer tests conducted at this site are plotted in figure 23. The values for this study are at the upper range of dispersivity values that have been found previously, an indication that the system is more heterogeneous than many others for which dispersivity has been evaluated at the same scales.

Numerical Methods

In order to evaluate the effects of boundaries and macroscopic heterogeneity not represented in the analytical model, a numerical model of the largest scale test (10 to 1) was constructed using SUTRA (Voss, 1984), a two-dimensional finite-element flow and transport model. The numerical model was conceptualized as representing layers 4, 5, and 6 of the more complex MODFLOW three-dimensional ground-water flow model used to interpret the aquifer test. The model was rotated in space 6° from the MODFLOW layer such that the line connecting wells 1 and 10 was in the direction of the x-axis, in order to minimize grid-orientation effects. The model was first gridded without this rotation, and the grid-orientation effect was found to be significant. The model was gridded finely around the injection and withdrawal wells (wells 10 and 1, respectively), where concentration (in the
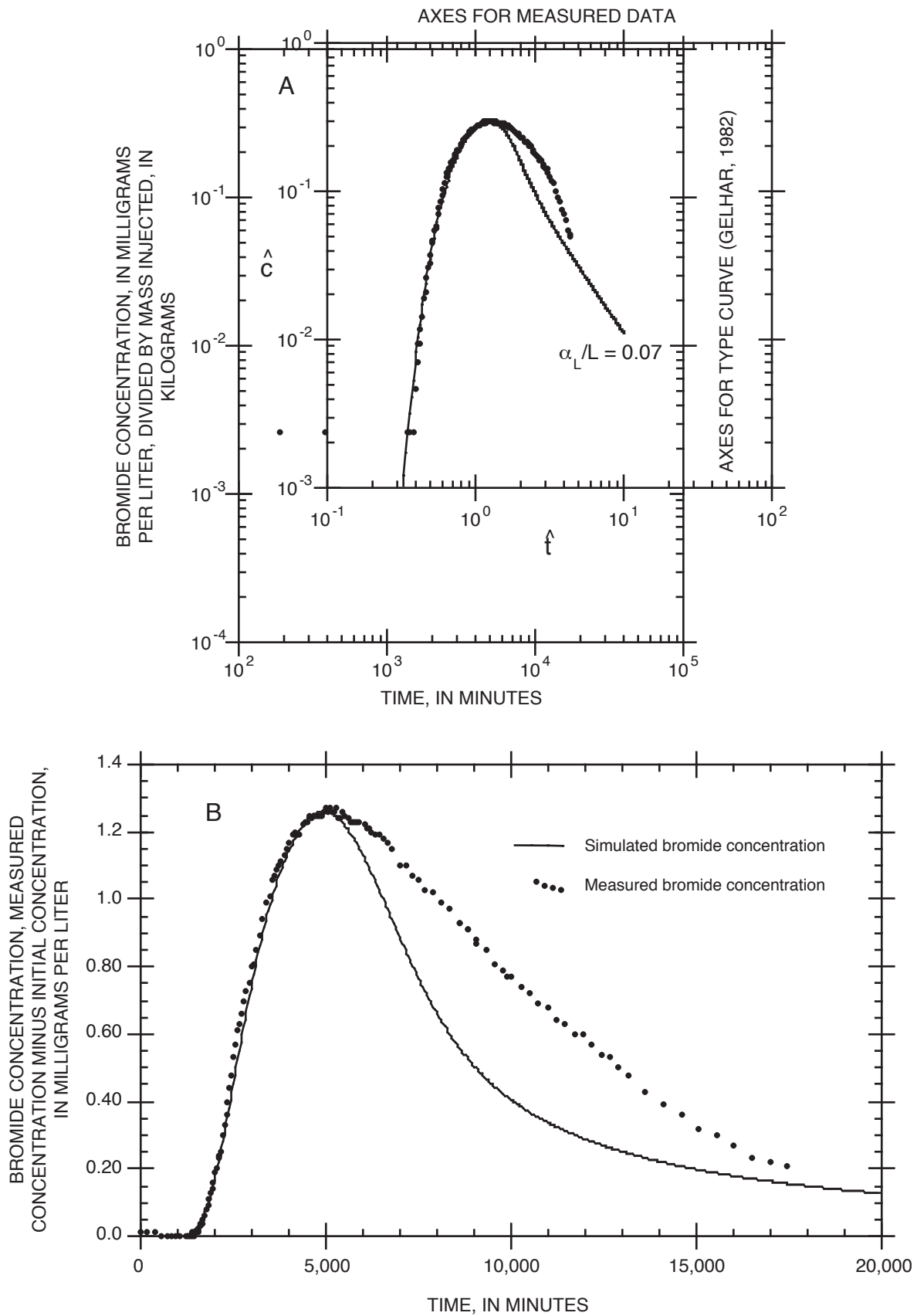
Figure 22. Best fit of the bromide breakthrough data from the well 10 to well 1 doublet tracer test, Hopewell Township, N.J., to the type curves shown in figure 16: (A) plotted on logarithmic (base 10) axes, ($\hat{t}$ dimensionless time and $\hat{c}$ dimensionless concentration) and (B) plotted on linear axes.

Table 5. Summary of evaluation of tracer tests at Hopewell Township, New Jersey, using analytical models

Tracer test	Scale (meters)	Dispersivity (meters)	Effective porosity	Percentage of mass recovered, analytical solution	Percentage of mass recovered, measured
Well 6 to well 1	30.5	4.6	1.6×10^{-3} to 3.0×10^{-3}	26	56
Well 2 to well 1	91.4	10.1	3.7×10^{-4} to 8.2×10^{-4}	29	53
Well 10 to well 1	183	12.8	3.7×10^{-4} to 7.6×10^{-4}	26	34
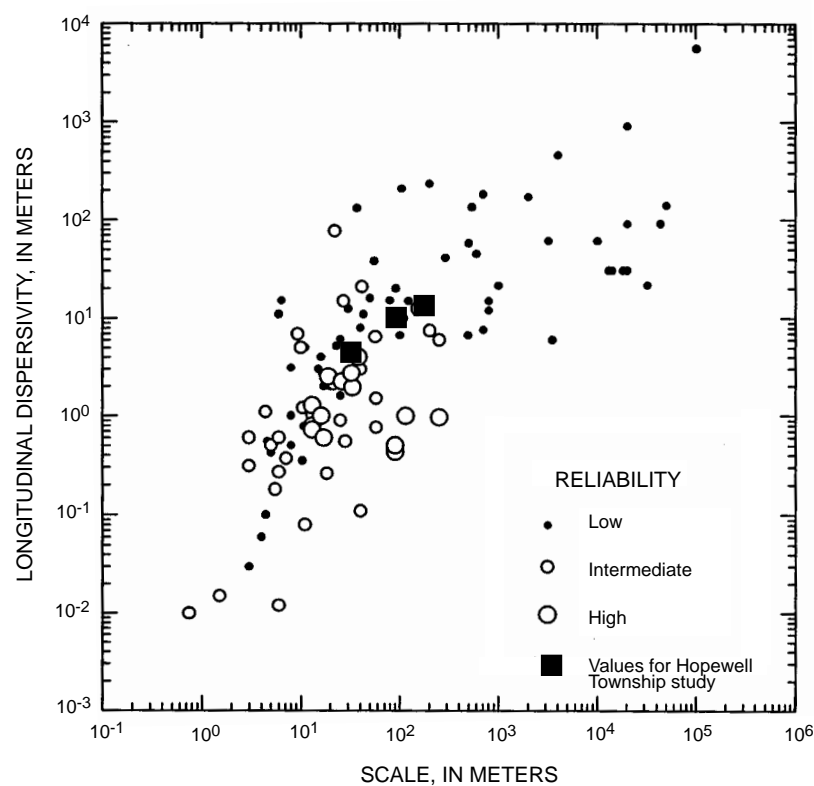
Figure 23. Dispersivity data from the Hopewell Township, N.J., study superimposed on longitudinal dispersivity data, plotted as a function of scale and classified by reliability (Modified from Gelhar and others, 1992).

53

case of the injection well) and hydraulic gradients were steep. The model extended 5,000 m and 325 m in the strike and dip directions, respectively. The maximum thickness was 35.7 m. Boundaries similar to those used in the MODFLOW flow model were used in the SUTRA model. The part of the model domain near the injection and pumped wells is shown in figure 24.

The SUTRA model was calibrated such that the simulated drawdowns were very close to measured aquifer-test drawdowns at wells 1, 2, 3, 6, and 10, resulting in best-fit values of hydraulic conductivity of $K_x = 8.9$ m/d and $K_y = 1.8$ m/d. With the addition of well 10 injecting, the large-time observed heads were underestimated at the pumping and injection wells using these values of hydraulic conductivity: the large-time measured drawdown at well 1 was 2.4 m compared to the model results of 1.5 m; the measured head buildup at well 10 was 8.8 m compared to the modeled value of 3.6 m. The difference between simulated and measured heads may be caused be well-loss effects that are not simulated in the model but have been shown to be significant in the Newark Basin (Goode and others, 1997).

Both the longitudinal-dispersivity and effective-porosity values (12.8 m and 3.9 x10^{-4}) from the analytic type-curve matching were used as initial estimates in the numerical model. The value of dispersivity did not need adjusting; the best-fit value of effective porosity was found to be 1.2×10^{-3}.

Figure 25 shows a close match between the simulated and measured first detection time, slope of the rising limb, and peak concentration time, all of which are indicative of a best-fit dispersivity and effective porosity. The calibrated dispersivity value from the SUTRA model (12.8 m) is the same as that from the analytical model, but the calibrated effective porosity is significantly larger (1×10^{-3}, compared to 3.7×10^{-4} to 7.6×10^{-4} from the analytical model). The match of the simulated and measured data is somewhat better in the tail (later time) region compared to the analytical model. Numerical tests indicated that the improvement arose solely as a result of the more exact nature of the numerical solution compared to the approximate analytical solution, where perfect agreement between the analytical and numerical solutions were found only at values of $\alpha_L/L < 0.01$.

The mass input to the numerical model had to be reduced by a factor of 2.43 (from 3.877 to 1.595 kg) to match the simulated to the observed peak concentrations. This factor is of the same order of magnitude as the mass-input discrepancy implied by comparison of the calculated values of effective porosity from the analytical type-curve match to the data (a factor of 2.04). The calculated mass recovery depicted in figure 25b is 29 percent if the mass under the simulation curve is scaled by the actual input mass (3.877 kg). The mass recovery calculated using the numerical model is slightly closer to the actual mass recovery (34 percent) than the mass recovery calculated using the analytical solution (26 percent). If the mass recovery is calculated on the basis of the mass input to the numerical model (1.595 kg), the percentage of mass recovered in the numerical solution is 70 percent compared to 84 percent if the measured data are scaled by this same number.

Although boundary effects and anisotropy were incorporated into the numerical model, the tail is still not well modeled by the numerical solution. Most likely, non-Fickian processes are not affecting the distribution of the solute tails because the shapes remained approximately the same at all scales. Diffusion into and out of the rock matrix is probably not significant because of the short duration of the tests (Tsang, 1995; Kuntsmann and others, 1997); however, faster diffusive processes, such as diffusion of the solute into immobile water in low-permeability zones, may be affecting the

Figure 24. Part of the finite-element domain used to model the well 10 to well 1 doublet tracer test, Hopewell Township, N.J.

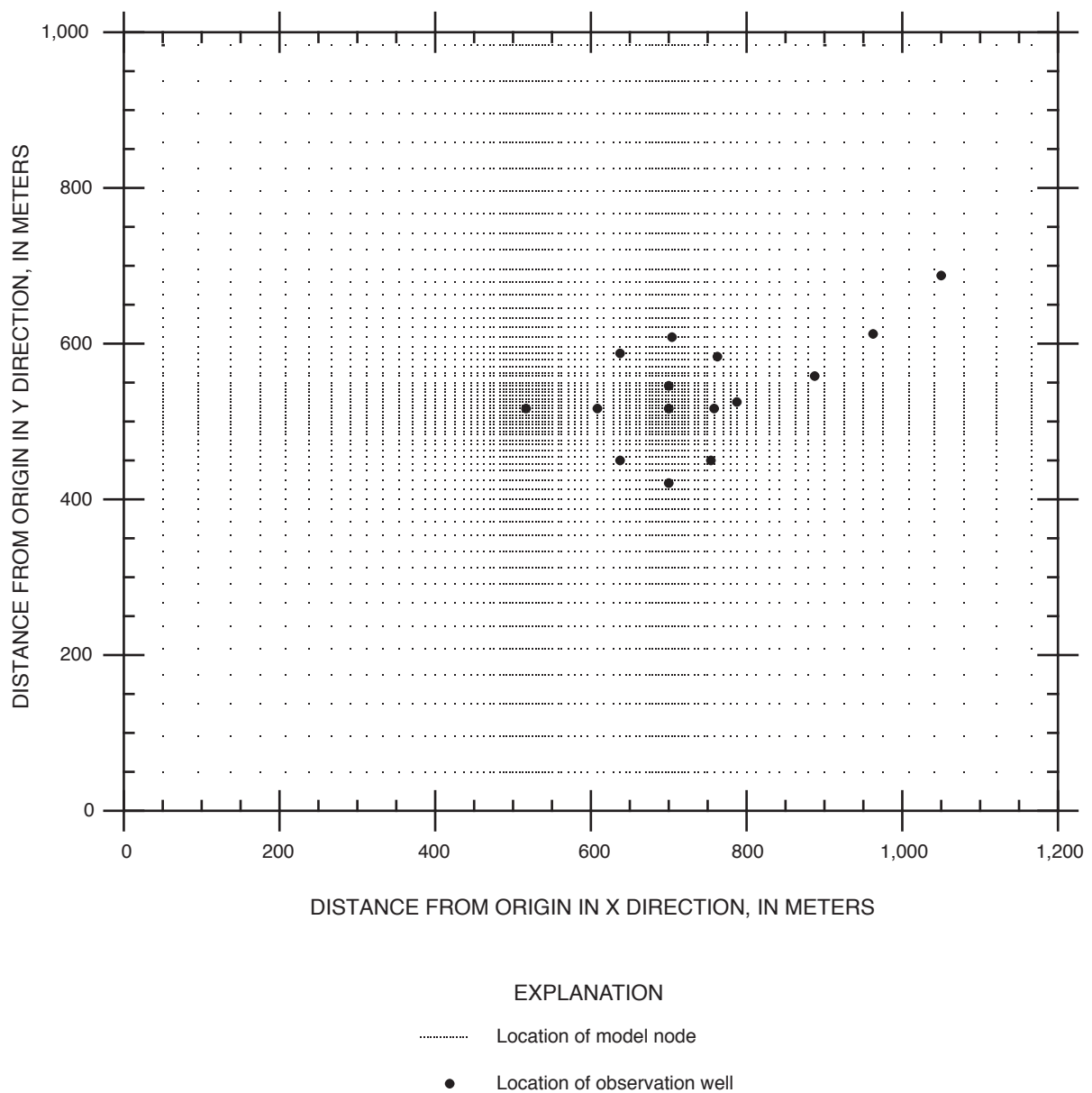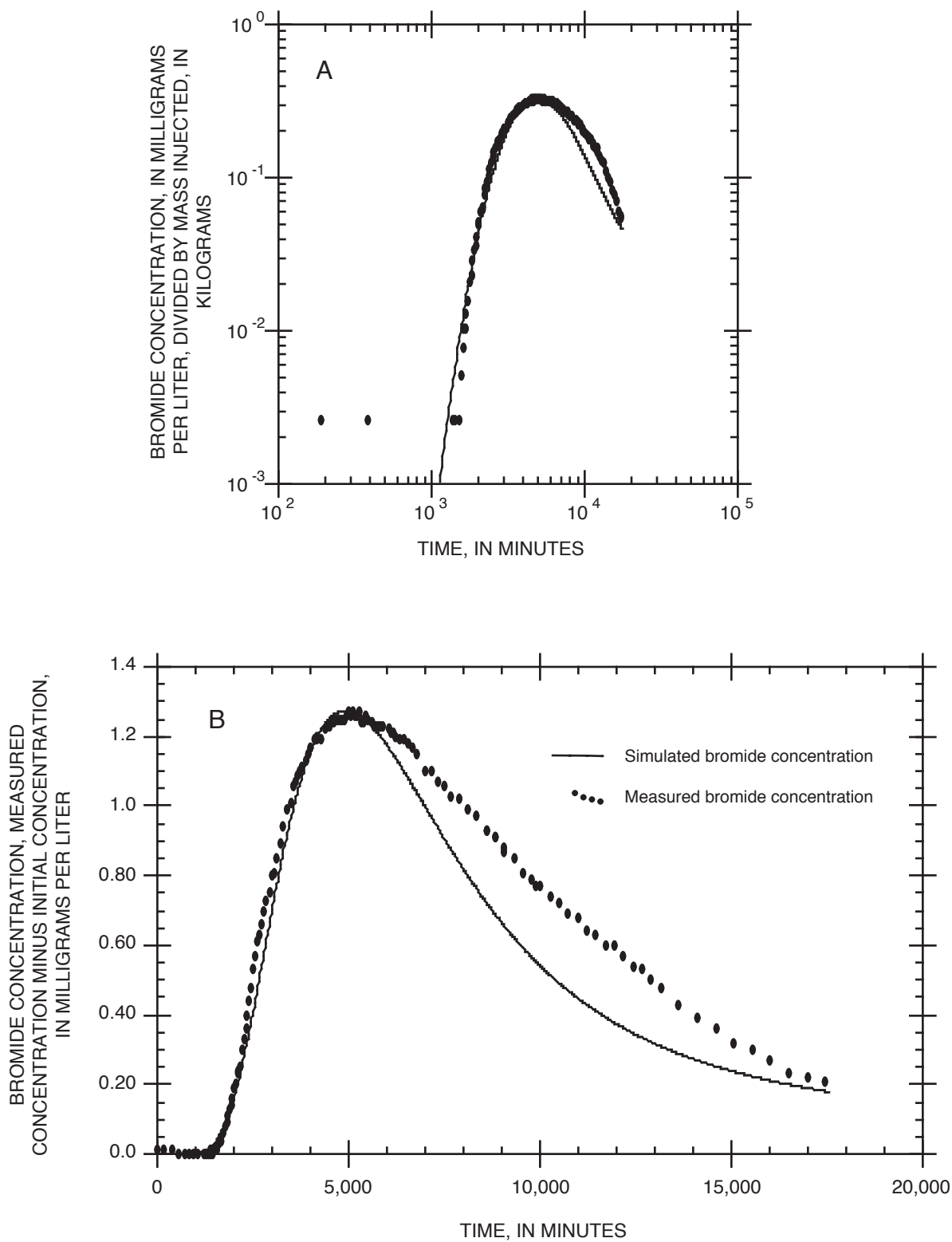**Figure 25.** Simulated scaled breakthrough curve from the well 10 to well 1 doublet tracer test, Hopewell Township, N.J. using SUTRA: (A) plotted on logarithmic (base 10) axes; (B) plotted on linear axes.

56

tailing behavior. An independent effort to resolve the issue of mobile/immobile diffusion would require estimates of mass-transfer rate and (or) distribution coefficients. Independent estimates of such coefficients from laboratory or complementary field data were not available; therefore, this avenue of analysis was not explored during this study.

The possible effect of leakage into the model layer on the breakthrough behavior was evaluated as follows. The net leakage as a function of space was determined for the layer of interest from the adjacent layers in the ground-water flow model and was distributed to each cell face of the transport model. The resulting SUTRA breakthrough curve showed a barely perceptible response to this change. An increase in the recharge values by four orders of magnitude also had no effect on the breakthrough curve. Therefore, it was concluded that the net leakage into and out of the model layer had a negligible effect on the test.

Particle-Tracking Method

The particle-tracking post-processor package MODPATH (Pollock, 1989) was applied to the numerical ground-water flow model (MODFLOW) to estimate the effective porosity of the aquifer layers represented in the model of the 10 to 1 tracer test. This approach allows consideration of flow patterns within the multilayer model of the site hydrogeologic framework and is assumed to provide a reasonable estimate of the time of arrival of the peak concentration (primarily a function of effective porosity and the hydraulic characteristics of the formation). The disadvantage, however, is that the particle tracker simulates advective transport only and thus does not account for dispersion.

The travel time of particles from introduction to the flow field at the injection well (well 10) to discharge at the withdrawal well (well 1) was determined using MODPATH. A total of 196,000 particles were introduced to well 10 by placing them on each of the four faces of the well cell in each of the three layers (layers 4, 5, and 6) intercepted by the well. Well 10 is only partially open to model layer 4; thus, most of the tracer mass (and therefore simulated particles) was injected into model layers 5 and 6. The number of particles introduced to each face was proportional to the flow across that face; thus, each particle represents approximately the same mass of tracer. Simulated data were plotted by graphing the number of particles that arrived at well 1 per 40-minute interval (the length of the tracer-injection period) (fig. 26).

Two principal peaks and a third, less significant, peak correspond to movement of particles through the three aquifer (model) layers in which the tracer was injected and withdrawn. The different peak arrival times are caused by the different hydraulic characteristics of the layers: the maximum transmissivities of layers 4, 5, and 6 are 140, 130, and 76 m^2/d, respectively. The trimodal arrival observed in the simulation, unlike the smooth breakthrough curve observed in the measured data, occurs because particle-tracking analysis does not include dispersion, and because heterogeneities of the natural system are simplified to be represented by three layers. The long tail of the simulated breakthrough curve, similar to that of the measured data, may be attributed in part to the macroscopic heterogeneity represented in this model. Heterogeneities affect the advective pattern, which in turn affects the shape of the tail of the breakthrough curve. The effect of heterogeneities on the shape of the breakthrough curve tail must be separated from effects of matrix diffusion to clarify why the shape of the breakthrough curve differs from the ideal case.
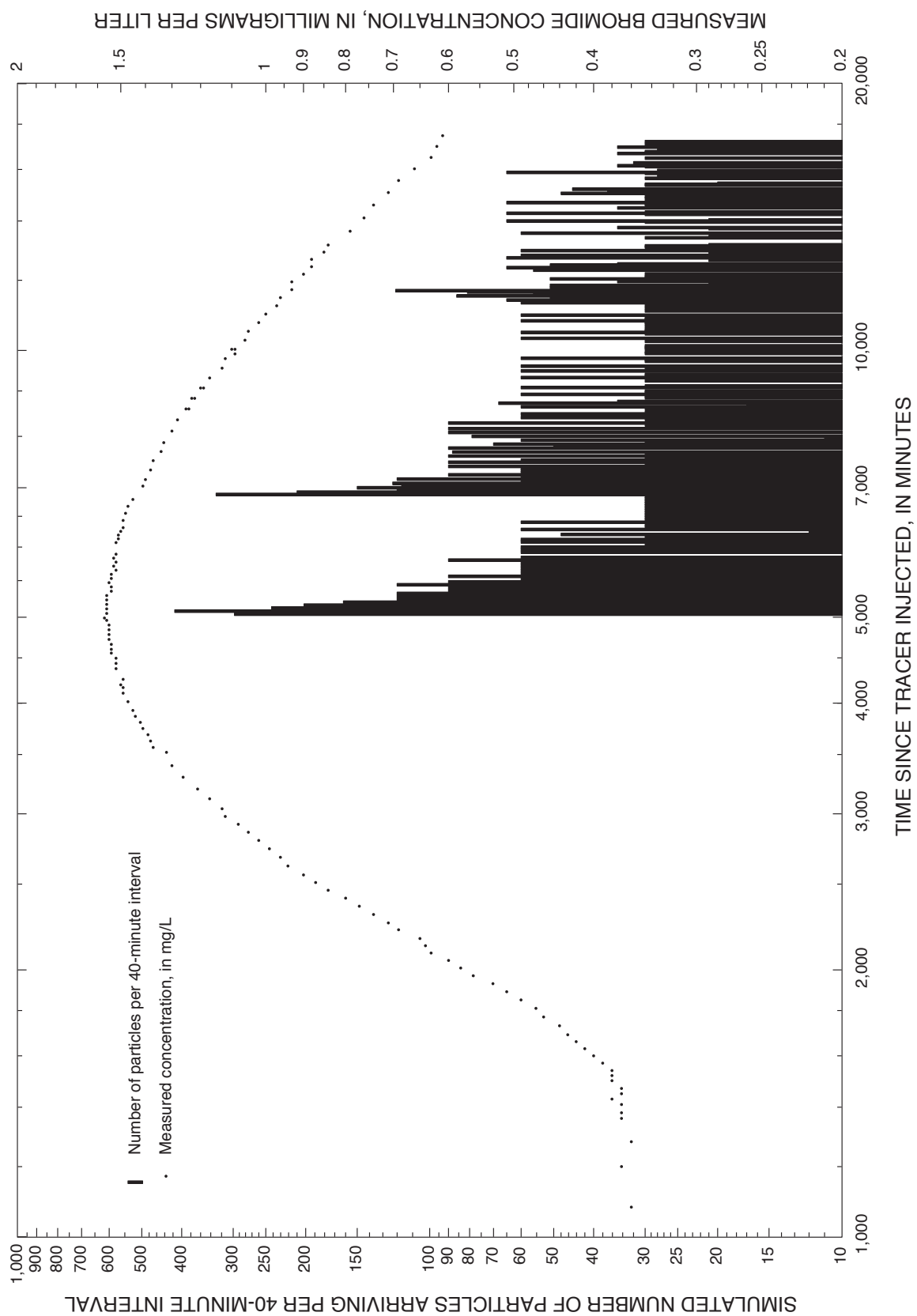
Figure 26. Number of simulated particles and measured bromide concentration at well 1 during the well 1 to well 10 doublet tracer test, Hopewell Township, N.J.

The effective porosity of the formation is estimated to be 1.4×10^{-3}, based on adjusting effective porosity until the arrival of the maximum number of particles (which approximately coincided with the first arrival) occurred at the same time as the peak concentration measured during the tracer test (5,100 minutes after injection began). Although the match of the simulated and measured peaks is subjective, the arrival times of the particles in the model are sensitive to the value of effective porosity used: a decrease of effective porosity from 1.4×10^{-3} to 1.0×10^{-3} resulted in a decrease in the arrival time of nearly 2,000 minutes.

Comparison and Results of Tracer-Test Analyses

The analytical and numerical solute-transport models and the advective-flow, particle-tracking model produced consistent results (table 6) despite the various assumptions and simplifications required by each model. The particle-tracking flow model used to estimate effective porosity contains the most detailed representation of the boundaries and three-dimensional geometry of the flow system of the three models used, but it does not include representation of any mixing processes. The advantage of using this model to estimate effective porosity is that it is relatively easy to implement when a flow model has already been constructed. Particle tracking can also provide insight into the effects of heterogeneities and complex flow geometries on the advective flow pattern.

Table 6. Results of analytical and numerical simulation of the well 10 to well 1 doublet tracer test, March 1995, Hopewell Township, N.J.

Simulation	Dispersivity (meters)	Effective porosity (dimensionless)	Effective borehole length (meters)	Effective porosity multiplied by layer thickness (meters)
Two-dimensional analytical solution for a doublet-well tracer test in a confined isotropic aquifer of infinite extent (from Welty and Gelhar, 1994)	12.8	3.7×10^{-4} to 7.6×10^{-4}	35.7	1.3×10^{-2} to 2.7×10^{-2}
Two-dimensional, solute-transport model (SUTRA, Voss, 1984) with horizontal and constant-head boundaries	12.8	1.2×10^{-3}	35.7	4.3×10^{-2}
Three-dimensional, advective-flow model (MODFLOW, McDonald and Harbaugh, 1988) with a particle tracker (Pollock, 1989) to represent the tracer chemical	--	1.4×10^{-3}	35.7	5.0×10^{-2}

The analytical solution used to generate curves that were matched to the measured data is based on the assumptions that the aquifer is isotropic, confined, and infinite in extent; that the tracer is injected instantaneously; that there is no matrix diffusion; and that transport is Fickian (Welty and Gelhar, 1994). Despite violations of these assumptions, the good fit of the rising limb of the type curves to the scaled measured data for the 2 to 1 and 10 to 1 tests indicates that the estimated values for dispersivity are reasonable. The dispersivity value of 12.8 m calculated from the 10 to 1 test may be an asymptotic value; this could possibly be verified by conducting a tracer test at a larger scale. The estimated values of effective porosity from the analytical type-curve matches are less reliable because of the discrepancy in the mass recovered when compared to the data.

The two-dimensional, numerical solute-transport model SUTRA (Voss, 1984) can simulate the boundary conditions, anisotropy, vertical leakage, and duration of injection. The simulated time-concentration curves match the measured data only slightly better than the analytical results. The dispersivity and effective porosity estimated with the numerical modeling are 12.8 m and 1.2×10^{-3}, similar to analytical model estimates; the effective-porosity estimate is very close to the estimate made with the particle-tracking model (1.4×10^{-3}). Because the SUTRA model includes the known boundaries of the system, the results of simulations made with this model were expected to be closer to the measured data than the more idealized analytical results, indicating that additional data and calibration may be warranted. None of the three models used accounted for diffusive processes, which were possibly significant, especially during the long-duration 10 to 1 tracer test.

SUMMARY AND CONCLUSIONS

A methodology to define the hydrogeologic framework (including the geometry of fracture pathways for ground-water flow), estimate values of hydraulic properties (hydraulic conductivity and specific storage), and estimate values of transport properties (effective porosity and dispersivity) was successfully demonstrated in a fractured sedimentary-rock aquifer in the Newark Basin, Hopewell Township, N.J. The methodology includes characterization of hydrogeologic framework using geologic mapping and borehole geophysical techniques, estimation of hydraulic properties using borehole and aquifer tests, and estimation of solute-transport properties using tracer tests. Multiple methods of analysis are presented to provide flexibility for application at other sites.

Geologic mapping of the site revealed the presence of a syncline that causes the bedding-plane strike to shift from about east to about northeast and two main fracture sets including bedding-plane partings that dip gently to the north and near-vertical structural fractures that dip steeply to the south (on the western limb of the syncline). Geophysical logs that detect changes in lithology, including gamma radiation and electromagnetic conductance and resistivity, were used to construct lithologic cross-sections to refine the understanding of the hydrogeologic framework. Borehole acoustic televiewer, caliper, and video logs were used to detect the location and orientation of fractures. Heat-pulse flowmeter and fluid temperature and resistivity logs were used to detect the location of water-producing fractures and the presence or absence of vertical flow within the boreholes. The heat-pulse flowmeter was also used while pumping the wells to determine the approximate transmissivity of the producing fractures, which ranged from below the detection limit of about 0.1 m^2/d to about 20 m^2/d. Although the near-vertical fractures were determined to be abundant, their water-transmitting properties are much lower than those of bedding-plane features. Bedding-plane partings had the highest transmissivities found at the site, but the transmissivities appeared to decrease with depth, probably because of the increase in overburden pressure.

A 9-day aquifer test was conducted during a rain-free period to measure the hydraulic conductivity and specific storage of the aquifer. The analytical method of Hsieh and Neuman (1985), in which the aquifer is assumed to be an equivalent homogeneous, anisotropic porous medium, was used to interpret the test. This analysis yielded estimates of principal hydraulic conductivity of 6.4, 0.30, and 0.0043 m/d and a specific storage of 9.2×10^{-5} m^{-1}. The aquifer test was also analyzed using a three-dimensional numerical model. The layers of the numerical model were aligned along the bedding planes of the formation and yielded best-fit, average values of hydraulic conductivity of about 7, 3, and 4×10^{-5} m/d in the strike, dip, and mutually perpendicular directions, respectively, and

a specific storage of about 10^{-7} m^{-1}. The analytical and numerical modeling results indicate that the system is highly heterogeneous and anisotropic, and is influenced by the boundary effects of a pond on the site (head-dependent boundary) and the lateral boundaries at the updip outcrop and downdip extinction depth (no-flow boundaries), but that the system can be successfully simulated using models developed for analysis of porous media.

Three doublet tracer tests were conducted at scales of 30.5 m, 91.4 m, and 183 m. The induced-gradient doublet test was chosen because of its advantages over radial flow tests, including better control over the flow field and faster solute-recovery times. The test was designed to measure properties of flow along an approximately 35-m-thick layer aligned with bedding-plane fractures. Effective porosities of 3.7 x 10^{-4} to 7.6 x 10^{-4} and a dispersivity of 12.8 m at a scale of 183 m were obtained using approximate analytical techniques. An effective porosity of 1.2 x 10^{-3} and a dispersivity of 12.8 m were obtained using the two-dimensional solute-transport model SUTRA. It is not known whether the value of dispersivity is asymptotic; this could be evaluated only by conducting a tracer test at yet a larger scale.   The dispersivity data are considered to be of medium quality on the basis of criteria of Gelhar and others (1992). This dispersivity value exceeds that of many high-quality data previously determined at this scale, a result that is not surprising given the highly heterogeneous nature of the formation. An effective porosity of 1.4 x 10^{-3} was estimated using a particle-tracking method with a three-dimensional numerical flow model.

The hydraulic and transport properties were determined in this study under stressed (that is, pumping) conditions. Findings based on such tests may not be adequately representative of those under ambient conditions. An ambient, three-dimensional tracer test could take several years, and considerable expense, to conduct because of the three-dimensional sampling that would be required.

The study site in Hopewell Township, N.J., offered a unique opportunity to conduct multiple tracer tests at multiple scales for a relatively low cost. Additional efforts at the site to improve understanding of the aquifer-transport properties could include (1) a tracer test across a massive layer between transmissive bedding-plane layers, (2) a tracer test perpendicular to strike and across both transmissive and massive layers, (3) a tracer test within the transmissive layer already tested, but at a still larger scale, to test the hypothesis that an asymptotic value of dispersivity may be reached in this setting, and (4) an evaluation of the effects of diffusive processes by extending the tracer test from well 10 to well 1 to obtain a complete definition of the late-time tracer breakthrough curve or using other tracers or tracer tests that specifically measure diffusion. Finally, the transfer-ability of the methodology could be tested by application in other geographic provinces in New Jersey.

REFERENCES CITED

Barton, C.A., and Zoback, M.D., 1992, Self-similar distribution and properties of macroscopic fractures at depth in crystalline rock in the Cajon Pass Scientific Drill Hole: Journal of Geophysical Research, v. 97, p. 5181–5200.

Bear, Jacob, 1972, Dynamics of fluids in porous media: New York, Elsevier, 764 p.

Boggs, J.M., Young, S.C., Beard, L.M., Gelhar, L.W., Rehfeldt, K.R., and Adams, E.E., 1992, Field study of dispersion in a heterogeneous aquifer: Water Resources Research, v. 28, no. 12, p. 3281–3291.

Garabedian, S.P., LeBlanc, D.R., Gelhar, L.W., and Celia, M.A., 1991, Large-scale natural gradient tracer test in sand and gravel, Cape Cod, Massachusetts. 2. Analysis of spatial moments for a nonreactive tracer: Water Resources Research, v. 27, no. 5, p. 911–924.

Gelhar, L.W., 1982, Analysis of two-well tracer tests with a pulse input: Richland, Wash., Rockwell International, Rockwell Hanford Operations, Report RHO-BW-CR-131 P, 103 p.

Gelhar, L.W., 1987, Applications of stochastic methods to solute transport in fractured rocks: Stockholm, Sweden, Swedish Nuclear Fuel and Waste Management Co., Technical Report 87–05, 54 p.

Gelhar, L.W., 1993, Stochastic subsurface hydrology: Englewood Cliffs, N.J., Prentice Hall, sections 4.6 and 5.5.

Gelhar, L.W., and Axness, C.L., 1983, Three-dimensional stochastic analysis of macrodispersion in aquifers: Water Resources Research, v. 19. no. 1, p. 191–180.

Gelhar, L.W. and Collins, M.A., 1971, General analysis of longitudinal dispersion in nonuniform flow: Water Resources Research, v. 7, no. 6, p. 1511–1521.

Gelhar, L.W., Welty, Claire, and Rehfeldt, K.R., 1992, A critical review of field-scale dispersion in aquifers: Water Resources Research, v. 28, no. 7, p. 1955–1974.

Gelhar, L.W., Gutjahr, A.L., and Naff, R.L., 1979, Stochastic analysis of macrodispersion in a stratified aquifer: Water Resources Research, v. 15, no. 6, p. 1387–1397.

Goblet, Patrick, 1984, Interpretation des Tracages aux Lanthanides. Part II, *in* Bigot and others, Etudie hydrodynamiques a l'aide traceurs d'un doublet hydrothermique in roches fissures: Commission des communautes Europeennes, Institut National d'Astonomie et de Geophysique.

Goode, D.J., Senior, L.A., and Amantia, Andrea, 1997, Aquifer tests and regional ground-water flow in fractured triassic rock, Lansdale, Pennsylvania: Boulder Colo., Geologic Society of America Abstracts with Programs, v. 29, no.1.

REFERENCES CITED--Continued

Greenman, D.W., 1955, Ground water resources of Bucks County, Pennsylvania: Pennsylvania Geological Survey, Fourth series, Bulletin W11, 67 p.

Hess, A.E., 1982, A heat-pulse flowmeter for measuring low velocities in boreholes: U.S. Geological Survey Open-File Report 82–699, 40 p.

Hess, A.E. and Paillet, F.L., 1990, Applications of the thermal-pulse flowmeter in the hydraulic characterization of fractured rocks: American Society for Testing of Materials, Special Publication 1101, p. 99–112.

Houghton, H.F., 1990, Hydrogeology of the Early Mesozoic rocks of the Newark Basin, N.J., *in* Brown, J.O., and Kroll, R.L, eds., Aspects of groundwater in New Jersey—Field guide and proceedings of the seventh annual meeting of the Geological Association of New Jersey, October 26-27, 1990, Kean College, Union, N.J.: p. E1–E36.

Hsieh, Paul and Neuman, S.P., 1985, Field determination of a three-dimensional hydraulic conductivity tensor of anisotropic media. 1. Theory: Water Resources Research, v. 21, no. 11, p. 1655–1665

Hsieh, Paul, Neuman, S.P., Stiles, G.K., and Simpson, E.S., 1985, Field determination of a three-dimensional hydraulic conductivity tensor of anisotropic media. 2. Methodology and application to fractured rocks: Water Resources Research, v. 21, no. 11, p. 1666–1676.

Keys, W.S., 1990, Borehole geophysics applied to ground-water investigations: U.S. Geological Survey Techniques of Water-Resources Investigations, book 2, chap. E2, 150 p.

Konikow, L.F., Goode, D. J., and Hornberger, G.Z., 1996, A three-dimensional method-of-characteristics solute-transport model (MOC3D): U.S. Geological Survey Water-Resources Investigations Report 96–4267, 87 p.

Koran, S.F., 1993, Bromide behavior in anion-adsorbing aquifer sediments: Eos, v. 74, no. 43, Supplement, Oct. 26, 1993, p. 240.

Kunstmann, H., Kinzelbach, W., Marschall, P., and Li, G., 1997, Joint inversion of tracer tests using reversed flow fields: Journal of Contaminant Hydrology, v. 26, p. 215–226.

LeBlanc, D.R., Garabedian, S.P., Hess, K.M., Gelhar, L.W., Quadri, R.D., Stollenwerk, K.G., and Wood, W.W., 1991, Large-scale natural gradient tracer test in sand and gravel, Cape Cod, Massachusetts. 1. Experimental design and observed tracer movement: Water Resources Research, v. 27, no. 5, p. 895–910.

REFERENCES CITED--Continued

Leonhart, L.S., Jackson, R.J., Graham, D.L., Gelhar, L.W., Thompson, G.M., Kanehiro, B.Y., and Wilson, C.R., 1985, Analysis and interpretation of a recirculating tracer experiments performed on a deep basalt flow top: Bulletin of the Association of Engineering Geologists, v. 22, no. 3, p. 259–274.

Lewis-Brown, J.C., and Jacobsen, Eric, 1995, Hydrogeology and ground-water flow, fractured Mesozoic structural-basin rocks, Stony Brook, Beden Brook, and Jacobs Creek drainage basins, west-central New Jersey: U.S. Geological Survey Water-Resources Investigations Report 94–4147, 83 p.

Lyttle, P.T., and Epstein, J.B., 1987, Geologic map of the Newark 1° x 2° quadrangle, New Jersey, Pennsylvania, and New York: U.S. Geological Survey Miscellaneous Investigations Map I–1715, scale 1:250,000.

McDonald, M.G., and Harbaugh, A.W., 1988, A modular three-dimensional finite-difference ground-water flow model: U.S. Geological Survey Techniques of Water-Resources Investigations, book 6, chap. A1, 528 p.

Michalski, Andrew, 1990, Hydrogeology of the Brunswick (Passaic) Formation and implications for ground water monitoring practice: Groundwater Monitoring Review, v. 10, no. 4, p. 134–143.

Michalski, Andrew, and Britton, Richard, 1997, The role of bedding fractures in the hydrogeology of sedimentary bedrock—evidence from the Newark Basin, New Jersey: Ground Water, v. 35, no. 2, p. 318–327.

Moench, A.F., 1995, Convergent radial dispersion in a double-porosity aquifer with fracture skin—Analytical solution and application to a field experiment in fractured chalk: Water Resources Research, v. 31, no. 8, p. 1823–1835.

Molz, F.J., Morin, R.H., Hess, A.E., Melville, J.G., and Guven, O., 1989, The impeller meter for measuring aquifer permeability variations—Evaluation and comparison with other tests: Water Resources Research, v. 25, p. 1677–1683.

Morin, R.H., Carleton, G.B., and Poirier, Stephane, 1997, Fractured-aquifer hydrogeology from geophysical logs; the Passaic Formation, New Jersey: Ground Water, v. 35, no. 2, p. 328–338.

Morin, R.H., Hess, A.E., and Paillet, F.L., 1988, Determining the distribution of hydraulic conductivity in a fractured limestone aquifer by simultaneous injection and geophysical logging: Ground Water, v. 26, p. 587–595.

National Research Council, Committee on Fracture Characterization and Fluid Flow, 1996, Rock fractures and fluid flow—Contemporary understanding and applications: Washington, D.C., National Academy Press, 551 p.

Olsen, P.E., 1980, The latest Triassic and early Jurassic formations of the Newark Basin (eastern North America, Newark Supergroup)—Stratigraphy, structure, and correlation: New Jersey Academy of Science Bulletin, v. 25, p. 25–51.

Parker, R.A., Houghton, H.F., and McDowell, R.C., 1988, Stratigraphic framework and distribution of early Mesozoic rocks of the Northern Newark Basin, New Jersey and New York, *in* Froelich, A.J., and Robinson, G.R. Jr., editors, Studies of the early Mesozoic basins of the eastern United States: U.S. Geological Survey Bulletin 1776, p. 31–39.

Pollock, D.W., 1989, Documentation of computer programs to compute and display pathlines using results from the U.S. Geological Survey modular three-dimensional finite-difference ground-water flow model: U.S. Geological Survey Open-File Report 89–381, 188 p.

Rajaram, Harihar, and Gelhar, L.W., 1995, Plume-scale dependent dispersion in aquifers with a wide range of scales of heterogeneity: Water Resources Research, v. 31, no. 10, p. 2469–2482.

Raven, K.G., Novakowski, K.S., and Lapcevic, P.A., 1988, Interpretation of field tracer tests of a single fracture using a transient solute storage model: Water Resources Research, v. 24, no. 12, p. 2019–2032.

Terzaghi, R., 1965, Sources of error in joint surveys: Geotechnique, v. 15, p. 287–304.

Tsang, Y.W., 1995, Study of alternative tracer tests in characterizing transport in fractured rocks: Geophysical Research Letters, v. 22, no. 11, p. 1421–1424.

Vecchioli, John, Carswell, L.D., and Kasaback, H.F., 1969, Occurrence and movement of ground water in the Brunswick Shale at a site near Trenton, N.J.: U.S. Geological Survey Professional Paper 650-B, p. B154–B157.

Voss, C.I., 1984, SUTRA—A finite-element simulation model for saturated-unsaturated, fluid-density-dependent ground-water flow with energy transport or chemically-reactive single-species solute transport: U.S. Geological Survey Water Resources Investigations Report 84-4369, 409 p.

Webster, D.S., Proctor, J.F., and Marine, I.W., 1970, Two-well tracer test in fractured crystalline rock: U.S. Geological Survey Water-Supply Paper 1544–I, p. I1–I21.

Welty, Claire, and Gelhar, L.W., 1989, Evaluation of longitudinal dispersivity from tracer test data: Cambridge, Mass., Massachusetts Institute of Technology, Ralph M. Parsons Laboratory Technical Report 320, R89-05, 107 p.

Welty, Claire, and Gelhar, L.W., 1994, Evaluation of longitudinal dispersivity from nonuniform flow tracer tests: Journal of Hydrology, v. 153, no. 1, p. 71–102.

Appendix A--Aquifer-Test Analysis Using the Technique of Hsieh and Neuman (1985)

Hsieh and Neuman (1985) present analytical solutions for aquifer tests for four different fluid-injection/observation scenarios. (The solutions are identical for fluid withdrawal.)   The cases are point injection/point observation (case 1), line injection/point observation (case 2), point injection/ line observation (case 3), line injection/line observation (case 4). Classification of a borehole interval as a line or a point depends on the values of the hydraulic conductivity tensor and the ratio of the length of the interval to the distance between the interval and the observation or injection location. Quantitative criteria for choosing a point or line representation are given, but are difficult to implement because they depend on the hydraulic-conductivity tensor, which is not known in advance. Using a point solution wherever possible is most desirable, however, because this simplifies the mathematics considerably.

The method published by Hsieh and Neuman (1985) allows determination of unknown principal directions and principal values of hydraulic conductivity for a homogeneous and anisotropic medium.   Adequate spatial distribution of observation data are required by the method. Specifically, at least six observation intervals must be available with adequate displacement in all three spatial dimensions in order to quantify the six independent components of the hydraulic-conductivity tensor. This spacing can be accomplished in a number of ways; for example, using three parallel boreholes that do not lie in a plane, or two nonparallel boreholes that can be packed off at several intervals. In both of these example alternatives, the various boreholes or borehole intervals would be required to alternate as fluid injection and withdrawal locations. The 14 observation boreholes at the Hopewell Township site are approximately parallel to the pumped well, where the centers of the observation boreholes are offset vertically from the center of the pumped well on the order of tenths of a meter to several meters.   This number and configuration of boreholes was considered to be marginally adequate to meet the data requirement for the analysis.

To evaluate the data from the Hopewell site, the line injection/line observation analytical solution (case 4) was selected, because long boreholes were used for fluid withdrawal and observation. For the simplified case of parallel pumping and observation boreholes, Hsieh and Neuman's (1985) solution for case 4 is given by their equation 39 as

$$\Delta h_{LD} = \frac{\beta_1}{4} \int_{w=1/(4t_D)}^{w=\infty} \frac{1}{w} exp[-(1-\alpha_2^2)w]\{ C_1 erf(w^{1/2}C_1) - C_2 erf(w^{1/2}C_2) -$$

$$C_3 erf(w^{1/2}C_3) + C_4 erf(w^{1/2}C_4) +$$

$$[exp(-wC_1^2) - exp(-wC_2^2) - exp(-wC_3^2) + exp(-wC_4^2)]/(\pi w)^{1/2}\}dw \quad ,$$

where

$$\Delta h_{LD} = (8\pi \Delta h\, G_{11}^{1/2})/Q ,$$

Δh is unscaled drawdown,

$$G_{11} = (L^2/4)A_{33},$$

L is length of injection interval,

A_{ij} is adjoint of K_{ij}; $i, j = 1, 2, 3,$

K_{ij} is hydraulic conductivity tensor, $i, j = 1, 2, 3,$

Q is volumetric pumping or injection rate,

t_D $= Dt/(S_s G_{xx}),$

t is unscaled time,

S_s is specific storage,

D is determinant of the K_{ij} tensor,

$$C_1 = \alpha_2 + 1/\alpha_1 + 1/\beta_1,$$

$$C_2 = \alpha_2 + 1/\alpha_1 - 1/\beta_1,$$

$$C_3 = \alpha_2 - 1/\alpha_1 + 1/\beta_1,$$

$$C_4 = \alpha_2 - 1/\alpha_1 - 1/\beta_1,$$

$$\alpha_1 = (G_{xx}/G_{11})^{1/2},$$

$$\beta_1 = (G_{xx}/G_{bb})^{1/2},$$

$$\alpha_2 = \beta_2 = (x_1 A_{13} + x_2 A_{23} + x_3 A_{33})/(G_{xx}A_{33})^{1/2},$$

$$G_{xx} = x_1^2 A_{11} + x_2^2 A_{22} + x_3^2 A_{33} + 2x_1 x_2 A_{12} + 2x_2 x_3 A_{23} + 2x_1 x_3 A_{13},$$

$$G_{bb} = (B^2/4)A_{33},$$

B is length of observation interval, and

x_i are cartesian coordinates of locations of centers of boreholes relative to the center of the observation borehole, $i = 1, 2, 3.$

Using the solution above, many sets of type curves can be constructed and an appropriate set identified that resembles the shape of the data. Although α_1, β_1, and $\alpha_2 = \beta_2$ cannot be determined individually beforehand because they contain the parameters sought from the analysis, the ratio of α_1/β_1 for the case of parallel boreholes reduces to the ratio of the observation-borehole length to the injection-borehole length. This relation can be used to advantage to aid in generating appropriate type curves.

Type curves were generated by numerical integration of the solution given above for various values of α_1, β_1, and $\alpha_2 = \beta_2$ by means of a Fortran program, which is available from the authors upon request. An example set of type curves is shown in figure A–1, for various values of $\alpha_1 = \beta_1$ and $\alpha_2 = \beta_2 = 0.9997$. That the code was working correctly was assumed from comparison of output with figure 8 in the Hsieh and Neuman (1985) paper (for $\alpha_2 = \beta_2 = 0$ and various values of α_1, β_1), a comparison that showed perfect agreement.

The type-curve matches to the data are shown in figure A–2. In these figures, the value of $\alpha_2 = \beta_2$ was held constant, and the value of $\alpha_1 = \beta_1$ was changed until a best fit of the type curve to the data was achieved. The ratio of α_1/β_1 was adjusted (compared to figure A–1, where $\alpha_1/\beta_1 = 1.0$) for cases where field notes indicted that the effective lengths differed between the pumping and observation boreholes.

From the type-curve matches, match points are chosen and the analysis of Hsieh and others (1985) can be carried out to calculate principal values of hydraulic conductivity and specific storage. The results of the curve matching are shown in table A–1. The procedure employed is similar to the step-by-step procedure outlined in Hsieh and others (1985), with the exception that case 4 is used here, whereas Hsieh and others (1985) used case 1 in their example. The procedure is the following:

1. The x_1, x_2, and x_3 coordinates of the center point of each observation well relative to the pumped well were calculated and entered in columns 2–4 of table A–1.

2. The values of $\alpha_2 = \beta_2$, α_1, and β_1 (columns 5–7) were recorded from the trial and error generation of type curves that appear to best fit the data. In cases where α_1 is not equal to β_1, the recorded ratio of the pumped and observation borehole lengths differs from 1.

3. For all type-curve matches, the type-curve coordinates $\Delta h_{LD} = 1$ and $t_D = 1$ (dimensionless) were chosen. The values of Δh and t in table A-1 (columns 8 and 9) are the coordinates of the match point from the data set, with drawdown given in meters and time in seconds.

4. The directional hydraulic diffusivities (K_d/S_s) for each observation well are shown in column 11 and are calculated as follows:

$$K_d/S_s = R_j{}^2\, t_D/t$$

where $R_j{}^2 = x_1{}^2 + x_2{}^2 + x_3{}^2$ (the distance from the center of the observation well to the center of the pumped well, squared)

When the square roots of the directional hydraulic diffusivities are plotted in space, if the resulting plot is ellipsoidal, this is an indication that the medium behaves as an equivalent, homogeneous, anisotropic one, and the analysis can proceed further to calculate the principal values and principal directions of hydraulic conductivity and specific storage. The directional hydraulic diffusivities for the Hopewell Township site did plot as an ellipsoid, so further analysis was done. An approximate horizontal slice through the best-fit hydraulic diffusivity ellipsoid is shown in figure A–3.
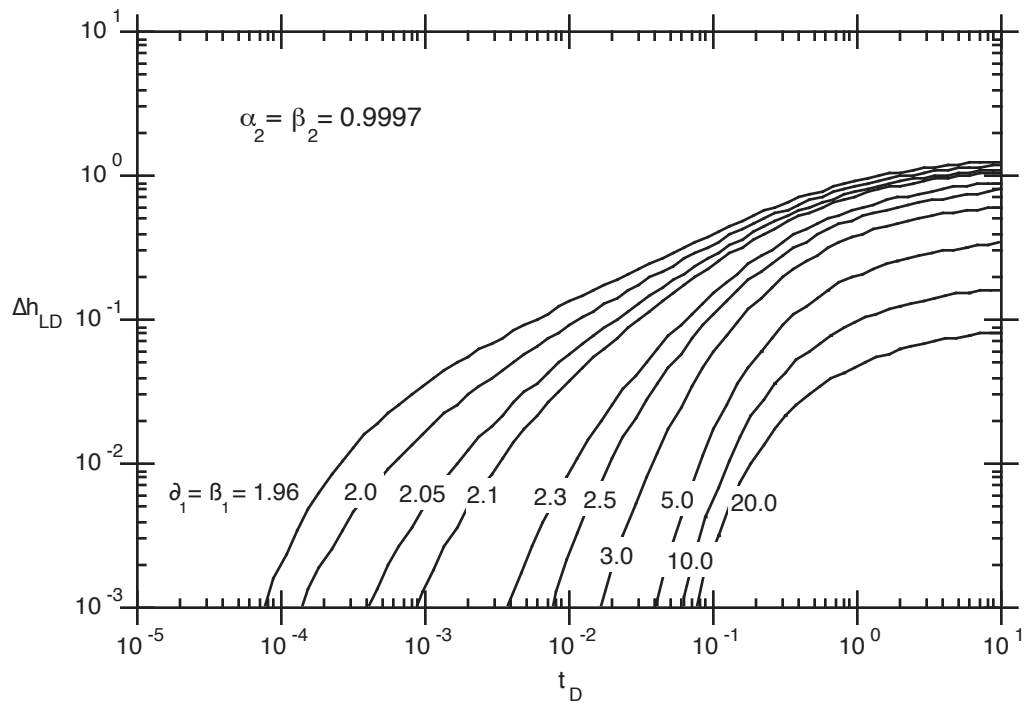
Figure A-1. Example type curves for Case 4 (line withdrawal, line observation), from Hsieh and Neuman (1985). (t_D is dimensionless time, and Δh_{LD} is dimensionless drawdown)
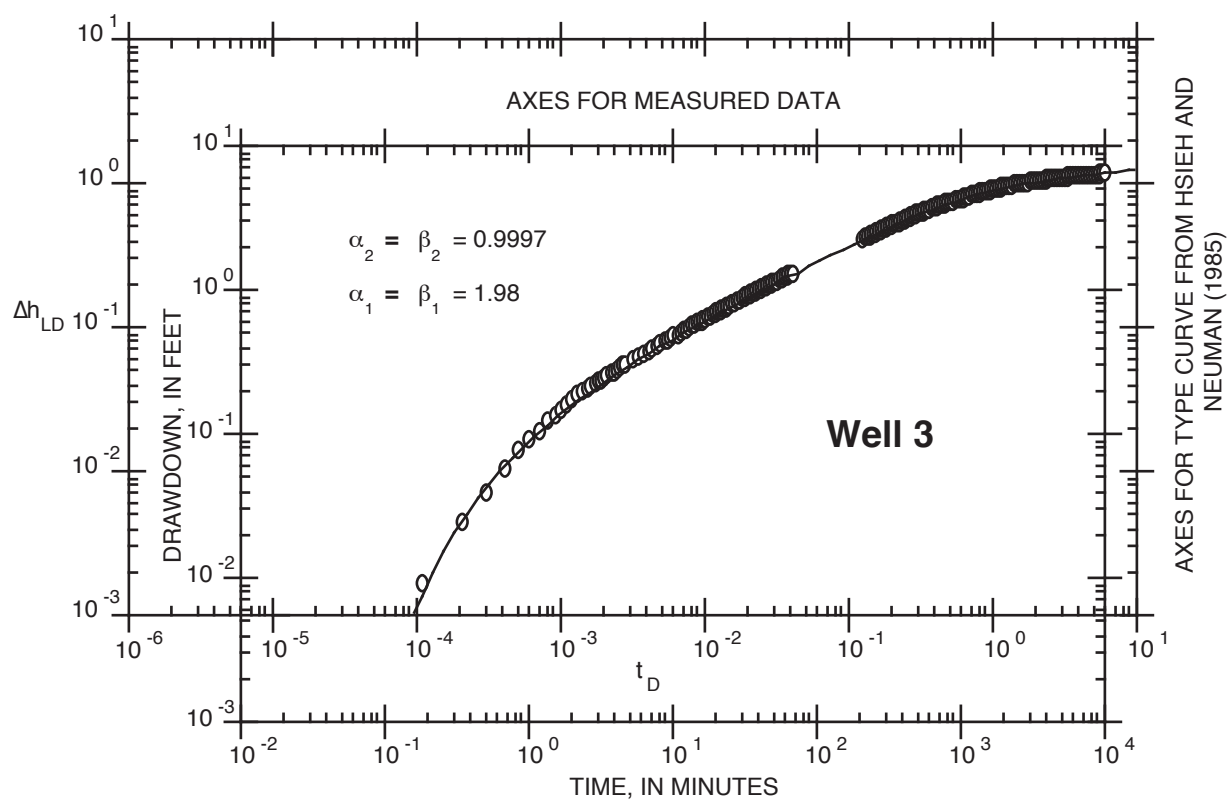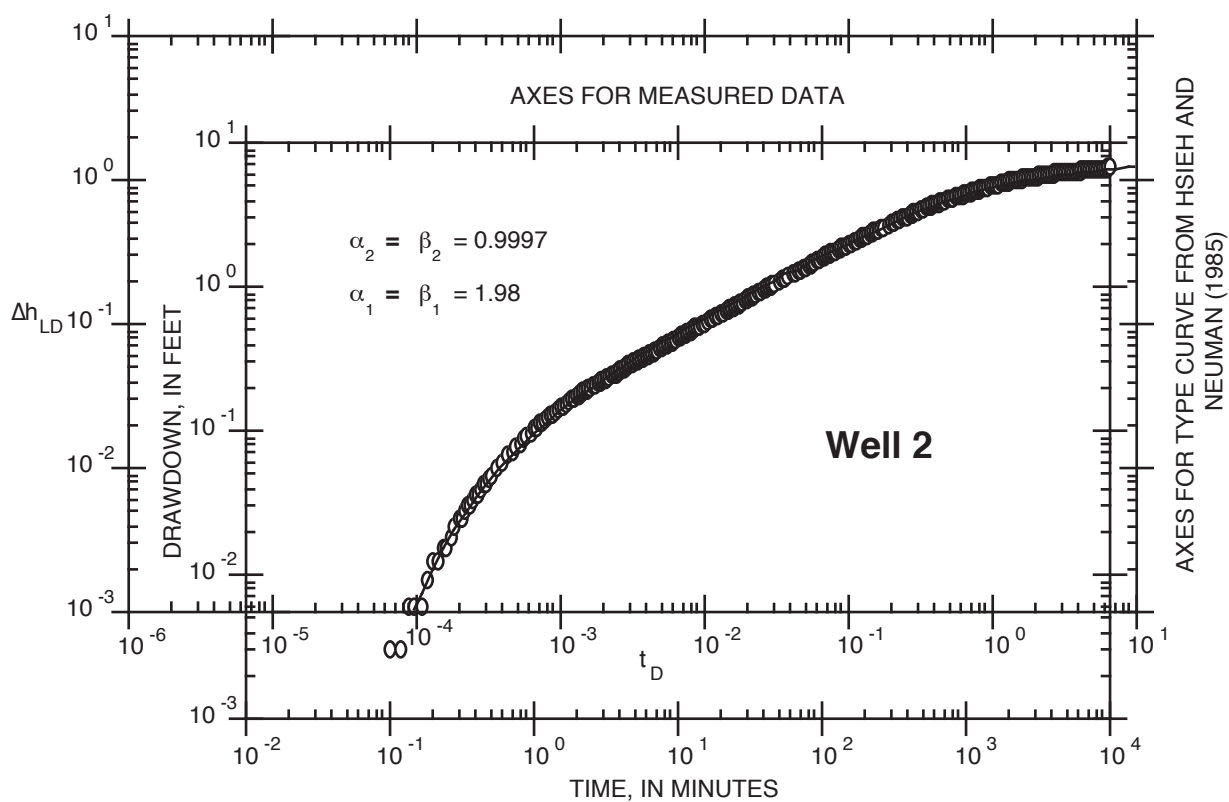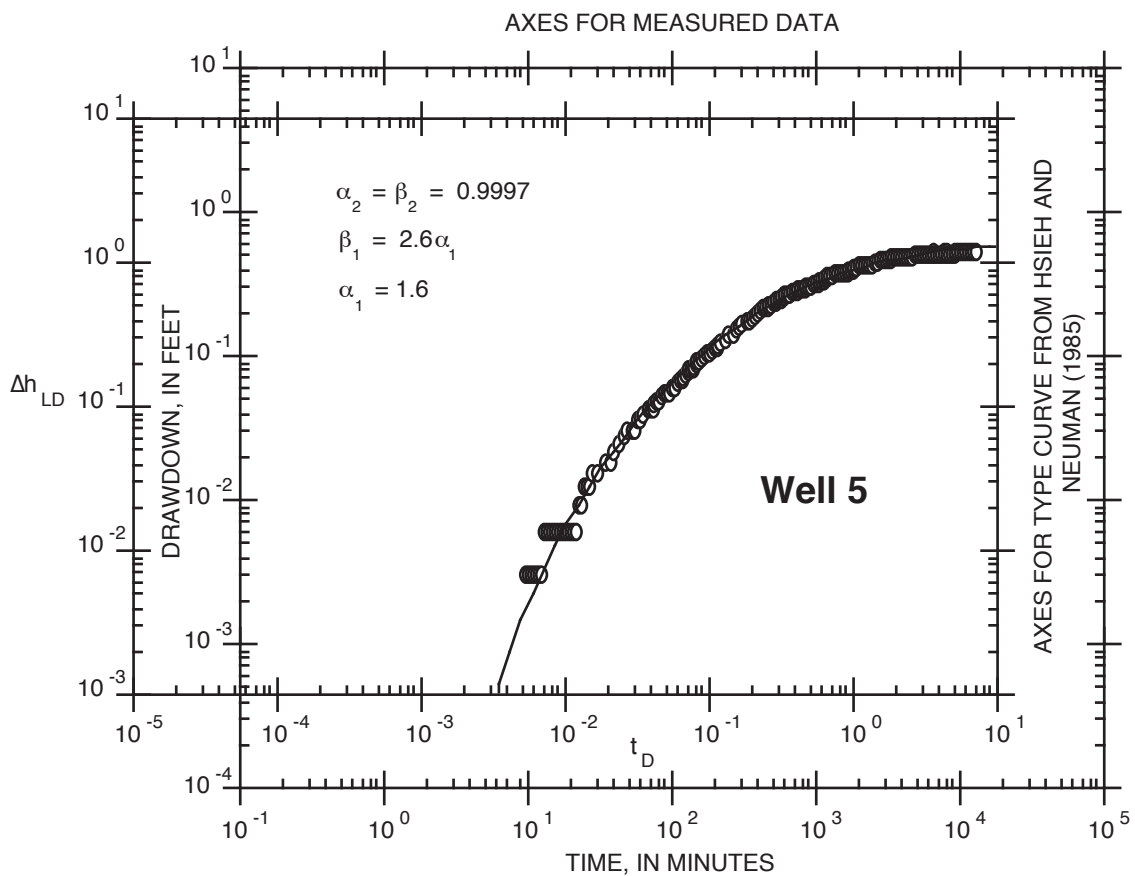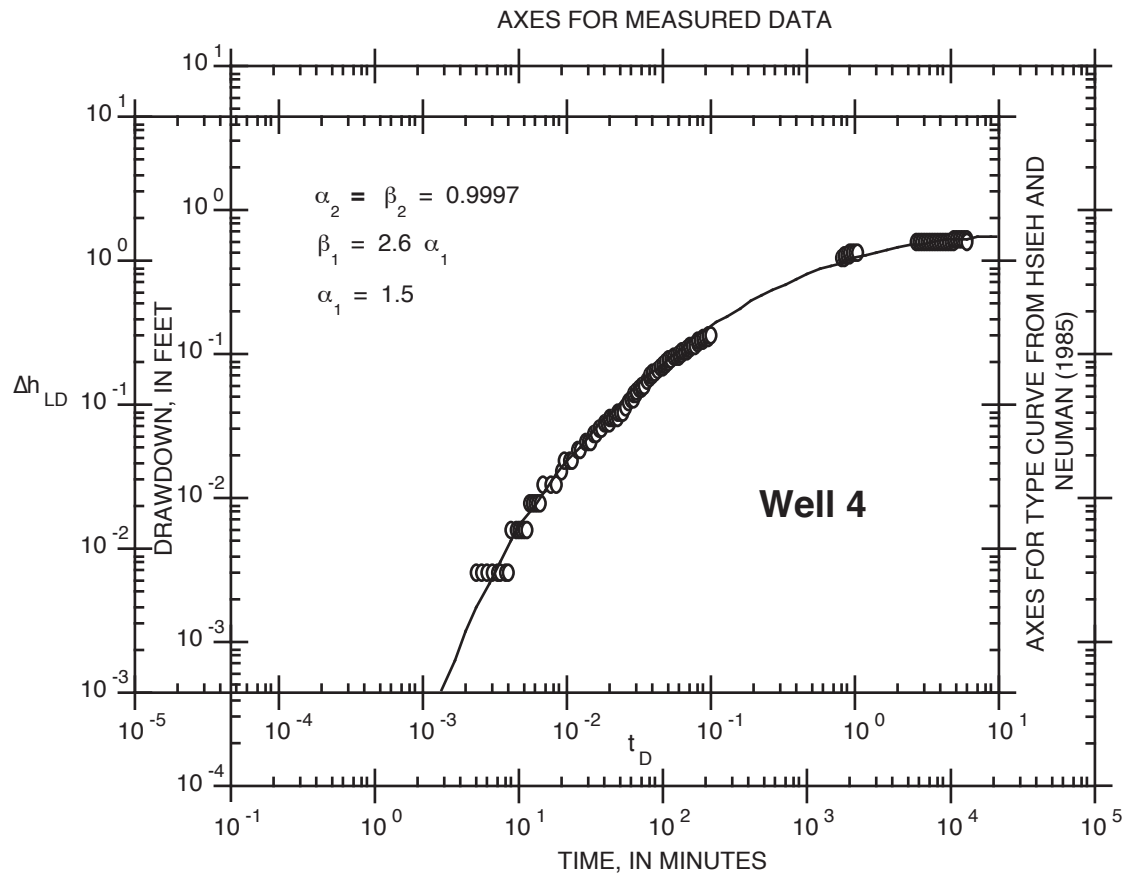
Figure A-2. Match of Hsieh and Neuman (1985) type curves with observed head drawdown in wells 2-15, Hopewell Township, N.J. (t_D is dimensionless time, and Δh_{LD} is dimensionless drawdown).

70

Figure A-2. Match of Hsieh and Neuman (1985) type curves with observed head drawdown in wells 2-15, Hopewell Township, N.J. (t_D is dimensionless time, and Δh_{LD} is dimensionless drawdown)--Continued.
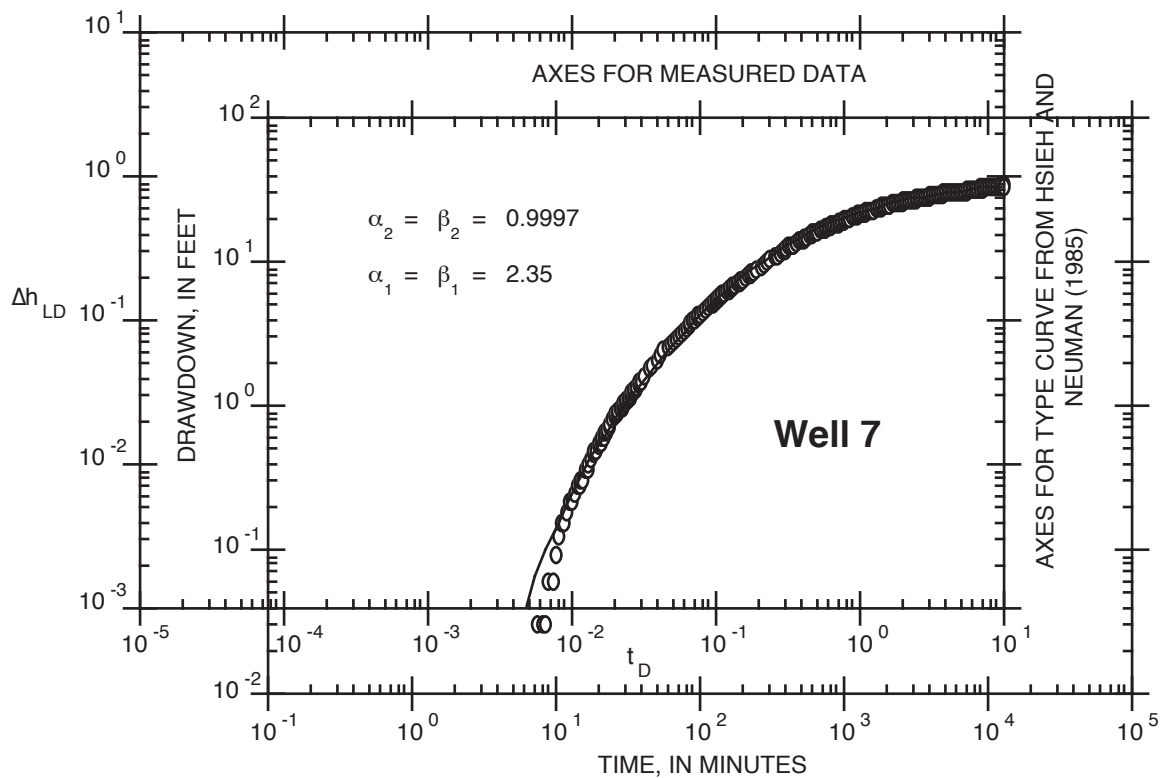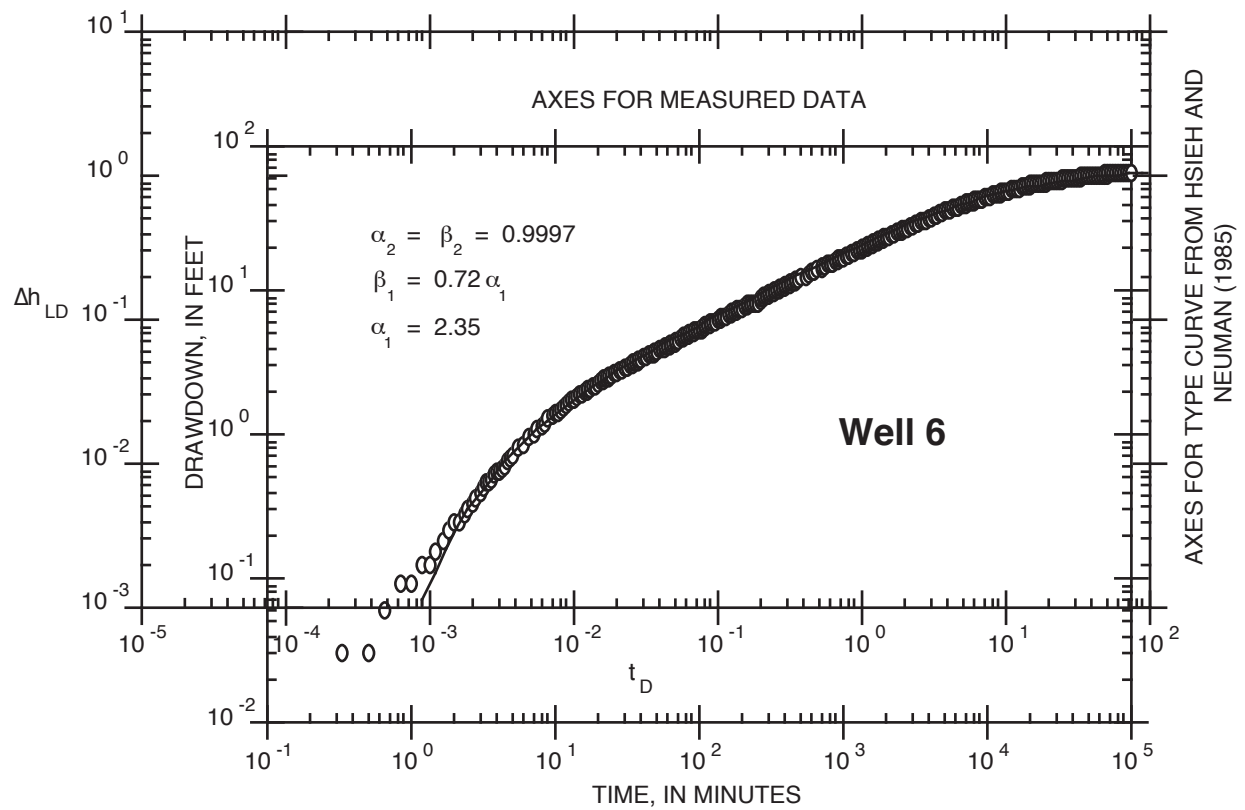
71

Figure A-2. Match of Hsieh and Neuman (1985) type curves with observed head drawdown in wells 2-15, Hopewell Township, N.J. (t_D is dimensionless time, and Δh_{LD} is dimensionless drawdown)--Continued.

Figure A-2. Match of Hsieh and Neuman (1985) type curves with observed head drawdown in wells 2-15, Hopewell Township, N.J. (t_D is dimensionless time, and Δh_{LD} is dimensionless drawdown)--Continued.
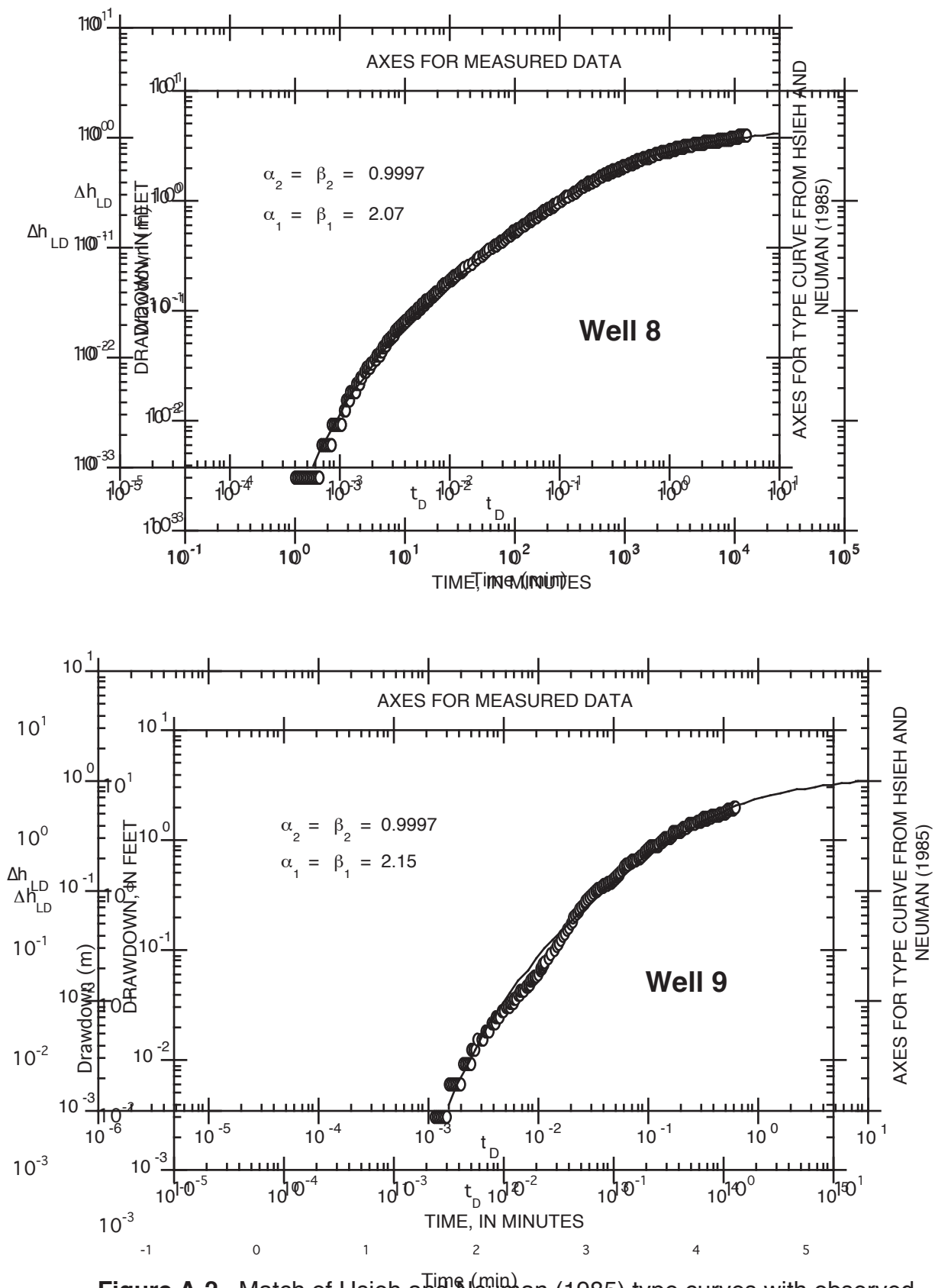
Figure A-2. Match of Hsieh and Neuman (1985) type curves with observed head drawdown in wells 2-15, Hopewell Township, N.J. (t_D is dimensionless time, and Δh_{LD} is dimensionless drawdown)--Continued.
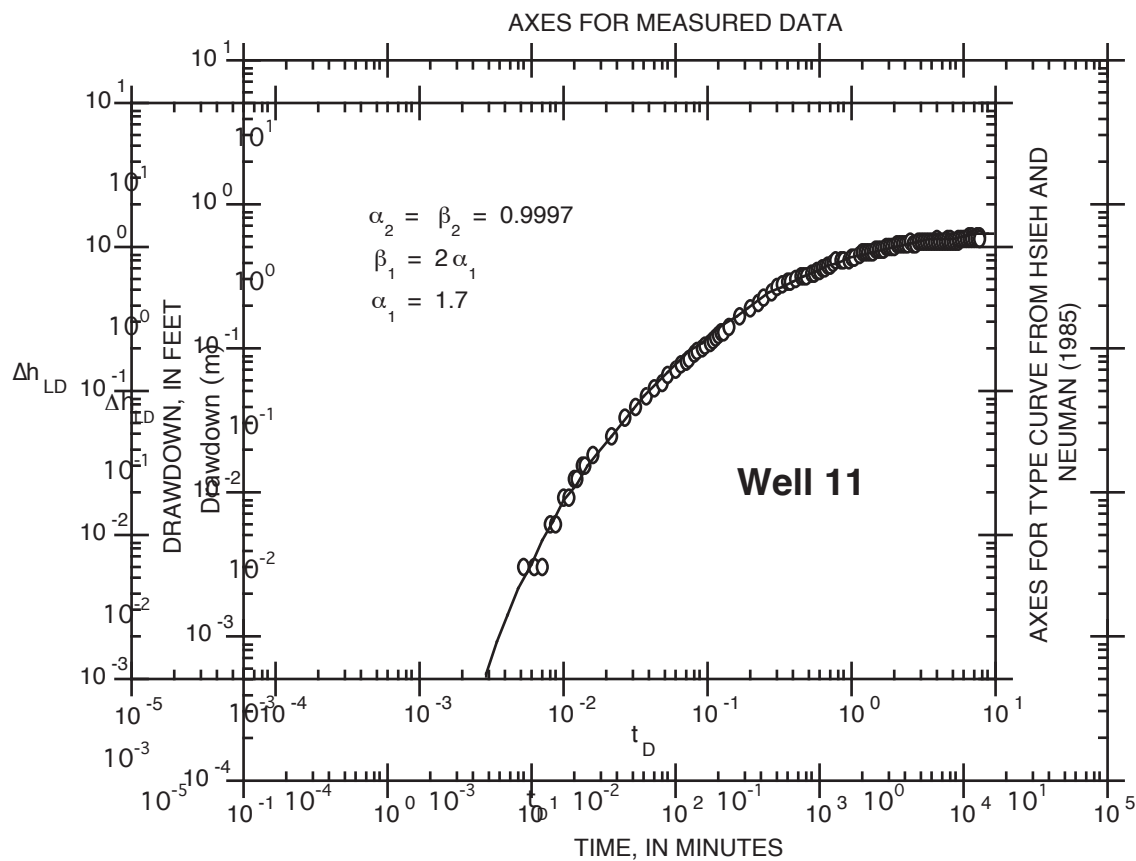
Figure A-2. Match of Hsieh and Neuman (1985) type curves with observed head drawdown in wells 2-15, Hopewell Township, N.J. (t_D is dimensionless time, and Δh_{LD} is dimensionless drawdown)--Continued.
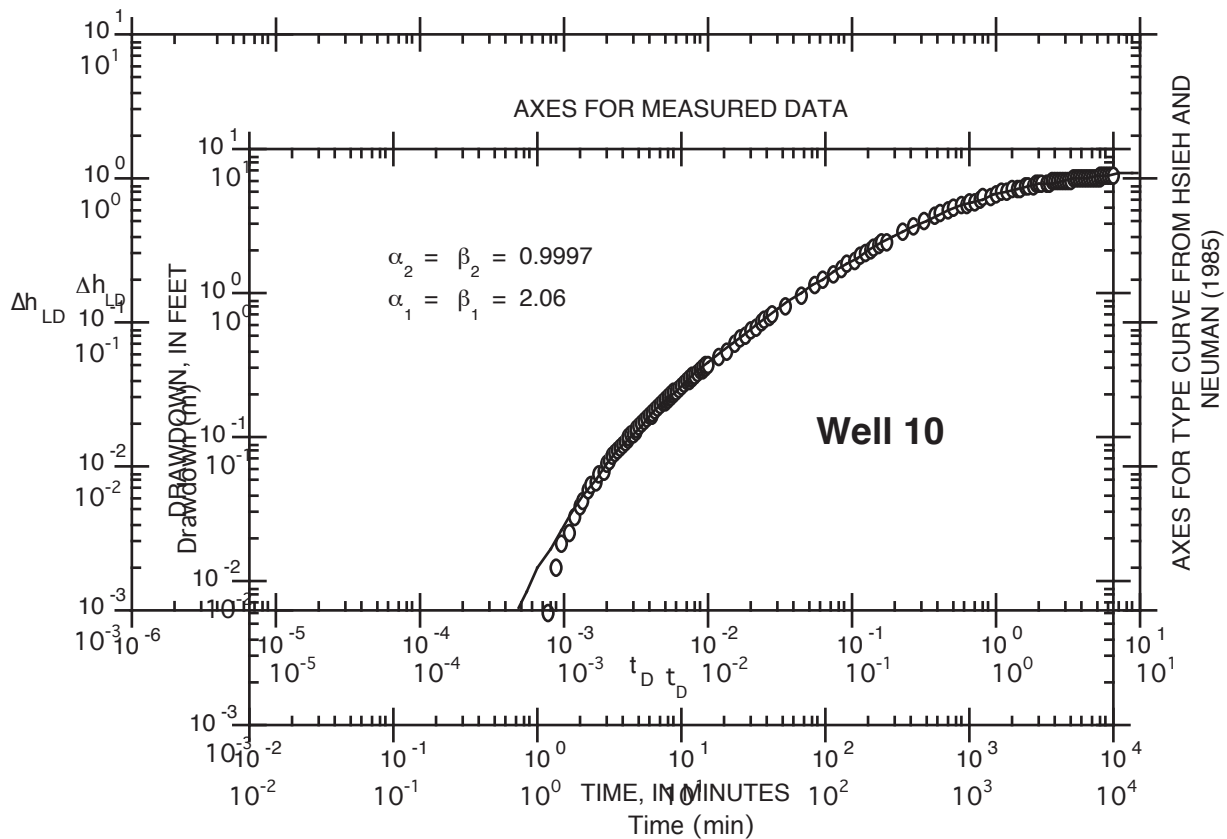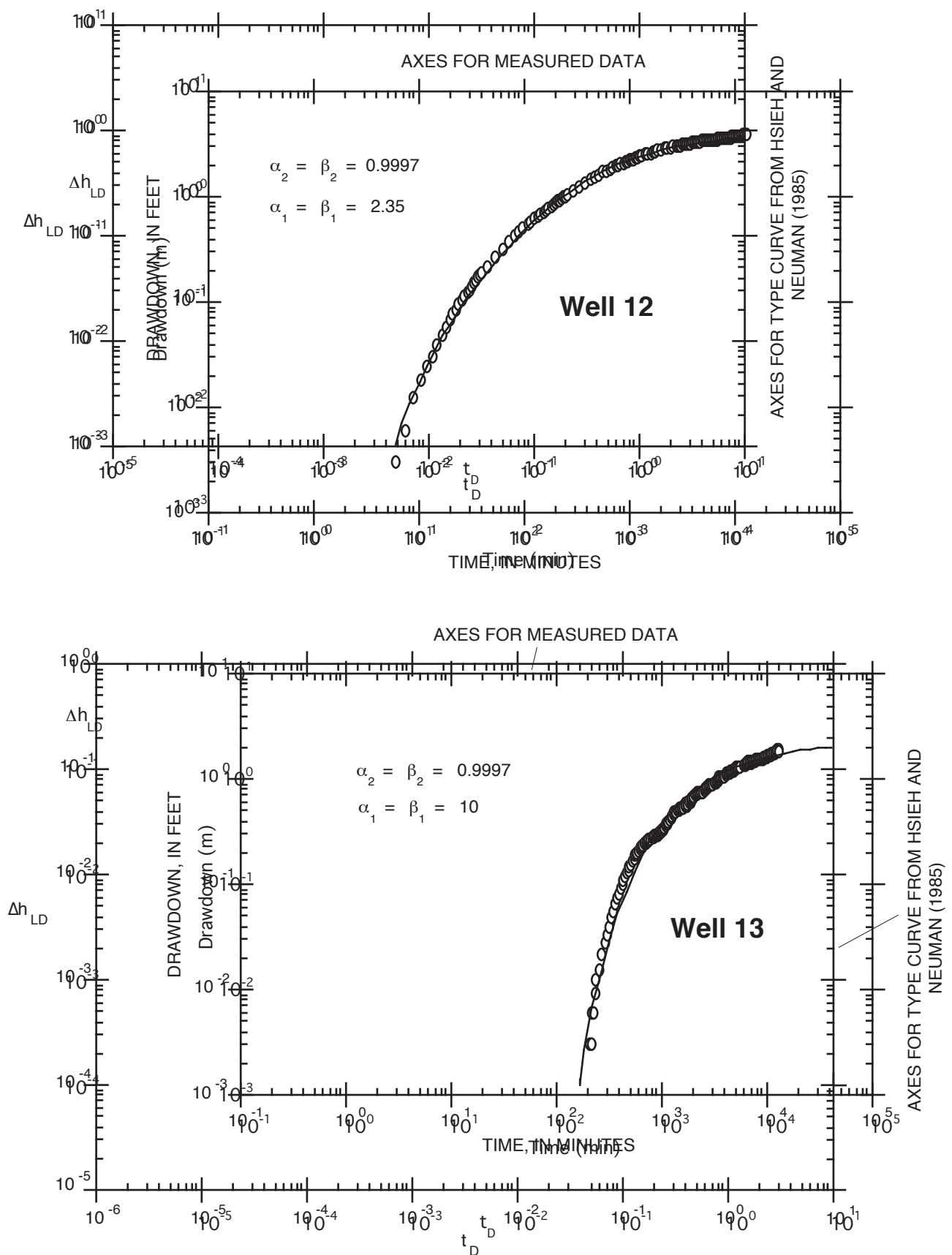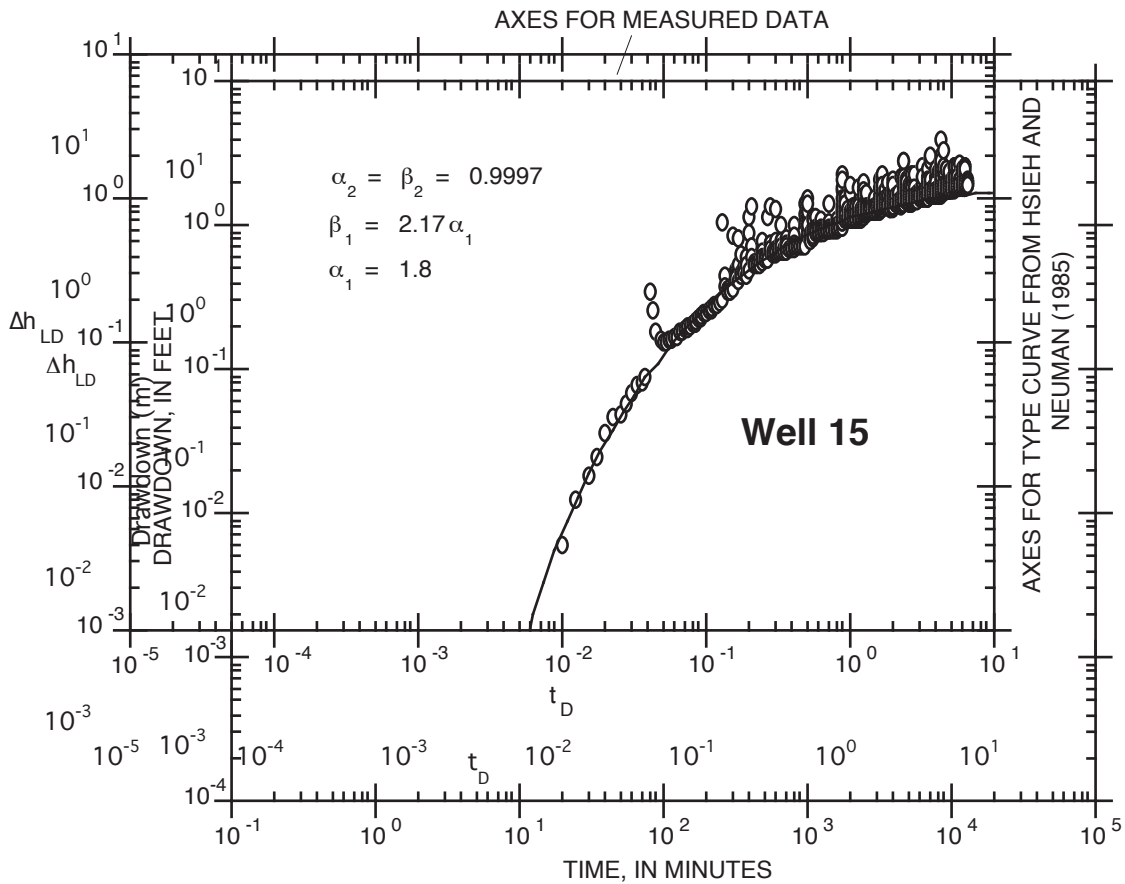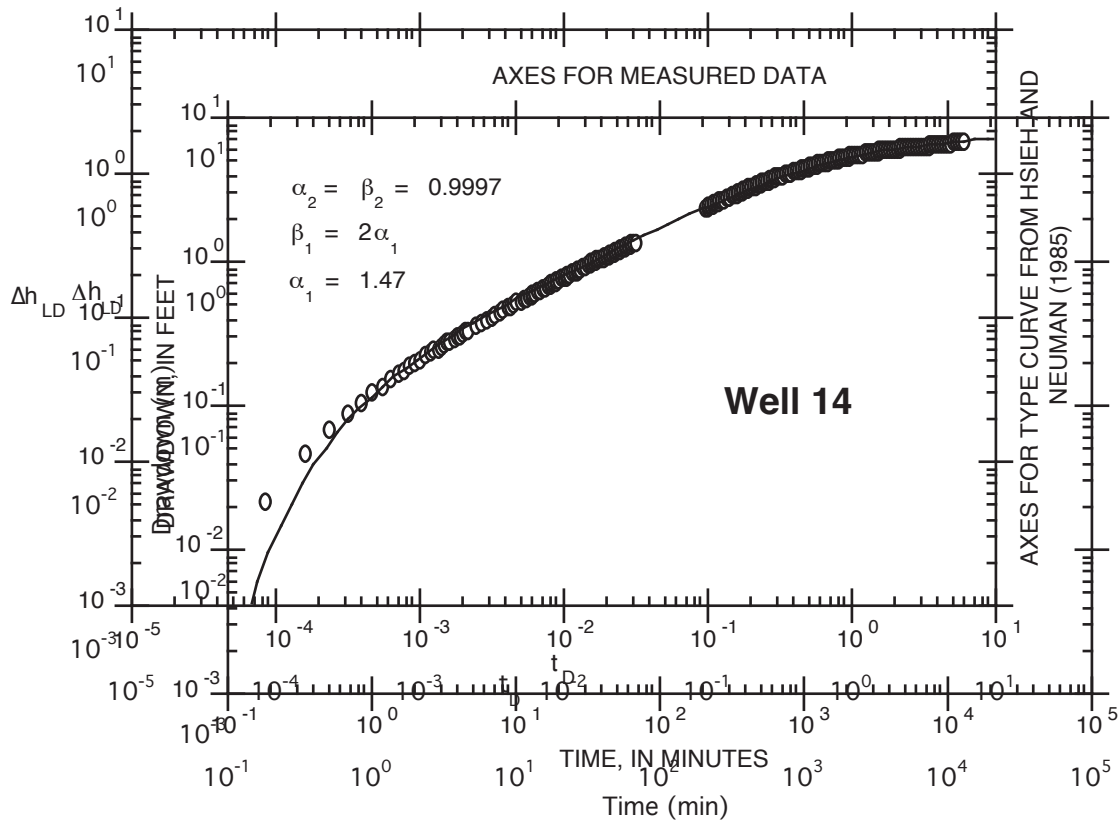
Figure A-2. Match of Hsieh and Neuman (1985) type curves with observed head drawdown in wells 2-15, Hopewell Township, N.J. (t_D is dimensionless time, and Δh_{LD} is dimensionless drawdown)--Continued.

Table A-1. Locations of centers of monitoring wells (relative to the center of the pumped well) and results of curve matching and weights assigned for nonlinear least-squares matrix inversion

[Q = 1.80x10^{-3} m3/s (28.5 gallons per minute) for the entire test. Well 1 is located at (0, 0, 0). m, meters; s, seconds]

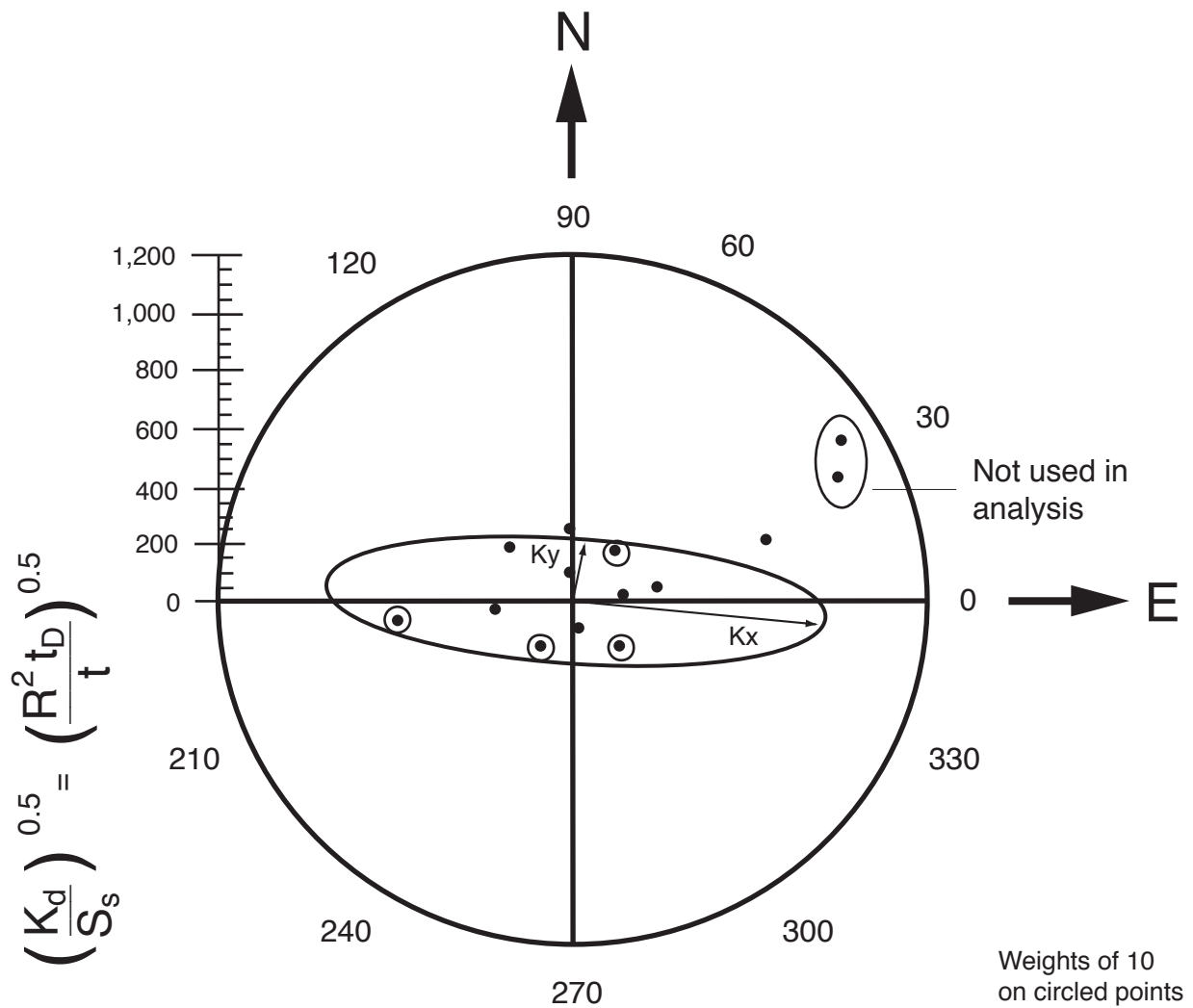| Well number	x_1 (m)	x_2 (m)	x_3 (m)	$\alpha_2=\beta_2$	α_1	β_1	Δh (m)	t (s)	D/K_d (m^2/s$^{2)}$)	K_d/S_s (m^2/s)	D/S_s (m^4/s^3)	Wt
2	-90.3	-10.0	2.6	0.99975	1.98	1.98	5.49	1.1x10^5	8.1x10^{-14}	7.9x10^{-2}	6.4x10^{-15}	1.0
3	90.0	17.0	-3.6	.99970	1.98	1.98	5.49	9,3x10^4	7.9x10^{-14}	9.0x10^{-2}	7.2x10^{-15}	1.0
4	57.8	74.0	-5.0	.99970	1.5	3.9	.49	1.5x10^5	5.5x10^{-12}	5.9x10^{-2}	3.2x10^{-13}	10
5	-4.6	93.0	-3.6	.99970	1.6	4.2	.43	1.2x10^5	8.3x10^{-12}	7.2x10^{-2}	6.0x10^{-13}	1.0
6	-2.2	30.0	-7.2	.99970	2.35	.72	6.10	7.8x10^4	8.0x10^{-13}	1.2x10^{-2}	9.8x10^{-15}	1.0
7	184.4	62.0	-4.2	.99970	2.35	2.35	3.66	7.5x10^4	5.6x10^{-14}	5.1x10^{-1}	2.8x10^{-14}	1.0
8	61.2	-59.0	-3.0	.99970	2.07	2.07	3.66	1.5x10^5	2.3x10^{-13}	4.8x10^{-2}	1.1x10^{-14}	10
9	11.2	-93.0	-1.1	.99970	2.15	2.15	3.35	1.1x10^6	2.4x10^{-13}	8.1x10^{-3}	2.0x10^{-15}	1.0
10	-180.8	-19.0	3.9	.99970	2.06	2.06	6.10	8.4x10^4	1.8x10^{-14}	3.9x10^{-1}	7.0x10^{-15}	10
11	-68.2	63.0	-.3	.99970	1.70	3.4	.46	9.6x10^4	3.2x10^{-12}	9.0x10^{-2}	7.4x10^{-13}	1.0
13	-53.9	-73.0	.4	.99970	10.0	10.0	2.44	2.2x10^5	4.2x10^{-13}	3.7x10^{-2}	1.6x10^{-14}	10
14	60.2	7.0	8.2	.99970	1.47	2.94	3.66	1.2x10^5	2.2x10^{-13}	3.1x10^{-2}	6.9x10^{-15}	1.0

Figure A-3. Polar coordinates of the square root of the directional diffusivity for each well and the two dimensional representation of the best-fit hydraulic conductivity ellipsoid, Hopewell Township, N.J.

The analysis required proceeded identically as outlined on pages 1669 to 1670 of Hsieh and others (1985). A synopsis follows:

1. The quantity D/K_d is calculated for each borehole as follows and is shown in column 10, table A–1:

$$D/K_d = ((Q\alpha_1 \Delta h_{LD})/(8\pi \Delta h R_j))^2.$$

2. The quantity D/S_s is calculated for each borehole by multiplying K_d/S_s by D/K_d and is shown in column 12, table A–1.

3. The inverse diffusivity tensor, which is unknown, is defined as follows:

$$U_{ij} = S_s K_{ij}^{-1}.$$

U_{ij} can be shown to be related to the directional diffusivities by

$$x_i x_j U_{ij}/(R_j^2) = S_s/K_d(e_j) \ (i, j = 1, 2, 3),$$

where e_j is a unit vector pointing between the observation well and the pumped well. Here, all information is known except the U_{ij}. This matrix represents a system of equations where the number of unknowns are the six values of U_{ij}, and the number of equations corresponds to the number of observation wells. The solution is found by solving the matrix for U_{ij}. A Fortran code written to invert U_{ij} is available from the authors upon request.

4. The diffusivity tensor, $S_s^{-1} K_{ij}$, is found by inverting U_{ij}. If U_{ij} is not positive definite, negative values of principal diffusivities will result, which can happen if the data exhibit pronounced scatter. If this is the case, additional data beyond the required six points can be collected, and an ordinary or weighted least-squares procedure can be used to fit an ellipse to the data. Weighted least squares can be tried if ordinary least squares fails to give a positive definite result, as was the case here. This behavior is common when the data exhibit wide deviations from the shape of an ellipsoid. This option for using weighted least squares is included in the Fortran code available from the authors.

Hsieh and others (1985) warn that the solution of ordinary least squares may be biased toward small K_d values if the small values differ significantly from the larger ones. In this case, the larger K_d values can be assigned weights so that they are not overlooked, and a weighted least-squares procedure can be used instead. As reported by Hsieh and others (1985), the process of assigning weights is a trial-and-error approach that is used until a positive definite result is obtained. A positive definite result could be obtained for the Hopewell site only by weighting the data from wells 4, 8, 10, and 13. The weights used are indicated in column 13. A weight of 1 indicates no weighting, whereas a weight of 10 was used to obtain a positive definite result for inverting U_{ij}. There is no particular significance attached to the weight of 10. Hsieh and others (1985) used weights of 4, but reported similar results using weights ranging from 2 to 10.

5. Once a U_{ij} is inverted to obtain $S_s^{-1}K_{ij}$, the diffusivity tensor, the determinant of the result is calculated to find D/S_s^3.

6. The average of the D/S_s values reported in column 12 of table A-1 is calculated $(\overline{D/S_s})$.

7. S_s is computed from

$$S_s = [\overline{(D/S_s)}/(D/S_s^3)]^{1/2} \quad .$$

8. The K_{ij} tensor is calculated by multiplying $S_s^{-1}K_{ij}$ by S_s.

9. The principal components and principal directions are found using standard tensor trans-formation rules. This calculation is also included in Fortran code available from the authors.

The data points from wells 12 and 15 were not used in the analysis (fig. A–3) because inclu-sion of the type-curve match data from these two wells did not produce a positive definite result using any combination of weights. This is likely because the strike of the formation and, therefore probably the direction of the principal components of hydraulic conductivity, change over the scale of the test.

The results of the analysis are summarized in table A–2.

Table A-2. Principal hydraulic conductivities, principal directions, and specific storage calculated by using weighted least squares

[m, meters; N., north; E., east; ^{o}, degrees]

Principal component	Bearing	Plunge
6.4	N. 94.7^{o} E.	1.1^{o}
.30	N. 4.6^{o} E.	4.6^{o}
4.3 x 10^{-3}	N. 192° E.	85.4^{o}

Specific storage	9.2 x 10^{-5} m^{-1}